Non-Volatile Particle Penetration Efficiencies: UTRC Line Loss Model Validation

A Thesis Presented for the
Master of Science
Degree
The University of Tennessee, Knoxville

Brandon Craig Hoffman
August 2017

Copyright © 2017 by Brandon Craig Hoffman
All rights reserved.

Distribution A: Approved for public release, Distribution unlimited.
PA Number: AEDC2017-074

ACKNOWLEDGEMENTS

First I would like to acknowledge my thesis committee (Dr. Trevor Moeller, Dr. Joseph Wehrmeyer, and Dr. Milton Davis) and Dr. Robert Howard for all their support that made this thesis possible. I would also like to acknowledge the United States Environmental Protection Agency National Vehicle and Fuel Emissions Laboratory (US EPA NVFEL) for funding the test campaign and the Arnold Engineering Development Complex (AEDC)/ University of Tennessee Space Institute (UTSI) for hosting this test. Thank you to both Dr. Robert Giannelli and Mr. John Kinsey from the US EPA who planned, managed, and helped make measurements for this test campaign. Next I would like to acknowledge, as well as thank, Dr. David Kittelson and Dr. Jacob Swanson of the University of Minnesota (UoM) for taking the time to check out all of the Scanning Mobility Particle Sizer (SMPS) instruments that made these penetration measurements possible. Thank you to United Technologies Research Center (UTRC) for supporting and providing much needed equipment at the last minute. Thank you also goes out to the rest of the EPA Variable Response In Aircraft Non-Volatile Particle Matter Testing (VARIAnT2) team which helped make the campaign a success.



EPA VARIAnT2 Test Team

ABSTRACT

The SAE E-31 Aircraft Engine Gas & Particulate Emissions Measurement Aerospace Recommended Practice (ARP) 6320 {Ref. 17} describes procedures recommended for continuous sampling conditions and instrumentation for measurement of non-volatile particle number and mass emissions from the exhaust of aircraft gas turbine engines. Throughout the creation of the ARP, many tests were conducted to determine the best way to collect and measure non-volatile particulate matter from turbine engines to preserve sample integrity and minimize the losses through the system; including sampling, conditioning, and measurement. Based on the results of these tests, a system was built by Missouri University of Science and Technology (MS&T), which they own and operate. A few other in-house systems were built by other organizations, but it wasn't until Anstalt für Verbrennungskraftmaschinen List (AVL) of Graz, Austria started to produce and manufacture an ARP6320 compliant sampling system that it was commercially available for purchase. The first prototype was delivered to Arnold Engineering Development Complex. Even though the AVL sampling system and the MS&T sampling system are compliant with the ARP6320, there were some differences between the two systems which begged the question, will each system produce the same or similar results? The Environmental Protection Agency (EPA) VAriable Response In Aircraft Non-Volatile Particulate Matter Testing (VARIAnT) 2 was established to answer these questions and more. This thesis concentrates on a small portion of this test campaign, specifically the ability of the systems to transport non-volatile or carbon black particles to instruments for measurement of mass, number, and size. The ratio of non-volatile particle concentration entering and leaving a sampling and measurement system segment is the Penetration Fraction which is the focus of this thesis.

The results in this thesis and other comparisons to the model have shown close correlation within the measurement uncertainties of 14%. The penetration efficiency model used in this work was developed by UTRC and has been improved over the years to account for various differences between measured and predicted. Using the results presented in this thesis, the UTRC model presents a better alternative to the measurements of the penetration efficiencies for the ARP compliant sampling systems.

TABLE OF CONTENTS

Chapter One Introduction and General Information 1
Background 1
The Sampling Systems 1
AVL Sample System 2
MS&T Sample System 3
Chapter Two Literature Review 5
Non-Volatile Particle Loss Theory and Models 5
UTRC Line Loss Model 6
Segment Calculations 7
Penetration Efficiencies due to only diffusional losses, $\eta_{difi}(D_m)$, i=1, 2, .., 10 8
Penetration Efficiencies due to only inertial particle losses, $\eta_{bi}(D_m)$ 9
Penetration Efficiency due only to Thermophoresis, $\eta_{thermoi}$ 9
Electrostatic Penetration Efficiencies, $\eta_{eleci}(D_m)$ 11
Diluter1 Penetration Efficiencies, $\eta_{dil}(D_m)$ 11
Splitter Penetration Efficiencies, $\eta_{spl}(D_m)$ 11
Cyclone Separator Penetration Efficiencies, $\eta_{cyc}(D_m)$ 11
AVL Particle Counter (APC) Penetration Efficiencies, $\eta_{APC}(D_m)$ 12
Total Penetration Efficiencies, $\eta_{total}(D_m)$ 13
Chapter Three VARIAnT2 penetration testing 14
Instrumentation 14
Scanning Mobility Particle Sizers 14
Non-Volatile Particle Sources 15
Jing Mini-CAST 15
General Electric J85 Engine with Afterburner 16
Testing 16
Data Collection 16
Test setup and Description 17
SMPS Functionality Checks 21
Source Setup 24
Jing Mini-CAST 24
General Electric J85 Engine with Afterburner 24
Chapter Four Results and Discussion 27
Instrumentation Issues 27
Penetration Efficiencies 30
AVL Sample System Penetration Efficiencies 30
Upstream Half of AVL Sample System Penetration Efficiencies 40
Downstream Half of AVL Sample System Penetration Efficiencies 45
MS&T Sampling System Penetration Efficiencies 50
APC Penetration Efficiencies 55
Penetration Efficiency Model Comparisons 64
Sampling System Model Comparison 64
VPR/Dilution System APC Model Intercomparison 66

Upstream and Downstream AVL Sampling System Model Comparison.....66
Error and Uncertainty 67
Standard Deviation Calculation.....67
Chapter Five Summary and Conclusions.....69
Results and Discussion 69
Recommended Additional Research 71
Final Remarks 71
List of References 72
Appendix.....76
Appendix 1. APC Calibrations 77
Appendix 2. SMPS Calibrations 83
Appendix 3. MSS, LII and APC Description 86
Appendix 4. Instrumentation List 89
Appendix 5. Measurement Parameters 91
Appendix 6. Additional Penetration Efficiency Measurements 99
Appendix 7. Acronyms and Symbols.....108
Appendix 8. UTRC Model Inputs and Assumptions.....116
Vita.....118

LIST OF TABLES

Table 3.1. Jing Mini-CAST Settings utilized during VARIAnT2 Test Campaign..16
Table A.4.1. Equipment & Description……..…….89
Table A.7.1. Acronyms definitions……..……..108
Table A.7.2. Symbols defined……..…..109
Table A.8.1. Sampling and measurement System Input Parameters {Ref.16}..116
Table A.8.2. Assumed Carrier Gas and Particle Properties used in the Particle Transport Calculations {Ref. 16}……..……117

LIST OF FIGURES

Figure 1.1. Diagram of any nvPM sampling and measurement system as defined in ARP6320 {Ref. 17} and AIR6241 {Ref. 18}……..4

Figure 2.1. UTRC calculated penetration efficiency model output for the AVL sampling system……..7

Figure 3.1. Po-210 aerosol neutralizer strips and cartridge holder……14

Figure 3.2. Jing Mini-CAST principle {Ref 1}……15

Figure 3.3. Configuration for penetration efficiency measurements……..19

Figure 3.4. Near source sampling system……..20

Figure 3.5. Test 1 calibration results during the UoM testing……..22

Figure 3.6. Test 2 calibration results during the UoM testing……..22

Figure 3.7. DOS Atomizer……23

Figure 3.8. Pre and post-test SMPS consistency check……..23

Figure 3.9. Mini-CAST setup illustration……24

Figure 3.10. Jing Mini-CAST setup……..25

Figure 3.11. Probes at GE J85 exit plane……..26

Figure 4.1. NRMRL SMPS and NVFEL SMPS daily DOS checks……28

Figure 4.2. Final test configuration……..29

Figure 4.3. TSI SMPS and AEDC SMPS mobility diameter distributions measured before and after the AVL Sampling system respectively, GE J-85 with Jet-A at idle……..31

Figure 4.4. Average size dependent penetration data determined from measurements on the GE J-85 with Jet-A at idle power setting compared to calculations from the UTRC model……..32

Figure 4.5. Measured Lognormal mobility diameter distributions produced by multiple sources, fuels, and settings recorded by the TSI SMPS located near the emissions source……33

Figure 4.6. Illustrating the split point determination between GE J-85 and Jing Mini-CAST distributions……34

Figure 4.7. Complete mobility diameter AVL sampling system penetration efficiency using measurements of mobility diameter distributions from two different particle sources compared to the UTRC model calculation……35

Figure 4.8. AVL Sampling System average penetration efficiency for the GE J-85 with 50/50 Camelina and Jet-A Blend Fuel at Idle power setting……..36

Figure 4.9. AVL Sampling System average penetration efficiency for the GE J-85 with Jet-A at Military (Mil) power setting……37

Figure 4.10. AVL Sampling System average penetration efficiency for the Jing Mini-CAST with the NRC Setting……38

Figure 4.11. AVL Sampling System average penetration efficiency for the Jing Mini-CAST with the VARIAnT1 Setting……..39

Figure 4.12. Complete mobility diameter average penetration efficiency for the upstream half of the AVL sampling system using measurements of mobility diameter distributions from two different particle sources compared to the UTRC model calculation……41

Figure 4.13. Upstream half of AVL sampling system average penetration efficiency for the GE J-85 with 50/50 Camelina and Jet-A Blend Fuel at Idle power setting……..43

Figure 4.14. Upstream half of AVL sampling system average penetration efficiency for the GE J-85 with Jet-A at Military (Mil) power setting……...43

Figure 4.15. Upstream half of AVL sampling system average penetration efficiency for the Jing Mini-CAST with the NRC Setting……..44

Figure 4.16. Measured Lognormal mobility diameter distributions produced by multiple sources, fuels, and settings recorded by the AFRL SMPS located at the dilutor one vent……46

Figure 4.17. Complete mobility diameter average penetration efficiency for the downstream half of the AVL sampling system using measurements of mobility diameter distributions from two different particle sources compared to the UTRC model calculation……...46

Figure 4.18. Downstream half of the AVL sampling system average penetration efficiency for the GE J-85 with 50/50 Camelina and Jet-A Blend Fuel at Mil power setting……..48

Figure 4.19. Downstream half of the AVL sampling system average penetration efficiency for the GE J-85 with Jet-A at idle power setting……..48

Figure 4.20. Downstream half of the AVL sampling system average penetration efficiency for the Jing Mini-CAST with the VARIAnT1 Setting……49

Figure 4.21. Complete mobility diameter average penetration efficiency for the MS&T sampling system using measurements of mobility diameter distributions from two different particle sources compared to the UTRC model calculation….51

Figure 4.22. NVFEL SMPS scan on GE J-85 burning Jet-A at a power setting of idle……52

Figure 4.23. MS&T sampling system average penetration efficiency for the GE J-85 with Jet-A at Military (Mil) power setting……54

Figure 4.24. MS&T sampling system average penetration efficiency for the Jing Mini-CAST with the NRC Setting……54

Figure 4.25. Average size dependent penetration data determined from measurements on the Jing Mini-CAST with an NRC setting compared to calculations from the UTRC model……..56

Figure 4.26. The average size dependent penetration curve determined from measurement on the Jing Mini-CAST with a VARIAnT1 setting compared to calculations from the UTRC model……..56

Figure 4.27. NVFEL SMPS mobility diameter distributions measured after the MS&T APC utilizing two settings on the Jing Mini-CAST……57

Figure 4.28. Measured Lognormal mobility diameter distributions produced by multiple sources, fuels, and settings recorded by the UTRC SMPS sampling from the outlet of the UTRC APC……59

Figure 4.29. Complete mobility diameter average penetration efficiency for the UTRC APC using measurements of mobility diameter distributions from two different particle sources compared to the UTRC model calculation……60

Figure 4.30. UTRC APC average penetration efficiency for the GE J-85 with 50/50 Camelina and Jet-A Blend Fuel at Idle power setting……61

Figure 4.31. UTRC APC system average penetration efficiency for the GE J-85 with Jet-A at Military (Mil) power setting……63

Figure 4.32. UTRC APC system average penetration efficiency for the Jing Mini-CAST with the NRC Setting……..63

Figure 4.33. UTRC calculated model penetration efficiencies for both sampling systems……...65

Figure 4.34. UTRC calculated model penetration efficiencies for both APC instruments……..66

Figure 4.35. UTRC calculated model penetration efficiencies for upstream and downstream of the AVL sampling system……67

Figure A.1.1. UTRC APC calibration certification (Page 1 of 2)……....77

Figure A.1.2. UTRC APC calibration certification (Page 2 of 2)……78

Figure A.1.3. UTRC APC calibration points fit to model……79

Figure A.1.4. MS&T APC calibration certification (Page 1 of 2)……80

Figure A.1.5. MS&T APC calibration certification (Page 2 of 2)……81

Figure A.1.6. MS&T APC calibration points fit to model……..82

Figure A.2.1. Day 1 – AEDC, NVFEL, and UTRC SMPS morning calibration results – Group 1……82

Figure A.2.2. Day 1 - AFRL and TSI SMPS morning calibration results – Group 2.....83

Figure A.2.3. Day 2 – AEDC, NVFEL, and UTRC SMPS morning calibration results – Group 1……83

Figure A.2.4. Day 2 - AFRL and TSI SMPS morning calibration results – Group 2…….84

Figure A.2.5. Day 3 – AEDC, NVFEL, and UTRC SMPS morning calibration results – Group 1……84

Figure A.2.6. Day 3 - AFRL and TSI SMPS morning calibration results – Group 2……85

Figure A.3.1. The principle of photoacoustic measurement (A) and the photoacoustic cell design (B) {Ref. 27}……...86

Figure A.3.2. Schematic of APC with key features specific to operation in aircraft engine emissions testing {Ref. 23}……..87

Figure A.3.3. Schematic showing the beam path used for measurement by the LII {Ref. 28}……...88

Figure A.6.1. Upstream half of AVL Sampling System average penetration efficiency for the Jing Mini-CAST with VARIAnT1 Setting……...99

Figure A.6.2. Upstream half of AVL Sampling System average penetration efficiency for the GE J-85 with Jet-A Fuel at idle power setting……...100

Figure A.6.3. Upstream half of AVL Sampling System average penetration efficiency for the GE J-85 with Jet-A Fuel at middle power setting……..…100

Figure A.6.4. Upstream half of AVL Sampling System average penetration efficiency for the GE J-85 with 50/50 Camelina and Jet-A Blend Fuel at middle power setting……101

Figure A.6.5. Upstream half of AVL Sampling System average penetration efficiency for the GE J-85 with Jet-A Fuel at Military power setting……101

Figure A.6.6. Downstream half of AVL Sampling System average penetration efficiency for the Jing Mini-CAST with NRC Setting……..…102

Figure A.6.7. Upstream half of AVL Sampling System average penetration efficiency for the GE J-85 with Jet-A Fuel at middle power setting……..…102

Figure A.6.8. Upstream half of AVL Sampling System average penetration efficiency for the GE J-85 with 50/50 Camelina and Jet-A Blend Fuel at idle power setting……103

Figure A.6.9. Upstream half of AVL Sampling System average penetration efficiency for the GE J-85 with 50/50 Camelina and Jet-A Blend Fuel at middle power setting……103

Figure A.6.10. Upstream half of AVL Sampling System average penetration efficiency for the GE J-85 with Jet-A Fuel at Military power setting……....104

Figure A.6.11. MS&T Sampling System average penetration efficiency for the GE J-85 with Jet-A Fuel at idle power setting……104

Figure A.6.12. MS&T Sampling System average penetration efficiency for the GE J-85 with Jet-A Fuel at middle power setting……..…105

Figure A.6.13. UTRC APC average penetration efficiency for the Jing Mini-CAST with VARIAnT1 Setting……..…105

Figure A.6.14. UTRC APC average penetration efficiency for the GE J-85 with Jet-A Fuel at idle power setting……..106

Figure A.6.15. UTRC APC average penetration efficiency for the GE J-85 with Jet-A Fuel at middle power setting……106

Figure A.6.16. UTRC APC average penetration efficiency for the GE J-85 with 50/50 Camelina and Jet-A Blend Fuel at middle power setting……107

Figure A.6.17. UTRC APC average penetration efficiency for the GE J-85 with 50/50 Camelina and Jet-A Blend Fuel at Military power setting……...107

CHAPTER ONE

INTRODUCTION AND GENERAL INFORMATION

Background

The SAE E-31 Aircraft Engine Gas & Particulate Emissions Measurement Aerospace Recommended Practice (ARP) 6320 {Ref. 17} outlines the requirements for the sampling system, mass and number measurements of non-volatile particle emissions from the exhaust of aircraft gas turbine engines. ARP6320 also provides equations for emission indices calculations for both mass and number, and operator guidance describing how to check, maintain, and operate a non-volatile Particle Matter (nvPM) system in compliance to the ARP6320.

Throughout the creation of the ARP, many tests were conducted to determine the best way to collect and measure non-volatile particulate matter from turbine engines to preserve sample integrity and minimize the losses through the system; including sampling, conditioning, and measurement. Based on the results of these tests, a system was built by Missouri University of Science and Technology (MS&T) which they own and operate. A few other in-house systems were built by other organizations, but it wasn't until Anstalt für Verbrennungskraftmaschinen List (AVL) of Graz, Austria started to produce and manufacture an ARP6320 compliant sampling system that it was commercially available for purchase. The first prototype was delivered to Arnold Engineering Development Complex. Even though the AVL sampling system and the MS&T sampling system are compliant with the ARP6320, there were some differences between the two systems which begged the question, will each system produce the same or similar results? The Environmental Protection Agency (EPA) VAriable Response In Aircraft Non-Volatile Particulate Matter Testing (VARIAnT) 2 was established to answer these questions and more. This thesis will concentrate on a small portion of this test campaign, specifically the ability of the systems to transport non-volatile or carbon black particles to instruments for measurement of mass, number, and size. The ratio of non-volatile particle concentration entering and leaving a sampling and measurement system segment is the Penetration Fraction which is the focus of this thesis.

The Sampling Systems

This section describes the two sampling systems, MS&T and AVL Sampling Systems, which were compared in the VARIAnT2 campaign.

AVL Sample System

The AVL Particle Emission Sampling System was built to the standard described in the SAE E-31 produced document ARP6320. The AVL design automated the sample system and conditions the exhaust from turbine engines. The AVL System provides continuous sample to the AVL Micro Soot Sensor (MSS) or Artium Technologies Inc. Laser Induced Incandescence (LII) for particle mass measurements, AVL Particle Counter (APC) for particle number measurements, and other instruments utilizing splitters may be connected to the sample system's auxiliary port only limited by the max flow rate, for all connected instruments, of 25 Lpm. The MSS, LII, and APC are described in more detail in Appendix 3.

Turbine engine exhaust is continually collected using an intrusive probe, shown in Section 1 of Fig. 1.1. The sample is routed through carbon impregnated polytetrafluoroethylene (PTFE) lines or stainless steel lines to minimize losses to the Front End Box of the AVL system, shown in section 2 of Fig. 1.1. Entering the front end box is a splitter. This splitter provides sample in 3 directions: Gas Line (GL) port, Particle Transport System (PTS), and an atmospheric vent to relieve any excess pressure. The GL port provides samples to an optional gas measurement suite. The Front End Box, section 2 in Fig. 1.1., regulates the pressure to ensure it is near atmospheric pressure by the use of a variable bypass valve. This box is designed to drop the temperature of the sample from 160 ºC to 60 ºC by adding a 10:1 dilution of nitrogen through the use of a Dekati Dilutor, Dilutor1 in Fig. 1.1. The sample is maintained at 60 ºC using heaters throughout the rest of the system. The sample is transported through a 25 meter carbon impregnated PTFE line, shown in section 3 of Fig. 1.1., from the front end box to the back end box, shown in sections 4 & 5 of Fig. 1.1. When the sample reaches the back end box, the sample flows through a cyclone separator to remove particles with diameters greater than 1.0 µm. The cyclone has a 50% penetration at 1.0 µm ± 0.1 µm. The sample is then split into 4 directions: MSS sample port (nvPM Mass Instrument in Fig. 1.1.), APC Sample Port (Consists of a dilution system, a VPR and nvPM Number Instrument from Fig. 1.1.), Auxiliary Sample Port (not shown in Fig. 1.1. but is off splitter 2), and Make-up Flow Port. The Make-up Flow Port provides make up flow to ensure the flow rate through the 25 meter line is 25 Lpm as is specified in AIR6241. The sample flow through the sample line, section 3 in Fig. 1.1., is determined by manually measuring the inlet flow of all attached instruments and subtracting this number from the ARP6320 specified 25 Lpm. The remaining flow that is required to achieve the 25 Lpm flow rate through section 3 is accomplished by controlling the mass flow controller in the Make-up Flow line. A CO_2 measurement, Diluted CO_2 in Fig. 1.1., is performed also pulled off the Make-up Flow line. This Diluted CO_2 measurement is compared with the GL CO_2 measurement to determine the Dilution Factor of the Dekati Dilutor, Dilutor 1 in Fig. 1.1. The other connections shown in Fig. 1.1. are self-explanatory. The Auxiliary Port, which is not shown in

Fig. 1.1. because it is not a requirement of the ARP6320 but is allowed, is found on the AVL Sample System and allows for the connection of other instruments to be connected. In this case, other instruments were needed and are explained in the setup section.

MS&T Sample System

The MS&T Sample system was one of the first sample systems built to the ARP6320 standard. This sample system is commonly referred to as the North American Reference system. There are cosmetic differences between the MS&T and AVL sampling systems, but the only difference in the sampling system control is a proportional valve in the front end box of the AVL system that is used to regulate the pressure at the inlet of the Dekati Diluter, Pressure control valve in Fig. 1.1. The MS&T system uses a manual vent valve to maintain a near ambient pressure at the Dekati Diluter inlet. Also, the MS&T system regulates the sample flow through section 3 of Fig. 1.1 based on the pressure differential between the inlet and the exit of section 3. Based on this pressure differential, the system will adjust the Make-up flow using the mass flow controller to ensure the required 25 Lpm.

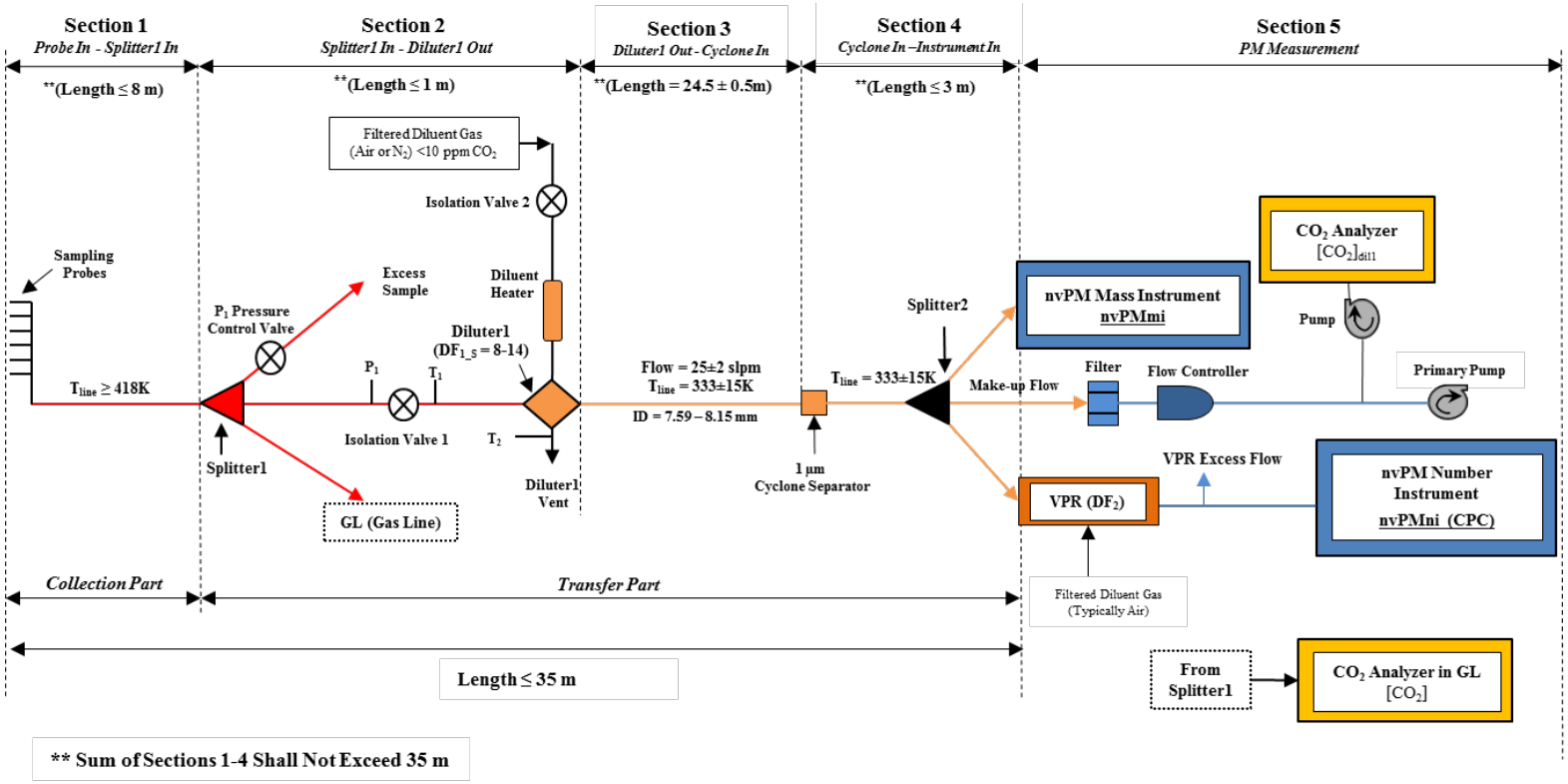

Figure 1.1. Diagram of any nvPM sampling and measurement system as defined in ARP6320 {Ref. 17} and AIR6241 {Ref. 18}.

CHAPTER TWO

LITERATURE REVIEW

Non-Volatile Particle Matter (nvPM) emissions from turbine engines have size diameters (also known as mobility diameter) for these type of particles ranging from 6 to 212 nm. Inherent with the small size of these particles, losses occur in the sampling system which is utilized to transport the particles to the measurement instruments. This chapter discusses these losses and the mechanisms around which they occur. It also discusses a theoretical model which is recommended by the AIR6241 to account for these losses in the ARP6320 prescribed sampling system in place of measuring these losses. The comparison of the theoretical model and the actual measurements is the concentration of this thesis.

Non-Volatile Particle Loss Theory and Models

Particles deposit on the wall of the sampling system due to many different physical mechanisms which change the velocity and direction of travel of the particle. The types of losses of primary significance in sampling from current turbojet and turbo fan engine exhaust are:

1. Thermophoretic – Occurs when the walls of the sample line have a lower temperature than the sample flowing through the line producing a thermal gradient across the flow. {Ref. 24}.
2. Diffusiophoresis – Also known as diffusional losses, occurs when aerosol particles suspended in a non-uniform, but isothermal gas mixture move due to existing concentration gradients. {Ref. 24}.
3. Inertial – Occurs in bends where the flow is redirected from a straight path. The particles impact the walls of the tube and are sometimes unable to move away from that wall. {Ref. 26}
4. Electrostatic – When particles become electrically charged they can be attracted to the walls and once on the surface the electrical resistance can prohibit the particles from moving down stream. This creates an electrostatic loss. {Ref. 26}

Due to the high temperature of turbine exhaust (~600 °C and up), the small particle size, and the length of sampling systems, the overall nvPM losses can be significant ranging from 50%-90%, seen in the results section of this thesis. To quantify and correct for these losses in each of the AVL and MS&T sampling systems, both the size dependent penetration functions and the size distribution of the particles need to be known.

Most particle size distributions are lognormal and are not mono-disperse. This is due to the particles being formed using a stochastic process. Based on a large number of measurements of different engine types {Ref. 3 - 14}, the size distribution width (geometric standard deviation) has been fairly well defined within the range of 10 nm to 100 nm.

The ARP 6320 only requires nvPM mass and number concentration measurements and the quantification of the dilution factors. A size measurement is not required. This presents a difficulty when calculating losses and correcting for them through the sample system because losses are size dependent. SAE has developed a method, described in AIR 6504 to estimate the size from a ratio of the mass and number. This thesis only concentrates on the nvPM particle penetration efficiencies when compared to the measured geometric size distribution and number measurements made by SMPS instruments.

UTRC Line Loss Model

The United Technologies Research Center (UTRC) developed a Line Loss Model in 2008 to predict the particle penetration performance of various sampling line configurations {Ref. 24}. The tool predicts particle transport as a function of particle size and assumes steady state flow. The tool calculates particle losses using standard equations from Yook and Pui {Ref. 14} and Willeke and Baron {Ref. 15}, but simplifies these equations by combining the effect of up to four different particle loss mechanisms. These four particle loss mechanisms described above consist of: diffusional, inertial, thermophoretic, and electrostatic. For steady state engine operation conditions, the expressions given for penetration efficiencies due to each specific loss mechanism are under conditions assumed to also be steady. This means a single factor will result for a single physical loss mechanism within a single segment of sample line of constant wall temperature and diameter. This allows the sample line to be divided into sections enabling a simpler method for the integration over the entire sample line. The UTRC Line Loss Model allows for up to 10 different sample line segments.

The UTRC Model predicts size dependent penetration efficiencies based on the sample line geometry, characteristics of the flow, pressure, and temperature. Table A.8.1. in Appendix 8, defines the required input parameters for the UTRC Model. Assuming the exhaust sample carrier gas can be approximated by standard ambient air properties, Table A.8.2. in Appendix 8 is utilized in the UTRC Model for the carrier gas of the particles and particle properties. These assumptions and estimates were agreed upon by the SAE E-31 technical committee. Even though these calculations are valid up to 10,000 nm, the size range is cut at 212 nm for this thesis because of the particles observed were below 212 nm.

The UTRC calculated penetration efficiency model will output values between zero and one, one meaning 100% of all particles at that specific mobility diameter has passed through the line segment of interest. An example of the UTRC calculated penetration efficiency model output for the AVL sampling system is shown in Fig. 2.1.

Note: The UTRC Model does not account for coagulation which can affect nvPM number and size in some Cases. However; coagulation was not observed during this test campaign based on the relatively high flow rates and low concentrations.

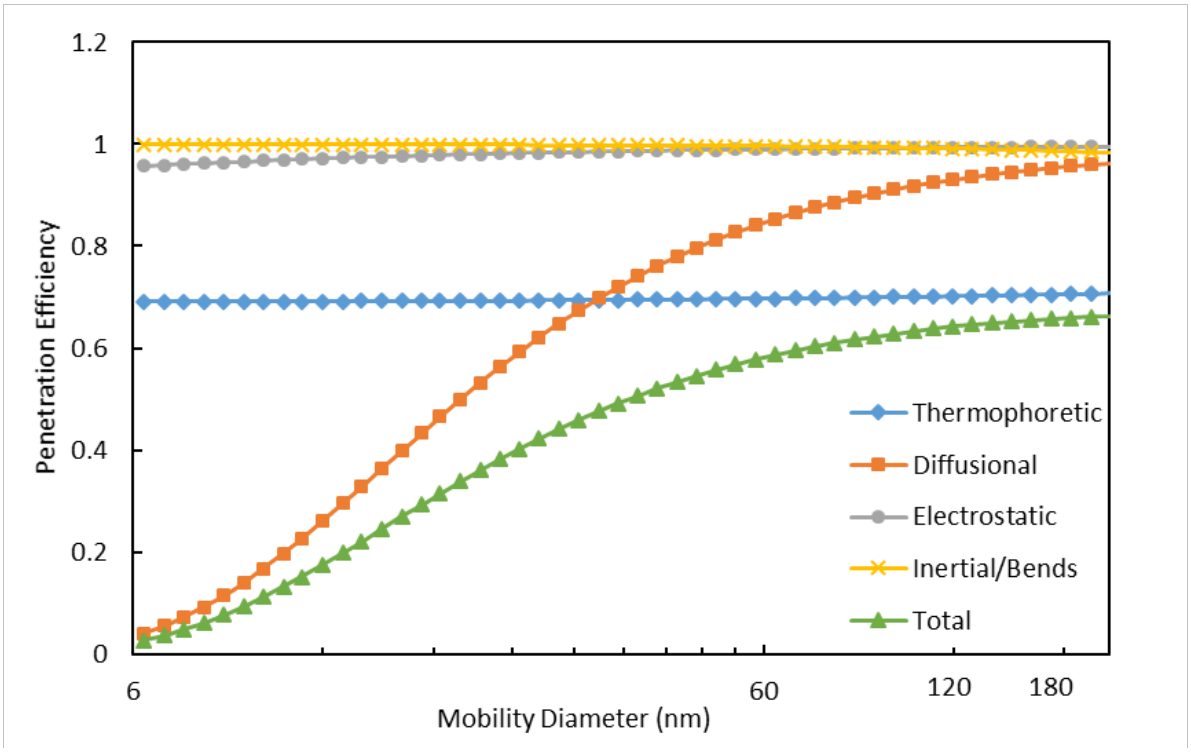

Figure 2.1. UTRC calculated penetration efficiency model output for the AVL sampling system.

Segment Calculations

Each section of the sampling system described above has a loss of particles through the ARP6320 prescribed sampling system which is dependent on the mobility diameter of the particle, D_m. The fraction of particles that remains (Penetration Efficiency, η) in each segment, i, and continues to travel through the sampling system is calculated and described in this section. The segment, i, in this section is a subset of the entire sampling system which again is sections one through four shown in Fig. 1.1. This is needed for some of the sections which are very complex. Breaking them down to smaller segments simplifies the

penetration efficiency calculations that are described below. All the calculations apply to the entire sampling section and are calculated by the UTRC model for each specified segment.

Penetration Efficiencies due to only diffusional losses, $\eta_{difi}(D_m)$, i=1, 2, .., 10

Diffusiophoresis losses, also known as diffusional losses, occur when aerosol particles suspended in a non-uniform but isothermal gas mixture move due to existing concentration gradients. {Ref. 24} The gradients in concentration occur when particles move towards the walls of the tube, in this case, and deposit on the walls due to mostly friction. Diffusional losses are modeled with standard models of particle diffusion in a turbulent flow which holds true for all sampling system sections up to the instrument inlets. Diffusional losses are calculated using the following equation {Ref. 16}

$$\eta_{difi}(D_m) = e^{\frac{-\pi ID_i L_i V_{d,diff}}{Q_i}} \qquad \text{Equation 2.1}$$

where, ID_i and L_i are the sampling line inner diameter (cm) and length (cm), respectively, $V_{d,diff}$ is the deposition speed and Q_i is the gas flow in the ith sampling line segment. {Ref. 16}

$$V_{d,diff} = 0.0118 \cdot Re^{\frac{7}{8}} \cdot Sc^{\frac{1}{3}} \cdot D/ID_i \qquad \text{Equation 2.2}$$

where Re is the Reynolds number, {Ref. 16}

$$Re = u_m \times \frac{\rho_{gas} \times ID_i}{\mu} = \left(\frac{4 \times Q_i}{\pi \times ID_i^2}\right) \times \frac{\rho_{gas} \times ID_i}{\mu} = \frac{4 \times Q_i \times \rho_{gas}}{\pi \times ID_i \times \mu} \qquad \text{Equation 2.3}$$

Sc is the Schmidt number, {Ref. 16}

$$Sc = \frac{\mu}{\rho_{gas} \times D} \qquad \text{Equation 2.4}$$

D is the diffusion coefficient, {Ref. 16}

$$D = \frac{k_B \times T_{gasi} \times C_c}{3 \times \pi \times \mu \times D_m} \qquad \text{Equation 2.5}$$

In these latter equations k_B (=1.38x10^{-16} g·cm^2/s^2) is the Boltzmann constant, ρ_{gas} is the carrier gas density, ρ is the particle density, T_{gasi} is in Kelvin, μ is the gas viscosity, {Ref. 16}

$$\mu = \mu_0 \times \left(\frac{T_{gasi}}{T_0}\right)^{3/2} \times \left(\frac{T_0 + 110.4}{T_{gasi} + 110.4}\right) \qquad \text{Equation 2.6}$$

where μ_0 = 1.83 x 10^{-4} g/(cm•s), T_0=296.15K, T_{gasi} is in Kelvin, and C_c is the Cunningham slip correction factor, {Ref. 16}

$$C_c = 1 + \frac{2\lambda}{D_m} \times (1.165 + 0.483 \times e^{-\frac{0.997 D_m}{2\lambda}}) \quad \text{Equation 2.7}$$

where λ is the carrier gas mean free path.

Penetration Efficiencies due to only inertial particle losses, $\eta_{bi}(D_m)$

Inertial particle losses occur in bends where the flow is redirected from a straight path. The losses are not dependent on just the bend angle but also the sum of the bend angles in a sampling system segment. Particles that cannot make the turn in the flow stream impinge on the wall of the tube in the bends.
Inertial losses, unlike diffusional losses, depend on the flow characteristics, especially whether the flow is laminar or turbulent. For clarity, we the SAE E-31 committee assumes laminar flow at a Reynolds number (Re) of 5000 or less and anything above is considered turbulent flow. For Laminar flow the penetration due to bends in the transport lines are calculated by {Ref. 16}

$$\eta_{\mathrm{bi}}(D_m) = 1 - 0.01745 \times Stk \times \theta_{bi} \quad \text{Equation 2.8}$$

For turbulent flow the penetration due to bends in the sample lines are calculated by {Ref. 16}

$$\eta_{bi}(D_m) = e^{-0.04927 \times Stk \times \theta_{bi}} \quad \text{Equation 2.9}$$

where θ_{bi} is the total angle of bends in the ith segment of the sampling line in degrees, and Stk is the dimensional Stokes number, {Ref. 16}

$$Stk = \frac{Q_i \times C_c \times \rho \times D_m^2 \times 10^{-3}}{27 \times \pi \times \mu \times ID_i^3} \quad \text{Equation 2.10}$$

Where Q_i is the gas flow in the ith sampling line segment, C_c is the Cunningham slip correction factor, ρ is the assumed nvPM effective density, 1 g/cm^3, D_m is the discrete particle size, μ is the carrier gas viscosity, and the ID_i is the Inner diameter of the ith segment of the sampling line.

Penetration Efficiency due only to Thermophoresis, $\eta_{thermoi}$

This loss occurs when the walls of the sample line have a lower temperature than the sample flowing through the line producing a thermal gradient across the flow. {Ref. 24} Therefore, the thermophoretic expression that is used depends on sample system segment gas temperature, T_{gasi}, and sampling system segment wall temperature, T_{linei}. This also assumes that for a given sampling system, the particle and gas properties are constant. As shown in the system diagram in Fig.

1.1., the sample lines are sufficiently long to allow the gas and particles to thermally equilibrate with the sampling wall temperature. This means the place where two connecting segments meet that differ in temperature is the only place where thermophoretic losses will take place. Hence, the thermophoretic loss will take place in the downstream segment and the sample will eventually reach equilibrium with the wall temperature. The only exception to this is where the sample enters the sampling system. The equation utilized by the UTRC model for penetration efficiencies due only to thermophoretic losses is as follows: {Refs. 5, 13, 14}

$$\eta_{thermoi} = \left[\frac{T_{linei}}{T_{gasi}}\right]^{Pr\times K_{th}} \cdot \left[1 + \left(\frac{T_{gasi}}{T_{linei}} - 1\right) e^{-\frac{\pi\times ID_i\times h_{gas}\times L_i}{\rho_{gas}\times Q_i\times C_p}}\right]^{Pr\times K_{th}} \qquad \text{Equation 2.11}$$

where T_{gasi} is the sample gas temperature in Kelvin, T_{linei} is the sample line wall temperature in Kelvin, ID_i is the line inner diameter, h_{gas} is the carrier gas convective heat transfer coefficient, L_i is the line length, ρ_{gas} is the carrier gas density, Q_i is the gas flow, C_p is the constant pressure carrier gas specific heat, Pr is the Prandtl number, and K_{th} is the thermophoretic coefficient, {Refs. 5, 13, 14}

$$K_{th} = \frac{2\times C_s\times C_c}{1+3\times C_m\times K_n}\left[2 + \frac{1}{\left({k_{gas}}/{k_p}\right)+C_t\times K_n}\right]^{-1} \qquad \text{Equation 2.12}$$

where C_s (= 1.17) is the slip coefficient, C_c is the Cunningham slip correction factor, C_m is the soot momentum, C_t is the thermal coefficient, k_{gas} is the thermal conductivity of the suspending gas, K_n(=2/λD_m) is the Knudsen number, λ is the carrier gas mean free path, and k_p is the particle thermal conductivity.
In section 1 of the sampling system, where most of the thermophoretic effect occurs, the above equation has shown {Refs. 20, 21, 25} to simplify to

$$\eta_{thermoi} \approx \left[\frac{T_{exit}}{T_{in}}\right]^{constant} \qquad \text{Equation 2.13}$$

where T_{in} is the temperature of the gas entering the sampling line which is approximately the engine exhaust temperature, T_{EGT}, i.e., $T_{in} \approx T_{EGT}$. T_{exit} is the equilibrated sample particulate and gas temperature which is approximately the temperature of the sampling line wall (the diluter inlet wall temperature, T1), $T_{exit} \approx T_{wall}$=T1=433.15K (specified in ARP6320), and the exponential constant is equal to 0.38 {Refs. 20 and 21}. Hence, the thermophoretic penetration fractions for segment 1 and 2 (probe to inlet of dilutor) are assumed to follow {Ref. 20, 21, 25}

$$\eta_{thermoi} = \left(\frac{T1}{T_{EGT}}\right)^{0.38} \qquad \text{Equation 2.14}$$

where T1 = 433.15K or the actual measured diluter inlet wall temperature, T1 and T_{EGT} is the engine exhaust gas temperature (in Kelvin). Note that if $T_{EGT} \leq T1$, then $\eta_{thermoi}=1$.

Electrostatic Penetration Efficiencies, $\eta_{eleci}(D_m)$

This loss occurs when electrically charged particles set up an electrostatic charge on sample line walls resulting in the creation of electrical fields. The electrical fields will interact with other charged particles resulting in perturbations in the flow stream that drive particles to the wall, thus creating losses. In the ARP 6320 prescribed sampling system all lines must be made of electrically conductive tubing (Carbon impregnated PTFE) or stainless steel tubing. The lines are electrically grounded to minimize this loss mechanism but is still accounted for by the UTRC penetration efficiency model. The penetration efficiency accounting only for electrostatic losses is calculated by the UTRC penetration efficiency model as follows: {Ref. 24}

$$\eta_{eleci}(D_m) = 1 - \left(\frac{C^2 \times L_i \times C_c}{\pi \times \varepsilon \times \mu \times D_m \times 10^{-7} \times ID_i \times Q_i}\right)^{1/3} \qquad \text{Equation 2.15}$$

where C is the Coulombic charge for a proton, 1.6E-19 C, L_i is the line length of the ith segment of line, C_c is the Cunningham slip correction factor, $\boldsymbol{\varepsilon}$ is the electrical permittivity of the particles through the sample lines, 8.85E-21 C2s2/g/cm^3, μ is the carrier gas viscosity, D_m is the particle mobility diameter, ID_i is the inner diameter of the ith segment of sampling line, and Q_i is the gas flow rate in the ith sampling line segment.

Diluter1 Penetration Efficiencies, $\eta_{dil}(D_m)$

A constant diluter1 penetration, $\eta_{dil}(D_m) = 1$ should be used for all particle sizes {Ref. 21}.

Splitter Penetration Efficiencies, $\eta_{spl}(D_m)$

Losses due to bends are calculated above, therefore splitters are treated as a straight tube and the penetration is constant, $\eta_{spl}(D_m) = 1$ and should be used for all sizes of particles. Any losses due to the flow changing direction should be included in the loss calculations due to bends.

Cyclone Separator Penetration Efficiencies, $\eta_{cyc}(D_m)$

The cyclone separator sharpness (the ratio of the particle aerodynamic diameter at 16% penetration, D_{16}, to the particle aerodynamic diameter at 84% penetration, D_{84}, i.e., $(D_{16}/D_{84})^{0.5}$) and its particle aerodynamic diameter at the

50% penetration point, D_{50}, were determined during commissioning of each of the sampling systems. Using the D_{50} and the Cyclone separator sharpness the following equation {Ref. 17} is utilized to calculate the cyclone penetration function.

$$\eta_{cyc}(D_m) = 1 - \int_{x>0}^{D_m} \frac{e^{-\frac{(\ln x - \mu_{cyc})^2}{2\sigma_{cyc}^2}}}{x\sigma_{cyc}\sqrt{2\pi}}\, dx \qquad \text{Equation 2.16}$$

where $\mu_{cyc}=\ln(D_{50})$ and $\sigma_{cyc}=\ln\{(D_{16}/D_{84})^{0.5}\}$.

AVL Particle Counter (APC) Penetration Efficiencies, $\eta_{APC}(D_m)$

The AVL Particle Counter (APC) (described in depth in Appendix 3) is an instrument connected to both the MS&T sampling system and the AVL sampling system to measure number of non-volatile particles. The APC consists of 3 main parts which effect the penetration efficiency the most: two stage dilution system, volatile particle remover (VPR), and the Condensation Particle Counter (CPC). Due to the way the CPC grows the particles and other loss factors, this thesis bypassed the CPC for simplicity. To avoid the losses in the CPC, the downstream SMPS instruments were connected to a port on the APC that supplied sample after the VPR and two stage dilution system but before the CPC. This means the SMPS instruments that are measuring the concentration upstream and downstream of the APC only measured the difference in the particles per mobility diameter between the inlet of the APC and after the two stage dilution system and VPR. It is assumed that the inertial and diffusional losses that occur in the APC, excluding VRP and two stage dilution system, are negligible, thus,

$$\eta_{APC}(D_m) = \eta_{VPR}(D_m) * \eta_{2Dil}(D_m) \qquad \text{Equation 2.17}$$

where, $\eta_{VPR}(D_m)$ are the penetration efficiencies per mobility diameter for the VPR, and $\eta_{2Dil}(D_m)$ are the penetration efficiencies per mobility diameter for the two stage dilution.

Note: The penetration efficiencies through the two stage dilution is a very complexed calculation and requires advanced calculations to determine. For this reason the penetration efficiencies for the APC must be must be experimentally measured. Appendix 1 shows the APC Calibration results for both the UTRC APC and the MS&T APC. The penetration efficiencies through the VPR are also included in this calibration.

Total Penetration Efficiencies, $\eta_{total}(D_m)$

The total penetration is the product of all the penetration functions multiplied together at each particulate mobility diameter size, D_m. However, not all of the above penetration efficiencies pertain to the sampling system. The APC penetration efficiencies only matters when trying to determine penetration efficiencies through the APC, which again is a number counting instrument attached to the sampling system. Therefore the total penetration efficiency for the sampling system is:

$$\eta_{totalslp}(D_m) = \eta_{difi}(D_m) \; x \; \eta_{bi}(D_m) \; x \; \eta_{thermoi} \; x \; \eta_{eleci}(D_m) \; x \; \eta_{dil}(D_m) \; x \; \eta_{spl}(D_m) \; x \; \eta_{cyc}(D_m)$$

Equation 2.18

The total penetration efficiency including the penetration efficiencies through the AVL Particle Counter (APC) is:

$$\eta_{total}(D_m) = \eta_{totalslp}(D_m) \; x \; \eta_{APC}(D_m) \qquad \text{Equation 2.19}$$

CHAPTER THREE

VARIANT2 PENETRATION TESTING

Instrumentation

Scanning Mobility Particle Sizers

The primary instruments utilized to measure size dependent concentration in various locations of the described sampling systems were TSI Scanning Mobility Particle Sizers (SMPS). The SMPS consists of 3 primary parts: particle charger/neutralizer, a differential mobility analyzer (DMA) and a condensation particle counter (CPC). The sample passes through the neutralizer, which in this experiment was Po-210, Fig. 3.1. The radioactive source provides a steady and known charge distribution to the particles as they pass by. Within the DMA the charged aerosol is pulled across a layer of clean air by an applied electric field while flowing down the length of the annular gap between two concentric tubes. Particles of different electric mobilities follow different paths, and the DMA selects only that fraction of positively charged particles having electric mobilities within a narrow window. This is the reason, within this thesis, that the particle size is also referred to as mobility diameter. Most of the selected particles will have one positive charge with a relatively small fraction having two (or more) positive charges, which the SMPS accounts for by a correction factor. The CPC then counts the number of the selected particles by enlarging the particles. Butanol vapor condenses on the particles, in turn growing the particle large enough for the laser beam and optics to see individual particles. The SMPS instruments were set up to scan the desired size range within a period of three minutes. Theoretical relationships developed by TSI are used to convert from scan time to electric mobility to particle diameter. Knowledge of the charge distribution is used to convert measured concentrations of charged particles to total concentration at each particle size. The SMPS then reports a size distribution with a resolution of 32 channels per decade of particle diameter over the size range of interest from 6 nm to 212 nm.



Figure 3.1. Po-210 aerosol neutralizer strips and cartridge holder.

Non-Volatile Particle Sources

For EPA VARIAnT2, two sources of particles were utilized: the combustion products of Jing Mini-Combustion Aerosol Standard (Jing Mini-CAST) and a General Electric (GE) J-85 turbine engine.

Jing Mini-CAST

In the Jing Mini-CAST burner, soot particles are formed within a co-flow diffusion flame due to the hydrocarbon pyrolosis that takes place as a consequence of the heat provided by the oxidation at the flame front. The CAST burner enables the soot particles to escape from the flame without contact with oxygen. Subsequently the particle stream is mixed with a quenching gas in order to prevent further combustion processes in the particle stream and to stabilize the soot particles. The quenching inhibits condensation in the particle stream at ambient air condition. To dilute the particle stream, compressed air is supplied to the quenched particle stream. {Ref 1}

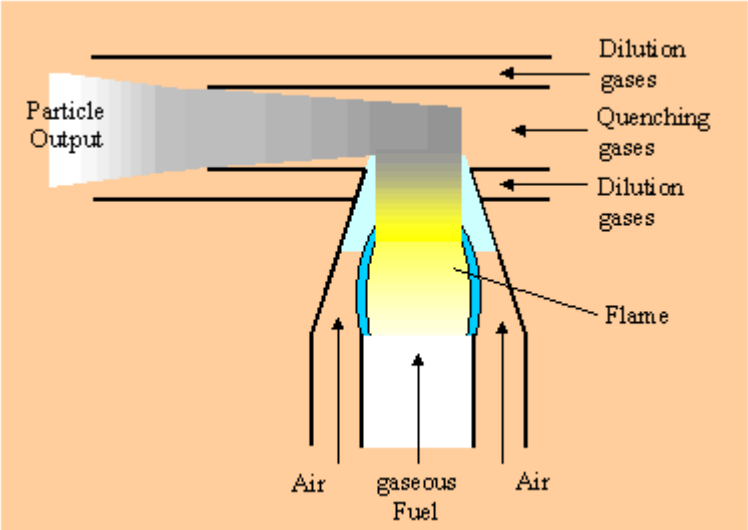

Figure 3.2. Jing Mini-CAST principle {Ref 1}.

Referring to Fig. 3.2., the gaseous fuel utilized for this CAST burner was propane, the air was dry shop compressed air, and the dilution/quenching gas was compressed nitrogen. Two specific settings were utilized for this experiment: the NRC Setting and the VARIAnT1 Setting. These settings are specific combinations shown in Table 3.1. These settings have nothing to do with the concentration that was observed from this source, because additional dilution in the form of compressed nitrogen was added downstream to occur various

concentrations. Only the data with acceptable concentrations were utilized in this thesis.

Table 3.1. Jing Mini-CAST Settings utilized during VARIAnT2 Test Campaign.

Gases	NRC Setting	VARIAnT1 Setting
Gaseous Fuel (Propane)	53 ml/min	60 ml/min
Downstream Dilution (nitrogen)	0 ml/min	250 ml/min
Air (Clean/Dry Compressed Air)	1.60 Lpm	1.5 Lpm
Dilution Gas (nitrogen)	20 Lpm	10 Lpm
Quenching Gas (nitrogen)	7.0 Lpm	3 Lpm

General Electric J85 Engine with Afterburner

The GE J85 is a 2850 – 3100 lbf max thrust (dry) turbojet engine and first entered service in 1960. Originally ordered by the U.S. Air Force strictly for the ADM-20 Quail, the J85 quickly found applications in other light-jet applications including the supersonic Northrop F-5/T-38 family. Over 13,500 J85s and 2,000 commercial CJ610s have been produced. {Ref. 2} This engine is located at the Propulsion Research Facility (PRF) at the University of Tennessee Space Institute (UTSI). The J85 is owned by Arnold Engineering Development Complex (AEDC) which is a U.S. Air Force organization. The engine is operated with collaboration between UTSI and AEDC. Three specific thrust settings were utilized for this test: idle, middle power, and Military (Mil) power. Military power is the highest thrust setting without activating the afterburner capability and the middle power is approximately midway between idle and Mil power. The afterburner was not used for this VARIAnT2 Test.

Testing

Data Collection

During testing, many other parameters were collected to fully characterize the system but are not discussed in this thesis. The parameters that were collected and utilized in this thesis are listed in Appendix 5. All AVL data were collected utilizing custom built, AVL proprietary software. MS&T sampling system control and data acquisition utilized National Instruments LabVIEW software. Data acquisition for the SMPS instruments utilized the TSI Aerosol Instrument Manager (A.I.M.) version 10 for TSI SMPS (Model Number: 3938) and version 9 for all others (Model Numbers: 3936 or older). Version 10 is not compatible with SMPS instruments with model numbers of 3936 or older. Data export utilized

version 10 exclusively. Details of the instrumentation configuration are provided in Appendix 4.

Test setup and Description

For testing, Scanning Mobility Particle Sizer (SMPS) instruments were utilized at various locations to determine the losses throughout the two sampling systems. Table A.4.1, Instrumentation Configuration, in Appendix 4 lists the configuration and specification of the SMPS instruments. Figure 3.3. below illustrates the locations of SMPS instruments, highlighted in green circles. This configuration accomplishes the simultaneous loss measurements of the following:

AVL Sampling System Penetration Efficiencies

When referring to the AVL Sampling System it is meant the point at which the sample enters the probe tip (TSI SMPS), downstream to the inlet of the mass or number instrument (AEDC SMPS) as illustrated in Fig. 3.3. Due to the high concentrations, pressures and temperatures produced by the GE J-85 (greater than ambient pressure and temperatures which are required for proper sampling), it was not possible to sample directly from the probe tip. A pressure relief valve and a diluter was utilized before the “TSI SMPS” as illustrated in Fig. 3.4. to reduce the pressures, temperatures, and concentrations to acceptable levels. Due to the extra hardware that was needed during engine tests, a true measurement of the penetration efficiencies of this sample system was not possible. To account for extra hardware before the TSI SMPS, the UTRC modeled penetration efficiency was calculated and utilized to determine the probe tip concentration per mobility diameter. The same hardware that was utilized for the GE J-85 engine was also utilized for the Jing Mini-CAST to simplify the setup. The ratio of these lognormal concentration vs. mobility diameter measurements from the SMPS instruments produce the penetration efficiencies for this sampling system. The final determination of the penetration efficiencies take into account the variability in SMPS instruments determined during the daily checks/calibrations (described in the next section), and any amount of sample line utilized between the SMPS and the point of interest.

Upstream Half of AVL Sample System Penetration Efficiencies

The AVL Sampling system had another SMPS instrument labeled “Air Force Research Laboratory (AFRL) SMPS” which sampled from the AVL Diluter 1 dump. This divided the sample system into two halves and allowed for a penetration efficiency measurement to be calculated for a segment of the sample system. This half is from the probe tip SMPS (TSI SMPS) mentioned above and

the AFRL SMPS. This portion of the system will account for most if not all of the thermophoretic losses in the system. Again the ratio of these lognormal concentration vs. mobility diameter measurements produces the penetration efficiency. Also, taking into account the variability in SMPS instruments determined during the daily checks/calibrations, and any amount of sample line utilized between the SMPS and the point of interest.

Downstream Half of AVL Sample System Penetration Efficiencies

This half of the AVL Sample System accounts for the section of sample line between the AFRL SMPS and the AEDC SMPS illustrated in Fig. 3.3. This half of the sample system, because of the long sample lines, accounts for most of the diffusional losses in the sampling system. Again the ratio of these lognormal concentration vs. mobility diameter measurements produces the penetration efficiency. Also, taking into account the variability in SMPS instruments determined during the daily checks/calibrations, and any amount of sample line utilized between the SMPS and the point of interest.

MS&T Sampling System Penetration Efficiencies

When referring to the MS&T Sampling System it is meant the point at which the sample enters the probe tip (TSI SMPS), downstream to the inlet of the mass or number instruments, in this case the National Risk Management Research Laboratory (NRMRL) SMPS, as illustrated in Fig. 3.3. Again the ratio of these lognormal concentration vs. mobility diameter measurements produces the penetration efficiency. Also, taking into account the variability in SMPS instruments determined during the daily checks/calibrations, and any amount of sample line utilized between the SMPS and the point of interest.

APC Penetration Measurement

SMPS instruments were placed before and after the APC instruments on the AVL Sampling System (AEDC SMPS and UTRC SMPS respectively) and the MS&T Sampling System (NRMRL SMPS and NVFEL SMPS respectively). Again the ratio of these lognormal concentration vs. mobility diameter measurements produces the penetration efficiency. Also, taking into account the variability in SMPS instruments determined during the daily checks/calibrations, and any amount of sample line utilized between the SMPS and the point of interest. This measurement was performed on both sampling systems because the penetration curves through the different VPR/dilution system of the APCs were different as shown in the calibration sheets attached in Appendix 1.

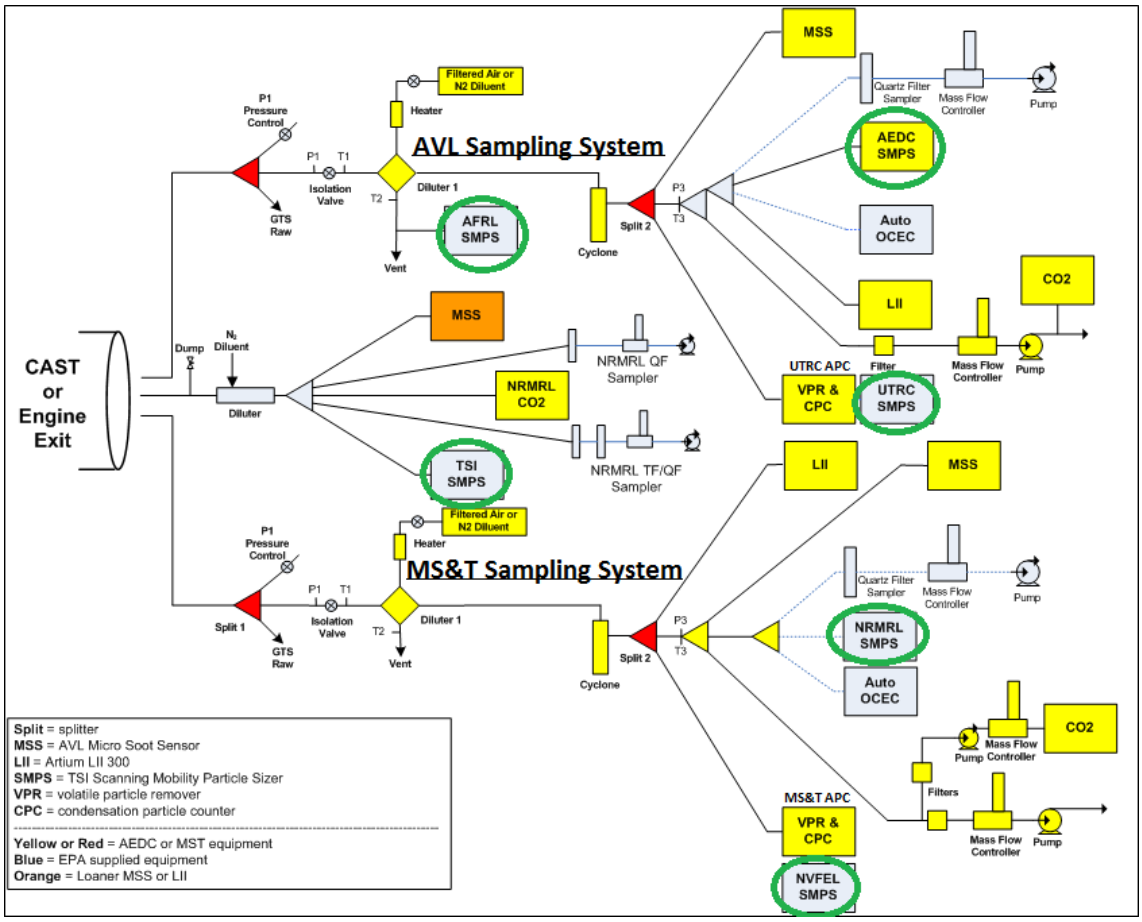

Figure 3.3. Configuration for penetration efficiency measurements.

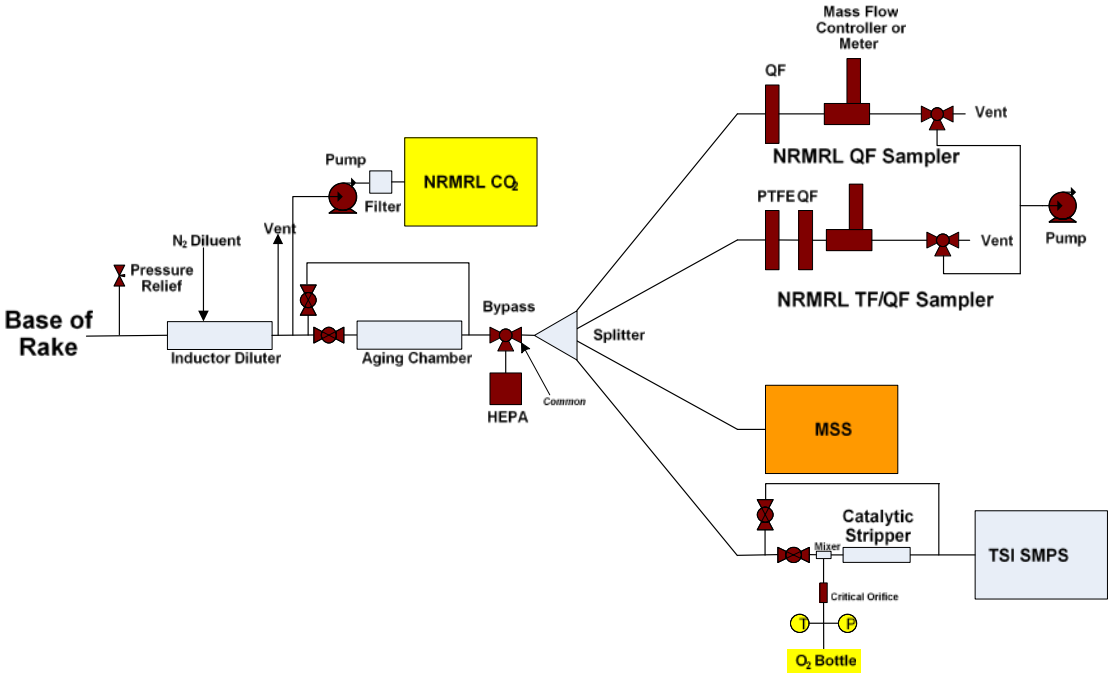

Figure 3.4. Near source sampling system.

SMPS Functionality Checks

Lab Functionality Check

Before testing started, all SMPS instruments were sent to the University of Minnesota (UoM) for calibration and functionality check. While at the UoM, the instruments were evaluated individually for deficiencies and were corrected/repaired if required. The instruments were simultaneously compared on various sources including a diesel engine. This testing what not performed by the author and will be described in future papers presented by UoM. The results, Figs. 3.5. – 3.6., show a max deviation between SMPS instruments of about 11% which is within the 14% measurement uncertainties provided by TSI.

SMPS Pre and Post Campaign Checks

At the beginning and end of the test campaign each SMPS was verified to be operating properly and consistently. This was accomplished by a zero test and a size distribution test. The zero test was accomplished by attaching a HEPA-filter to the inlet of each SMPS and verifying the instrument measured zero particles within the uncertainty of the instrument. The size distribution test was accomplished by using dioctyl sebacate (DOS), sodium chloride (NaCl) particles generated with an atomizer seen in Fig. 3.7. The test setup for the size distribution test is shown in Fig. 3.8. Plots of these checks are shown in Appendix 2. The plots in Appendix 2 illistrate the deviations in the SMPS instruments, which is compensated for throughout this thesis.

SMPS Daily Checks

Each morning before testing started, The SMPS instruments were verified for operation and consistency using the DOS particles and procedure described in the post campaign checks above. For daily testing, simultaneous sampling was not feasible due to the locations of the instruments but results were comparable and are shown in Appendix 2. An issue with the NRMRL SMPS was discovered in the daily checks early in the test campaign and it was removed from operation for repair. This is discussed more in the test results section.

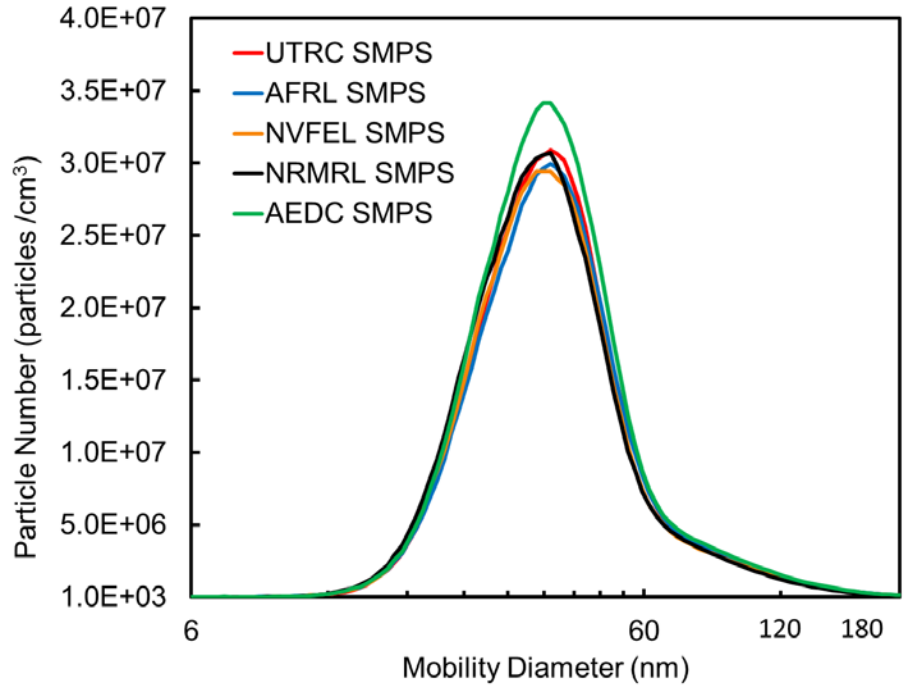

Figure 3.5. Test 1 calibration results during the UoM testing.

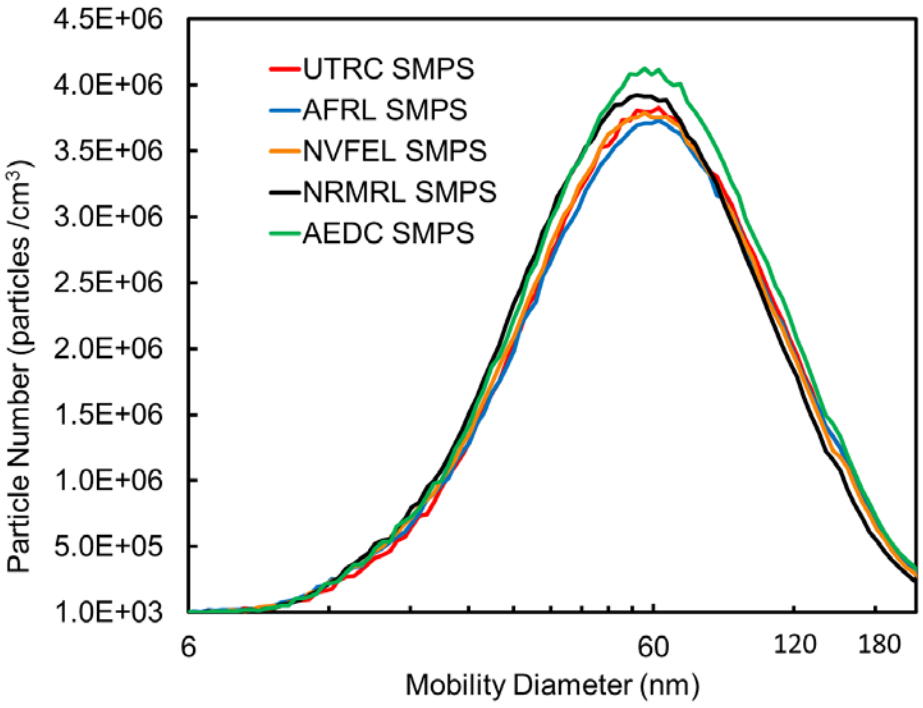

Figure 3.6. Test 2 calibration results during the UoM testing.



Figure 3.7. DOS Atomizer.

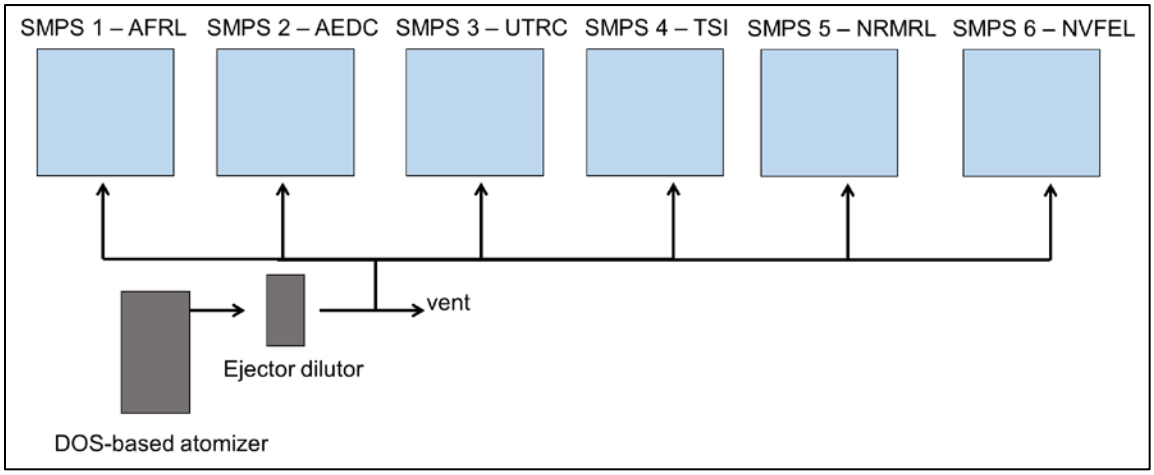

Figure 3.8. Pre and post-test SMPS consistency check.

Source Setup

Jing Mini-CAST

The Mini-CAST was set up as illustrated in Figs. 3.9. – 3.10. The Mini-CAST exhaust was diluted twice in the setup, once with ambient air and then with nitrogen to acquire the desired concentration. CO_2 of 100% concentration flowed into the bottom of the cone to increase the CO_2 concentration. CO_2 analyzers are utilized to determine and monitor the dilution ratio of the Dilutor 1 in both systems.

General Electric J85 Engine with Afterburner

The J85 was operated by AEDC personnel at the UTSI Propulsion Research Facility (PRF). Three specific thrust settings were utilized for this test: idle, middle power, and Military (Mil) power utilizing both Jet A and a 50/50 blend of Jet A and Camelia fuel. Military power is the highest thrust setting without activating the afterburner capability and the middle power is approximately midway between idle and Mil power. The afterburner was not used for this VARIAnT2 Test. The probes of the sampling systems were located a couple inches above center line of the J85 at the exit plane, as shown in Fig. 3.11.

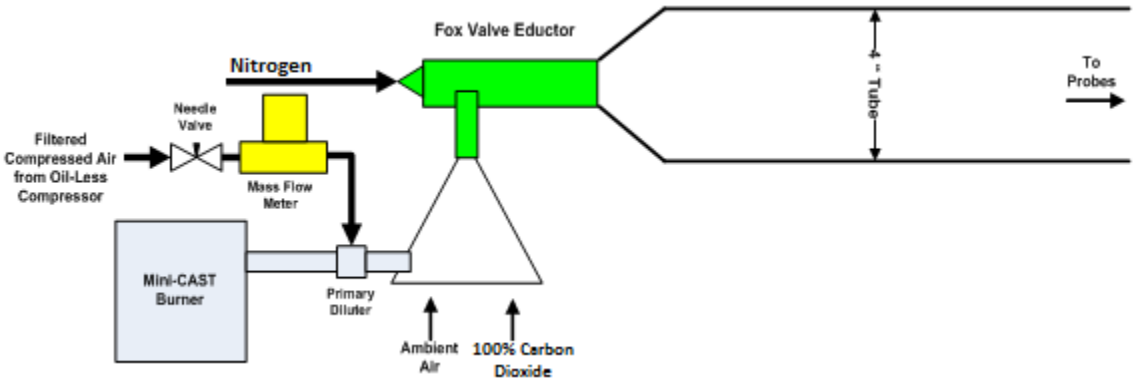

Figure 3.9. Mini-CAST setup illustration.

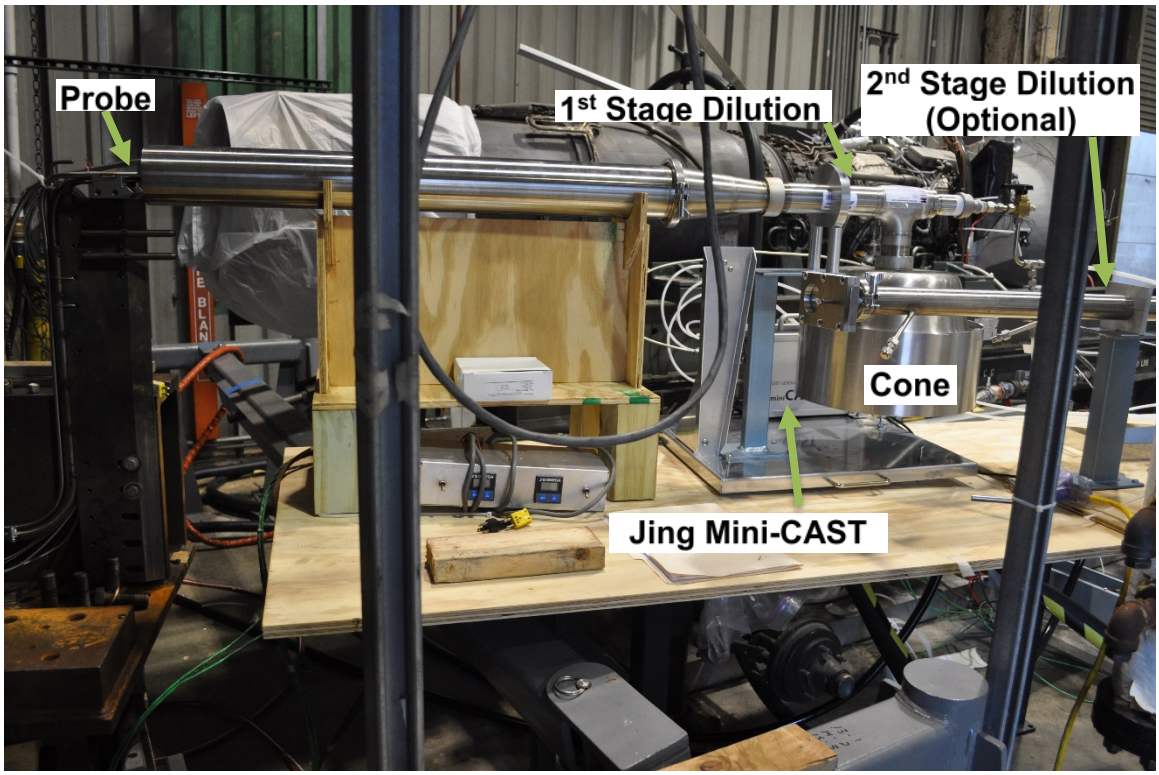

Figure 3.10. Jing Mini-CAST setup.

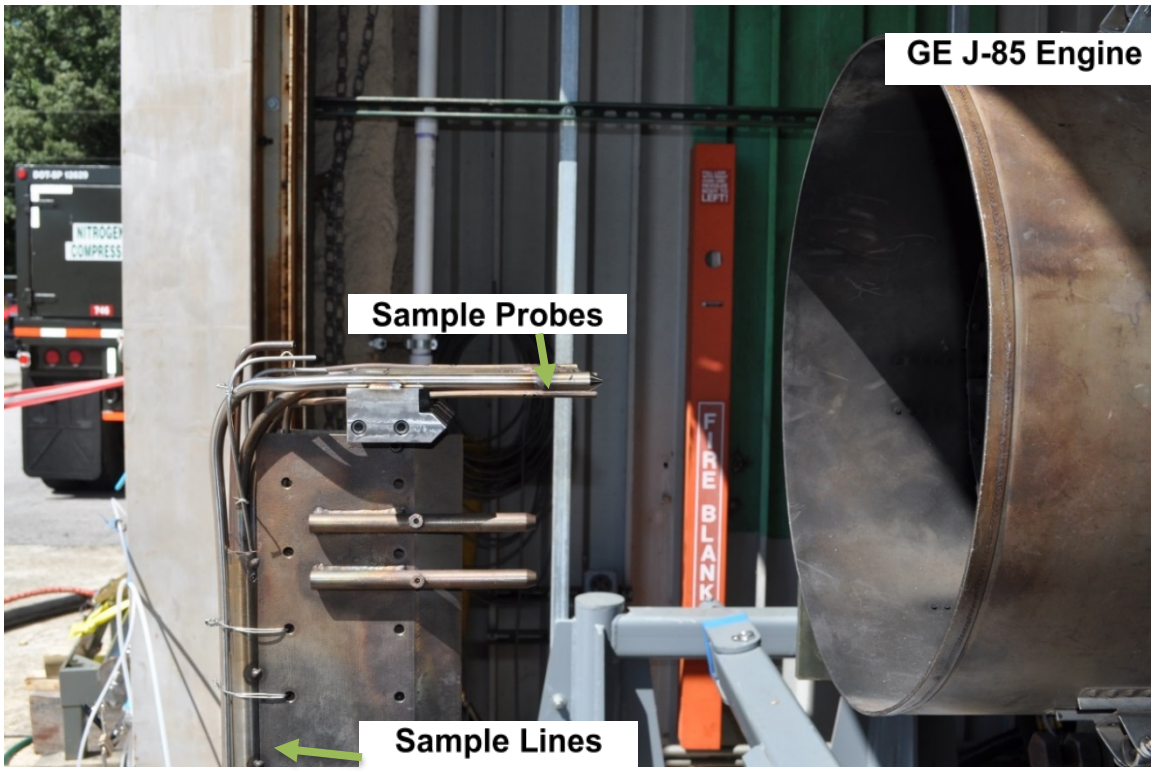

Figure 3.11. Probes at GE J85 exit plane.

CHAPTER FOUR

RESULTS AND DISCUSSION

This chapter describes issues with instrumentation, the results from measured penetration efficiencies to the calculated UTRC modeled penetration efficiencies, and comparisons between each sampling system and APC (AVL Particle Counter) where applicable. Six different sections of the particle measurement systems are discussed below: AVL Sample System Penetration Efficiencies, Upstream Half of AVL Sample System Penetration Efficiencies, Downstream Half of AVL Sample System Penetration Efficiencies, MS&T APC Penetration Efficiencies, UTRC APC Penetration Efficiencies, and MS&T Sampling System. This chapter also presents the error/uncertainty in the models and measurement, while also providing suggestions for future testing to reduce these uncertainties.

Instrumentation Issues

Early in the test campaign, it was discovered during one of the morning checks with dioctyl sebacate (DOS) particles that the National Risk Management Research Laboratory (NRMRL) Scanning Mobility Particle Sizer (SMPS) was not operating properly. Fig. 4.1. below shows the NRMRL SMPS compared to the National Vehicle Fuels and Emissions Lab (NVFEL) SMPS, which was sampling the same DOS particles. The graph indicates that the lower mobility diameters were not being counted correctly. At this time the NRMRL SMPS was removed from the system. The new configuration shown in Fig. 4.2. was the configuration used for the remainder of the campaign. This new configuration indicates that no direct SMPS measurements of the Missouri Science and Technology (MS&T) sampling system were acquired. Also because of this failure, NRMRL SMPS data were not acquired on the GE J-85. For analysis purposes it was assumed that the VPR/dilution system penetrations were constant through the rest of the campaign and there was no dependency on the source (GE J-85 or Jing Mini-CAST).

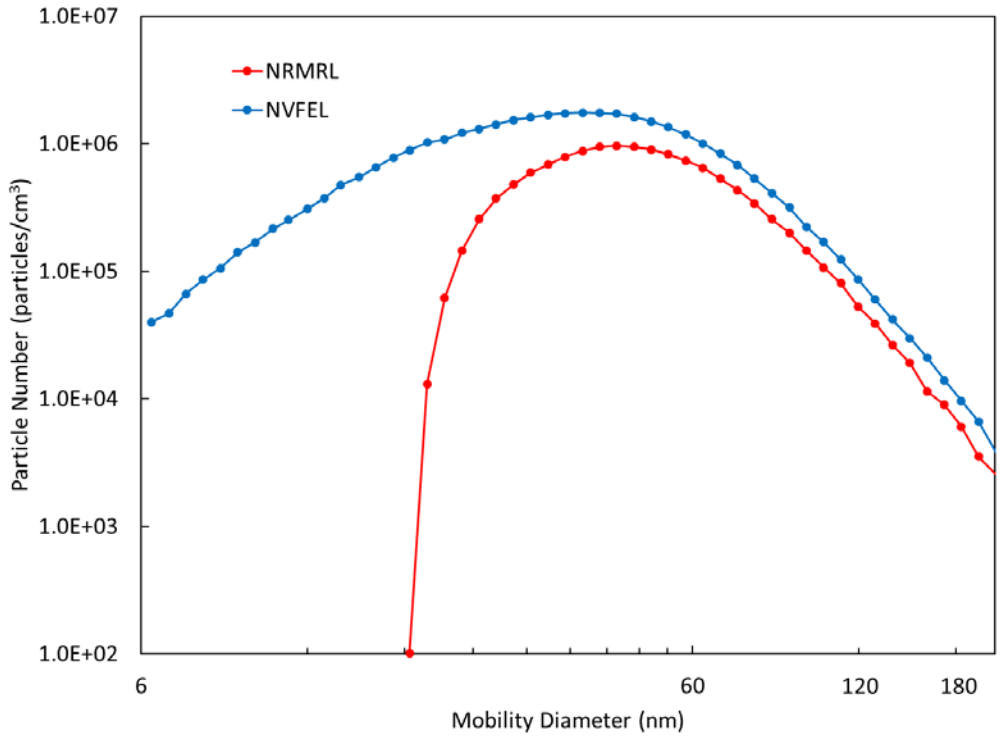

Figure 4.1. NRMRL SMPS and NVFEL SMPS daily DOS checks.

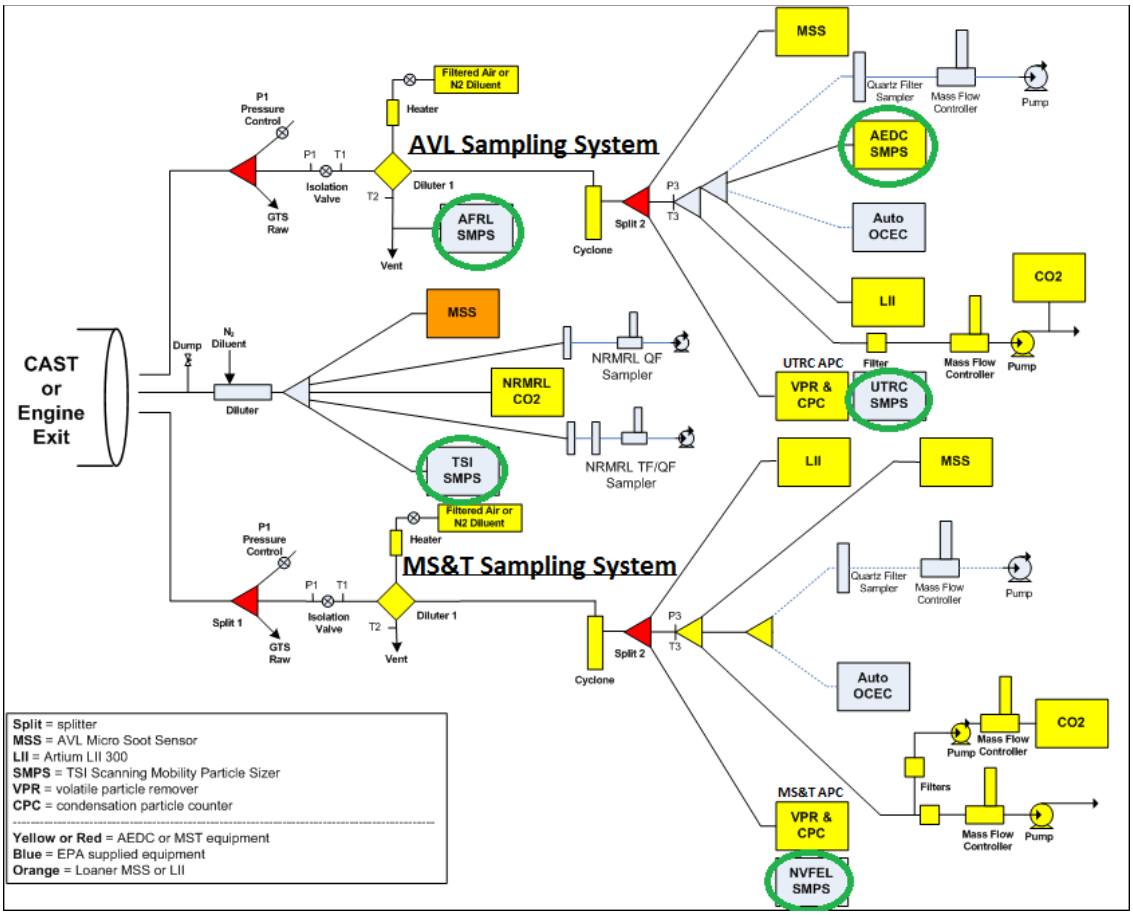

Figure 4.2. Final test configuration.

Penetration Efficiencies

AVL Sample System Penetration Efficiencies

The graph in Fig. 4.3. shows two measured lognormal mobility diameter distributions scanning the range from 6 nm to 212 nm that were produced in one scan taking three minutes from two different SMPS instruments. The TSI SMPS measured the size distribution at the probe tip, after correcting for its sample system losses, and the AEDC SMPS measured the size distribution after the sample passed through the AVL sample system. These measurements were performed while sampling from the exhaust of the GE J-85 at idle power and burning Jet-A fuel. The measurement uncertainty of the SMPS instruments has been quoted by TSI (Manufacturer of the SMPS instruments) to be approximately ±14% at a 95% confidence level.

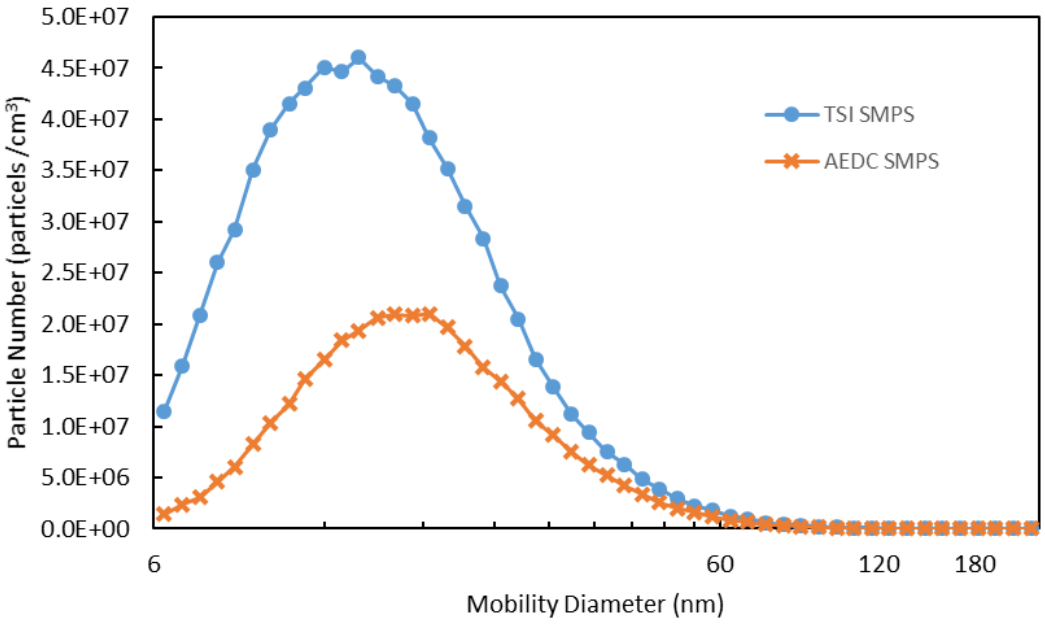

Figure 4.3. TSI SMPS and AEDC SMPS mobility diameter distributions measured before and after the AVL Sampling system respectively, GE J-85 with Jet-A at idle.

The ratio of a pair of scans (an AEDC SMPS scan over the TSI SMPS scan) of the individual mobility size distributions determines the size dependent penetration. To get a better statistical average, this procedure was completed on each of five sets of mobility size distribution measurements acquired during steady state operations, thus producing five individual penetration efficiencies for

each mobility diameter. The resulting five penetration efficiency vs. mobility diameter data sets are then averaged together to obtain an average penetration efficiency vs. mobility diameter dataset for this test point as shown by the diamonds in Fig. 4.4. Any penetration efficiencies of zero in the graphs illustrate no data were available for that mobility diameter. The error bars in this graph represent the standard deviation of the five penetration efficiencies utilized to create the average penetration efficiency. The average size dependent penetration efficiency is compared to the penetration efficiency curve calculated using the UTRC penetration model. As seen in Fig. 4.4. the standard deviation increases significantly above 60 nm. This is due to the small number of particles at these mobility diameters as seen in Fig. 4.3. Many issues can be seen when approaching the limit of detection for the SMPS instruments. Four of those issues can be seen in Fig. 4.4 and other average penetration efficiency graphs to follow: standard deviations above one, standard deviations below zero, average penetration efficiencies above one, and exponential increase in penetration efficiencies at smaller mobility diameters. The standard deviation bars that are above one in the average penetration efficiency graphs occur due to the downstream SMPS reporting a higher concentration than the upstream SMPS. The downstream SMPS instrument reporting a higher concentration than the upstream SMPS, again occurs when the concentration approaches the limit of detection of the instruments and an accurate reading of the concentration is not possible. When this occurs, the average penetration efficiencies for a given mobility diameter can be reported as high as ten, which will enable the standard deviation to be greater than the mean value if most of the calculated penetration efficiencies for a mobility diameter are below one. In this case, since the standard deviation is just added or subtracted from the mean to create the bars illustrated on the graphs, the standard deviation bar can be much above one or even below zero. Also when the concentration starts to approach the limit of detection at the smaller mobility diameters, an exponential increase in the penetration efficiencies is noticed in Fig. 4.4 and is more pronounced in other average penetration efficiencies presented later in this paper, which have a much lower concentration overall.

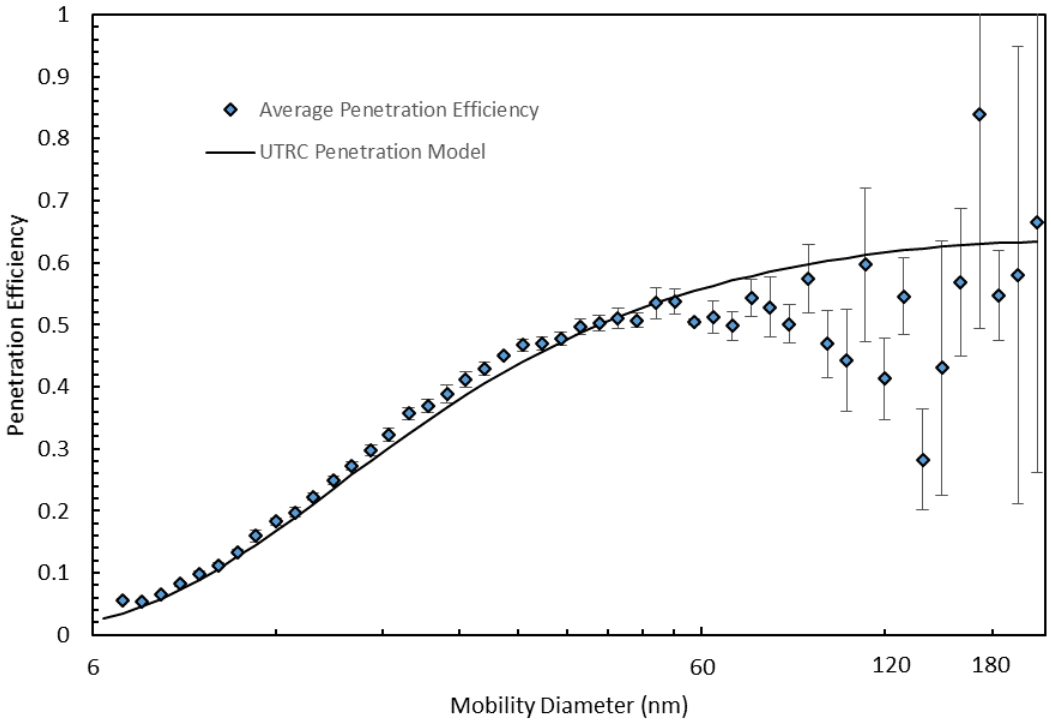

Figure 4.4. Average size dependent penetration data determined from measurements on the GE J-85 with Jet-A at idle power setting compared to calculations from the UTRC model.

In order to get a meaningful penetration efficiency dataset across all mobility diameters, adequate concentrations are needed at all mobility diameters of interest. To achieve this, multiple sources, fuels, and power settings were used. Fig. 4.5. illustrates the mobility diameter distributions recorded for various power settings, fuels, and particle source types. These were measured using the TSI SMPS instrument and represent the size distribution at the probe tip. Referring to Fig. 4.5., the GE J-85 with Jet-A fuel at a power setting of idle has the highest concentration from 6 nm to about 12 nm. After 12 nm the GE J-85 with Jet-A fuel at a power setting of Military (Mil) has the highest concentrations until approximately 96 nm where the Mini-CAST, at the NRC Setting, has the highest concentrations through the remaining size range of interest. Selecting the mobility sizes from Fig. 4.5. with the highest concentrations, the resulting average penetration efficiencies will account for the small amount of particles in individual average penetration efficiencies. By utilizing at least one set of average penetration efficiencies from the GE J-85, (for small diameters) and one from the Mini-CAST(for large diameters), an average penetration can be determined across the entire 6 nm to 212 nm mobility diameter range.

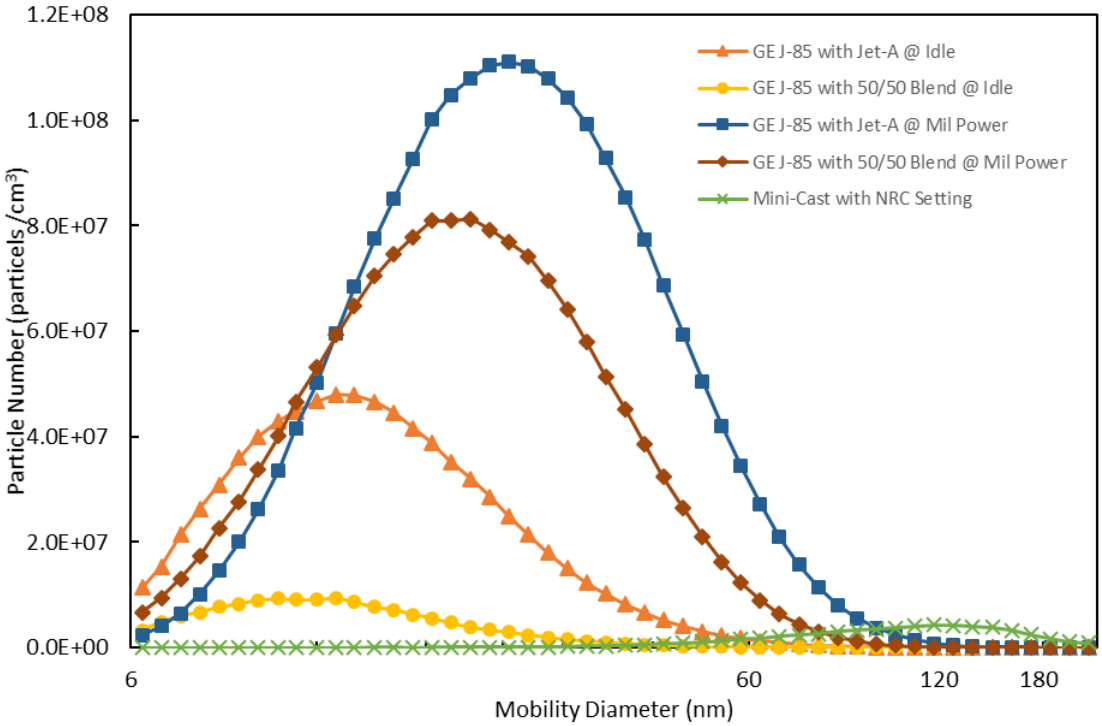

Figure 4.5. Measured Lognormal mobility diameter distributions produced by multiple sources, fuels, and settings recorded by the TSI SMPS located near the emissions source.

To calculate the average penetration efficiency across the entire mobility diameter range, a split point needs to be determined in order to systematically change from one average penetration to the other. This was determined by the point at which the concentration of the GE J-85 burning Jet-A fuel at a power setting of idle falls below the concentration of the Mini-CAST operating at the NRC Setting, here-in referred to as the split point. For instance, zooming in on the intersection of the GE J-85 burning Jet-A fuel at a power setting of idle and Mini-CAST with NRC Setting curves in Fig. 4.5., Fig. 4.6. shows the split point for the GE J-85 with Jet-A at Idle and the Mini-CAST with NRC Setting occurs at about 62 nm. Therefore, only the average penetration efficiencies for the GE J-85 that are smaller in mobility diameter than the 62 nm split point are combined with the average penetrations for the Jing Mini-CAST that have mobility diameters larger than 62 nm.

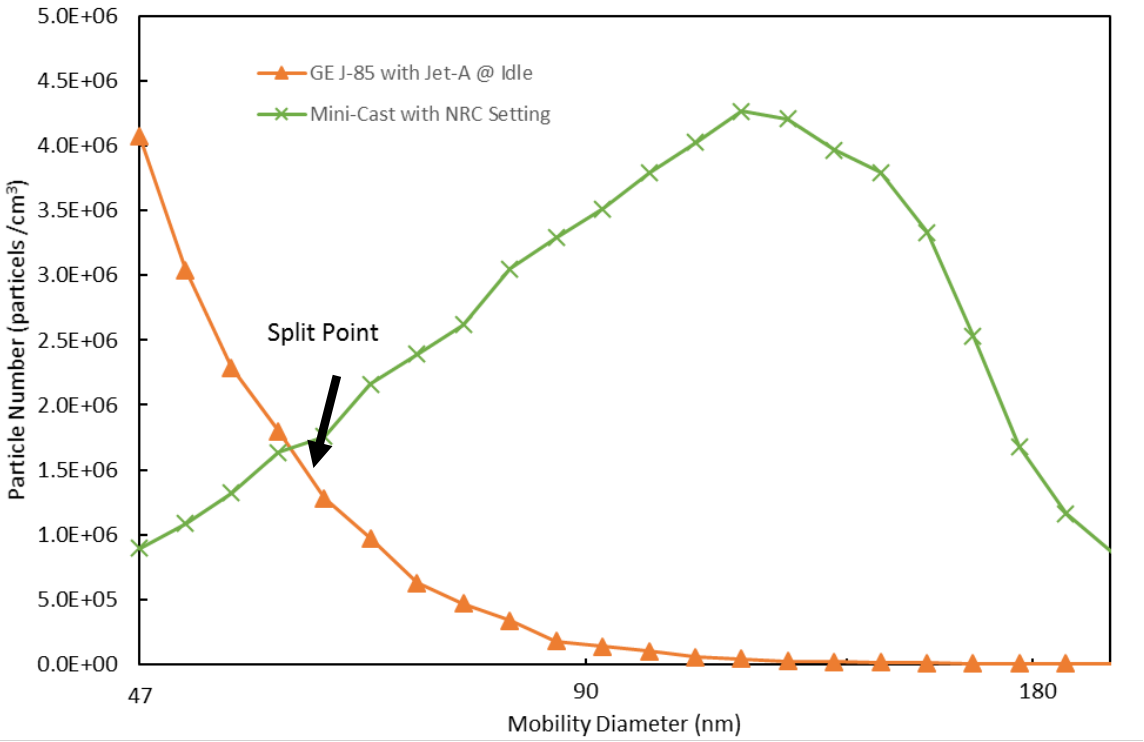

Figure 4.6. Illustrating the split point determination between GE J-85 and Jing Mini-CAST distributions.

By accounting for the split point and utilizing the average penetration efficiencies with the greatest concentrations per mobility diameter, a full average penetration efficiency dataset is graphed in Fig. 4.7. When comparing the full average penetration efficiency from measurements to the UTRC penetration efficiency

model calculations, the full average penetration efficiency deviates from the model by an average of 6.71%, which is well within the measurement uncertainties of 14% that are quoted by TSI for a single measurement. To determine the difference between the model and the measured penetration efficiency data, the penetration efficiencies at each mobility diameter were subtracted from the reference (the UTRC model) and then is divided by the reference. The average is taken of these values and is then multiplied by 100 to get a percent. This calculation is performed throughout the rest of this thesis when comparing the penetration efficiencies from the measured data to the calculated values using the UTRC model.

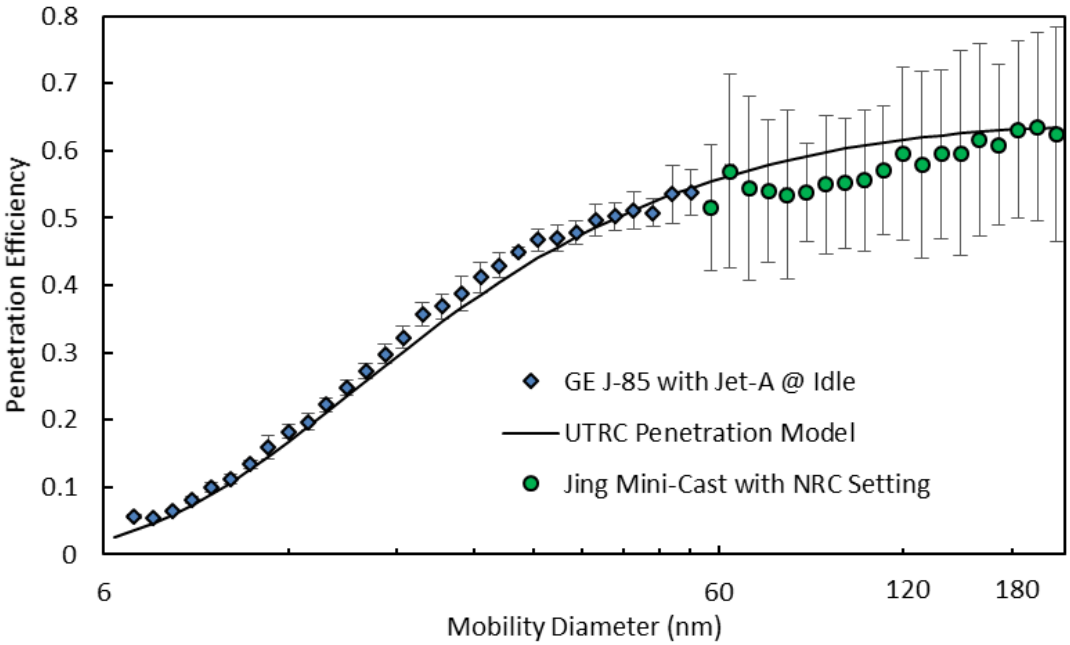

Figure 4.7. Complete mobility diameter AVL sampling system penetration efficiency using measurements of mobility diameter distributions from two different particle sources compared to the UTRC model calculation.

The difference in the standard deviations of the two penetration efficiency calculations is due to the GE J-85 producing a more constant soot and gas composition over time compared to the Jing Mini-CAST. The TSI and AEDC SMPS instruments were set up to start the 3 minute measurement scan at the same point in time. This means they will be determining the concentration for a particular size bin at the same point in time. This measurement method would

not create an issue if both SMPS instruments were analyzing the same sample simultaneously. Due to transit times of the particles from the front of the sampling system to the back where the AEDC SMPS was located, characteristics of the sample may be different. If the source is variable, then the SMPS instruments have the potential of sampling a different composition of particles.

Various Fuel, Source, and Setting Penetration Efficiencies

Using the procedure described above for Fig. 4.4., additional average penetration efficiencies were determined for different fuel types, combustion sources, Mini-CAST settings, and power settings which are shown below.

The alternative fuel can be seen in Fig. 4.8. where the same GE J-85 with a power setting of Idle was utilized as in Fig. 4.4., but the fuel was a mixture of 50% Camelina and 50% Jet-A. This average penetration efficiency dataset shows close correlation, within about 14%, to the UTRC modeled penetration efficiency from 6 nm up to about 35 nm (dashed vertical line on Fig. 4.8.) where the concentration is well above zero as can be seen in Fig. 4.5., but this is not the case after 35 nm where the concentration approaches zero.

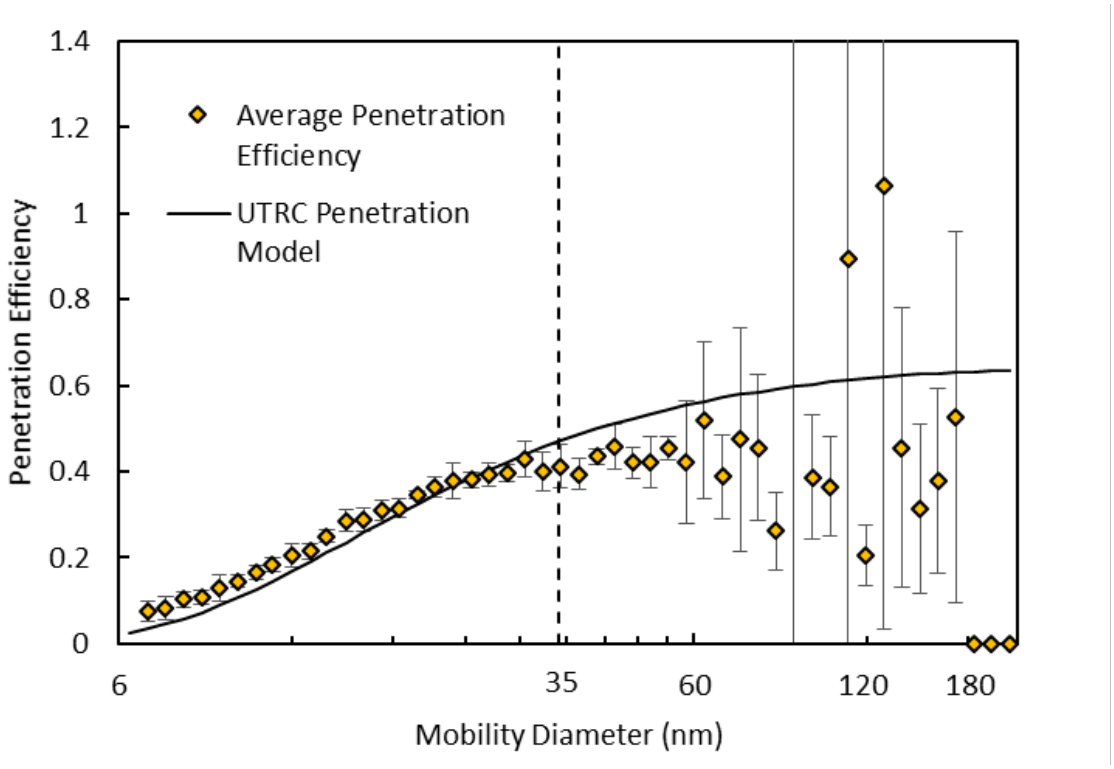

Figure 4.8. AVL Sampling System average penetration efficiency for the GE J-85 with 50/50 Camelina and Jet-A Blend Fuel at Idle power setting.

Multiple settings are shown in Fig. 4.9., where the GE J-85 with Jet-A was utilized as in the above Fig. 4.4. but a power setting of Military (Mil) was utilized. The Military setting represents the max thrust without entering afterburner. This average penetration efficiency dataset shows a close trend to the UTRC Modeled Penetration Efficiency from about 8 nm up to about 110 nm where the concentration is well above zero as can be seen in Fig. 4.5., but this is not the case after 110 nm where the concentration approaches zero. From 6 nm to approximately 8 nm the concentration starts to approach zero which is the reason this graph was not utilized for the full penetration efficiency shown in Fig. 4.7. Another reason these penetration efficiency data were not selected is due to the offset from the model. The reason for the offset is unknown, however, with the steady incline in the standard deviation from about 32 nm (first dashed vertical line on Fig. 4.9.) up to the 110 (second dashed vertical line on Fig. 4.9.) where there is still a sufficient amount of concentration, indicates some type of issue, possibly with the downstream SMPS. This could also be due to the setup being changed during the middle of a steady state test point which would affect the average of the penetration efficiencies in question.

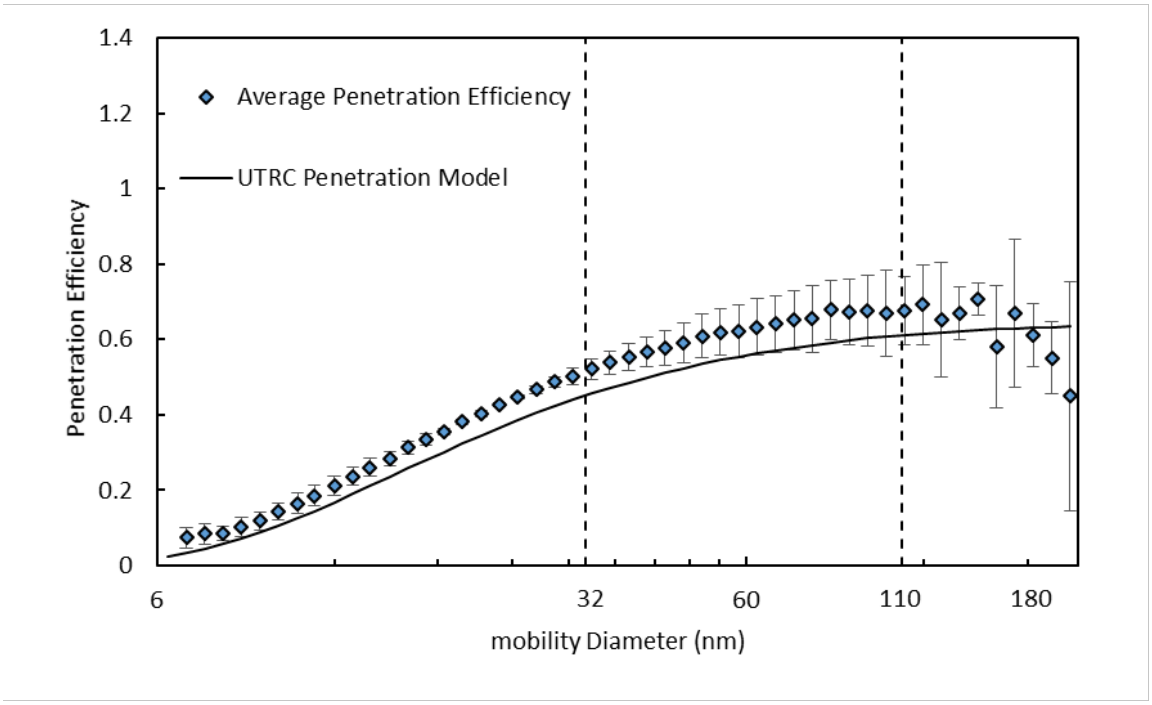

Figure 4.9. AVL Sampling System average penetration efficiency for the GE J-85 with Jet-A at Military (Mil) power setting.

Another source, fuel, and multiple settings can be seen in Figs. 4.10. and 4.11. where the Jing Mini-CAST was utilized. The Mini-CAST utilizes compressed propane and dry shop air to produce the soot source. The VARIAnT1 and NRC settings are a specific fuel to air ratio as well as other parameters that affect the particle morphology. This average penetration efficiency dataset for the NRC setting shows close correlation, within approximately 5%, to the UTRC Modeled Penetration Efficiency from about 27 nm to 212 nm, where the concentration is well above zero as can be seen in Fig. 4.5., but this is not the case for mobility diameters smaller than about 27 nm (dashed vertical line in Fig. 4.10.) where the concentration approaches zero. This average penetration efficiency dataset for the VARIAnT1 setting shows close correlation, within about 13%, to the UTRC Modeled Penetration Efficiency from about 62 (Dashed vertical line in Fig. 4.11.) to 212 nm where the concentration is well above zero, but this is not the case for mobility diameters smaller than about 62 nm, where the concentration approaches zero.

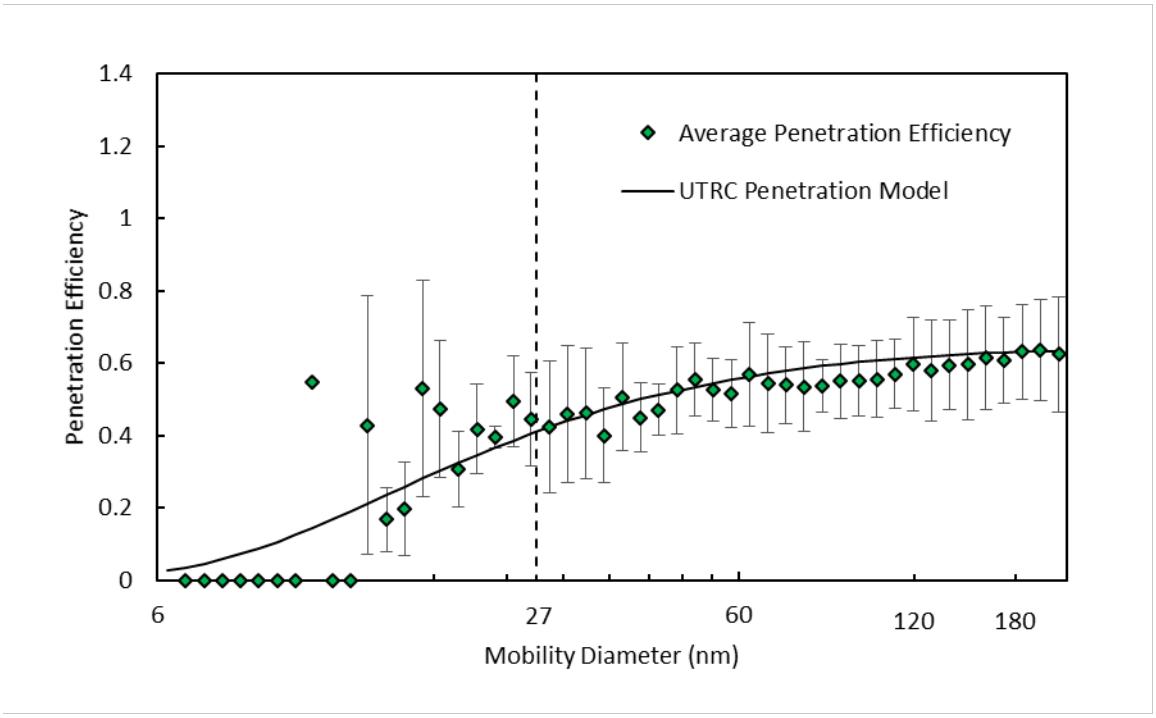

Figure 4.10. AVL Sampling System average penetration efficiency for the Jing Mini-CAST with the NRC Setting.

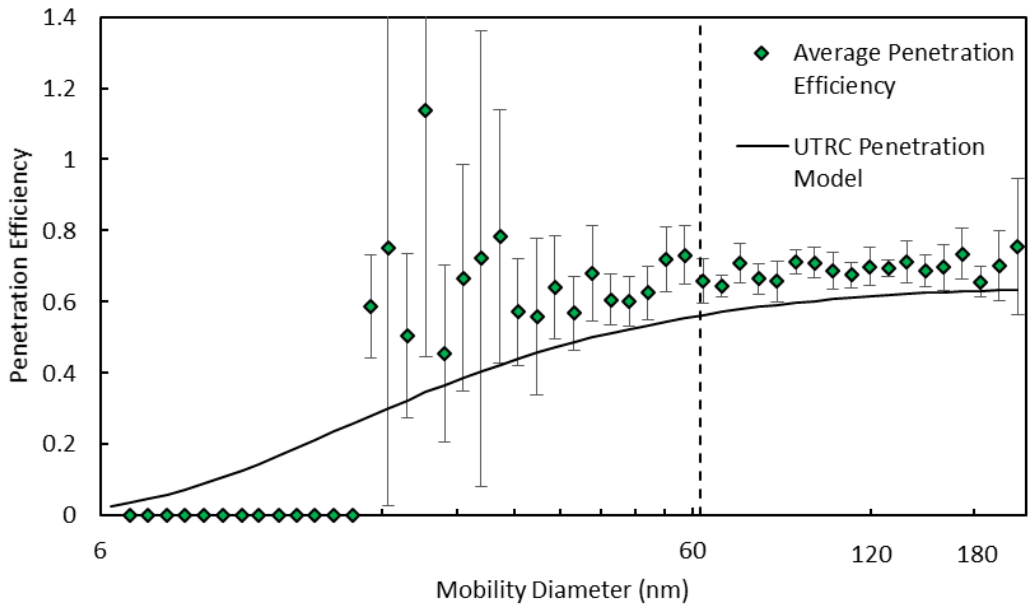

Figure 4.11. AVL Sampling System average penetration efficiency for the Jing Mini-CAST with the VARIAnT1 Setting.

All of the average penetration calculations show close correlation, within measurement uncertainties to the model, at least where the standard deviation is consistently small. As the standard deviation increases, the average penetration greatly deviates from the model, which is due to the lack of particles at that mobility diameter. Using the standard deviation as the indicator, the Mini-CAST has a close agreement at the larger mobility diameter sizes, while the GE J-85 has a closer agreement at the larger sizes.

Upstream Half of AVL Sample System Penetration Efficiencies

The same procedures utilized to calculate the penetration efficiency for the full AVL sampling system were also utilized for only the front half of the sampling system. As described in the setup section and Fig. 1.1., the front half of the AVL Sampling system refers to the section between the probe tip (TSI SMPS) and the dilutor1 vent (AFRL SMPS). The Jing Mini-CAST with the VARIAnT 1 Setting, and the GE J-85 with Jet-A at a power setting of idle was utilized to create the full average penetration efficiency. The reason the Jing Mini-CAST with the VARIAnT1 setting was utilized in place of the NRC setting in this case was because the VARIAnT1 setting showed a closer correlation to the model. The same split point at about 54.2 nm was utilized to determine the average penetration efficiencies for the upstream half of the AVL sampling system as was utilized for the full average AVL sampling system penetration efficiencies. Utilizing the average penetration efficiencies with the greatest concentrations per mobility diameter, a full average penetration efficiency dataset is graphed in Fig. 4.12. When comparing the full average penetration efficiency from measurements to the UTRC penetration efficiency model calculations, the full average penetration efficiency deviates from the model by an average of 5.52%, well within the measurement uncertainties of 14% that are quoted by TSI for a single measurement.

The difference in the standard deviations of the two penetration efficiency calculations is again due to the GE J-85 producing a more constant soot and gas composition over time compared to the Jing Mini-CAST. The TSI and AFRL SMPS instruments were set up to start the 3 minute measurement scan at the same point in time. This means they will be determining the concentration for a particular size bin at the same point in time. This measurement method would not create an issue if both SMPS instruments were analyzing the same sample simultaneously. Due to transit times of the particles from the front of the sampling system to the back where the AFRL SMPS was located, characteristics of the sample may be different. If the source is variable, then the SMPS instruments have the potential of sampling a different composition of particles.

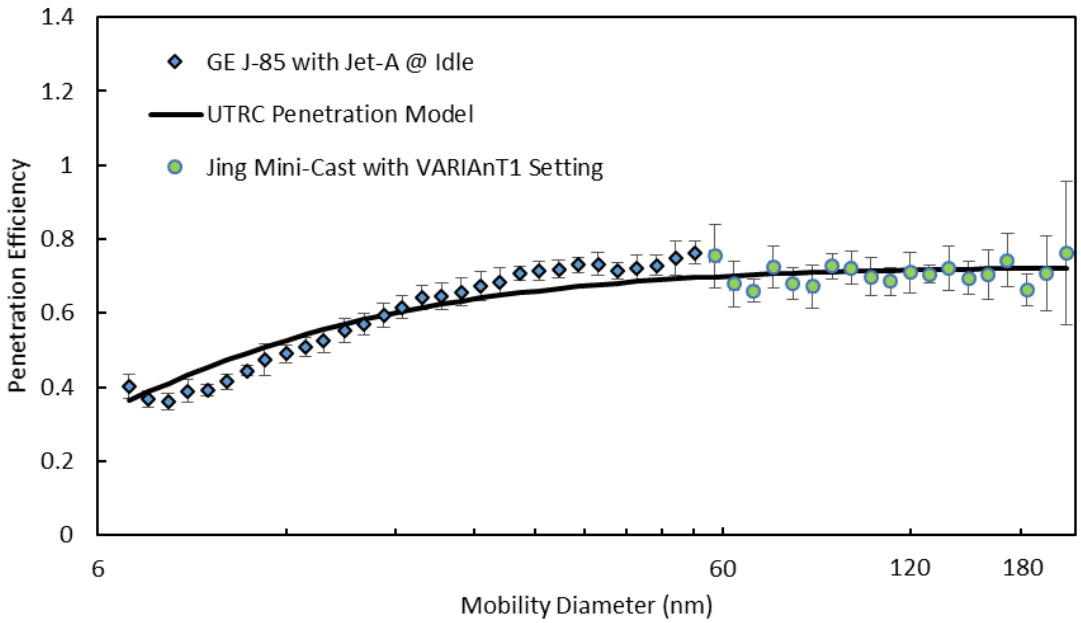

Figure 4.12. Complete mobility diameter average penetration efficiency for the upstream half of the AVL sampling system using measurements of mobility diameter distributions from two different particle sources compared to the UTRC model calculation.

Various Fuel, Source, and Setting Penetration Efficiencies

Using the procedure described above for Fig. 4.4., average penetration efficiencies were determined for different fuel types, combustion sources, Mini-CAST settings, and power settings. These are shown in Figs. A.6.1. - A.6.5. in Appendix 6. The procedure described above for Fig. 4.1.a.1 was not performed due to the many combinations that could be created from the Figs. A.6.1. - A.6.5.

An example of the alternative fuel can be seen in Fig. 4.13. where the same GE J-85 with a power setting of Idle was utilized as in Fig. 4.12., but the fuel was a mixture of 50% Camelina and 50% Jet-A. This average penetration efficiency dataset shows close correlation, within about 14%, to the UTRC Modeled Penetration Efficiency from about 12 nm (First vertical dashed line in Fig. 4.13.) up to about 35 nm (Second vertical dashed line in Fig. 4.13.) where the concentration is well above zero, as can be seen in Fig. 4.5. (Same TSI SMPS data were utilized for the split determination). The concentration after 35nm starts to approach zero, and it is only a coincidence that the penetration efficiency still matches the model until about 60 nm. The penetration efficiency shows a gradual exponential increase in penetration efficiency from 12 nm to about 6 nm. This is an indication the penetration efficiency for the AFRL instrument may not be correct. After checking the penetration efficiency and concentrations all calculations look correct. This indicates there is something occurring that is unknown or there was an issue with the setup.

An example of multiple settings is shown in Fig. 4.14. where the GE J-85 with Jet-A was utilized as in the above Fig. 4.12. but a power setting of Military (Mil) was utilized. This average penetration efficiency dataset shows a close trend to the UTRC Modeled Penetration Efficiency from about 11 nm (first dashed vertical line on Fig. 4.14.) up to about 110 nm (third dashed vertical line on Fig. 4.14.) where the concentration is well above zero as can be seen in Fig. 4.5., but this is not the case after 110 nm where the concentration approaches zero. Also from 6 nm to about 10 nm the concentration starts to approach zero. The reason this penetration efficiency was not selected is due to the offset from the model and the exponential increase in penetration efficiency from about 10 nm down to the 6 nm mobility diameter. The reason for the offset and exponential increase is unknown; however, with the steady increase in the standard deviation from about 32 nm (second dashed vertical line on Fig. 4.14.) up to the 110, where there is still a sufficient amount of concentration, indicates some type of issue or misunderstanding of the setup.

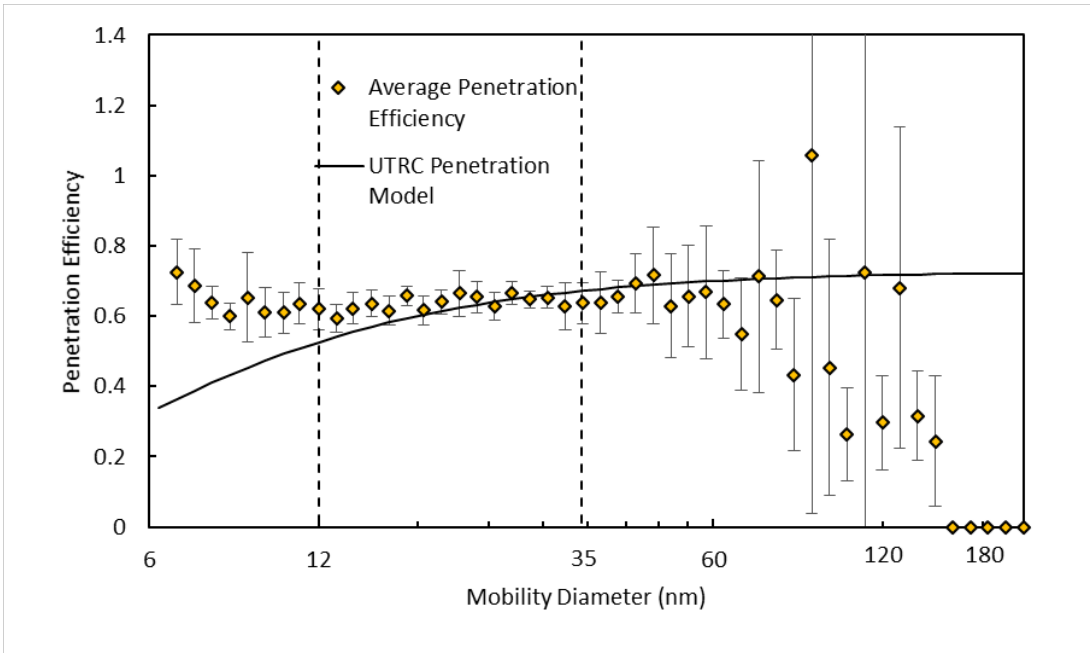

Figure 4.13. Upstream half of AVL sampling system average penetration efficiency for the GE J-85 with 50/50 Camelina and Jet-A Blend Fuel at Idle power setting.

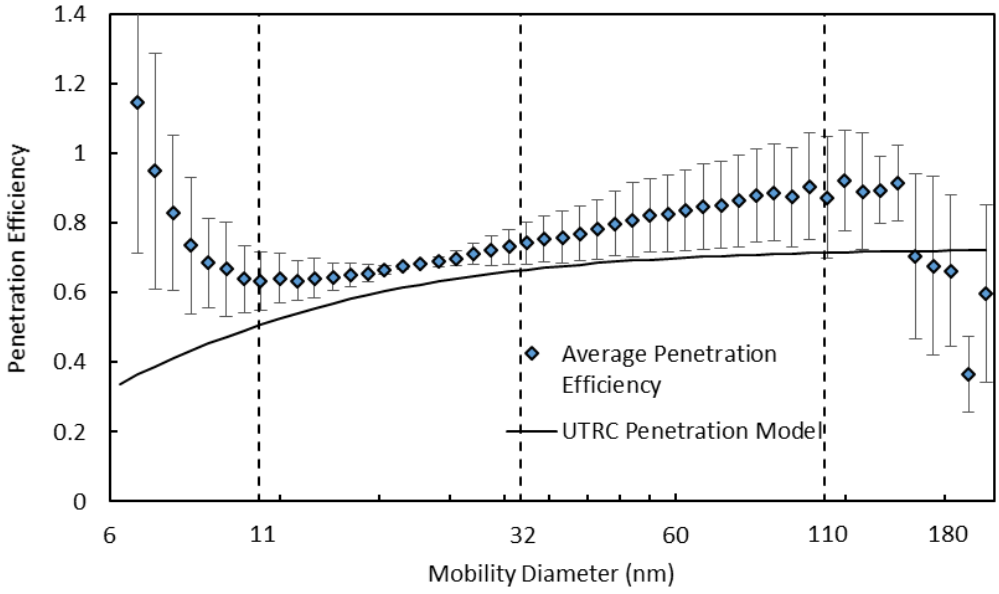

Figure 4.14. Upstream half of AVL sampling system average penetration efficiency for the GE J-85 with Jet-A at Military (Mil) power setting.

An example of another source and fuel can be seen in Fig. 4.15., where the Jing Mini-CAST with an NRC setting was utilized. The Mini-CAST utilizes compressed propane and dry shop air to produce the soot source. The NRC setting is a specific fuel to air ratio as well as other parameters that affect the particle morphology. This average penetration efficiency dataset shows close correlation, within about 12%, to the UTRC Modeled Penetration Efficiency from about 40 nm (dashed vertical line in Fig. 4.15.) to 212 nm where the concentration is well above zero as can be seen in Fig. 4.5. This is not the case for mobility diameters smaller than about 40 nm where the concentration approaches zero.

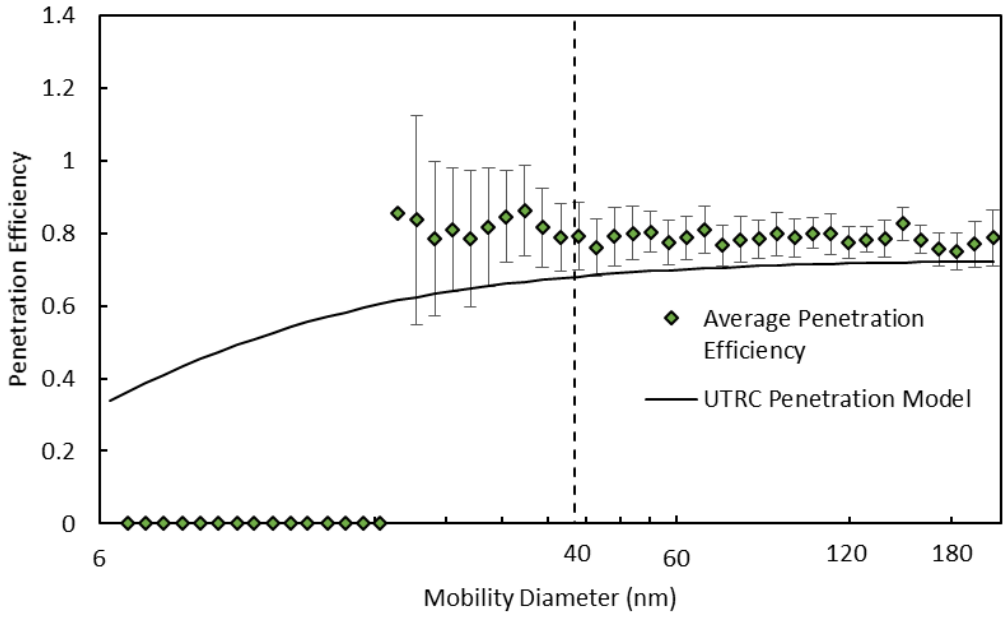

Figure 4.15. Upstream half of AVL sampling system average penetration efficiency for the Jing Mini-CAST with the NRC Setting.

All the average penetration functions have portions of them that show close correlation to the model, within measurement uncertainties, at least where the standard deviation is consistently small. As the standard deviation increases, the average penetration greatly deviates from the model which is due to the lack of particles at that mobility diameter. Using the standard deviation as the indicator, the Mini-CAST has a close agreement at the larger mobility diameter sizes while the GE J-85 has a closer agreement at the larger sizes. There is still question as

to the exponential increase in the penetration efficiencies at the lower sizes. This is shown in most of the penetration functions where there is enough concentration to determine a penetration efficiency. This is due to the concentration approaching the limit of detection for the SMPS instruments. The other issue that was observed that cannot be explained is the steady increase in offset from the model and steady increase in standard deviation, discussed in Fig. 4.14. The deviation of the measured data from the model in Fig. 4.14. is presumed to result from issues with the upstream SMPS or the setup somehow changing during a steady state data point. This would affect the final average over multiple penetration efficiencies. This portion of testing would need to be conducted again to determine the true cause of the discovered issues.

Downstream Half of AVL Sample System Penetration Efficiencies

The same procedures utilized to calculate the penetration efficiency for the full AVL sampling system was also utilized for only the downstream or back half of the sampling system. As described in the setup section, the back half of the AVL sampling system refers to the section between the Dilutor 1 vent (AFRL SMPS) and the inlet to the mass or number instruments (AEDC SMPS). In this subsection of the AVL sampling system, the Jing Mini-CAST with the NRC Setting and the GE J-85 with Jet-A at a power setting of Mil was utilized to create the full average penetration efficiency. A split point at approximately 104 nm was utilized to determine the average penetration efficiencies for the upstream half of the AVL sampling system, as was utilized for the full average AVL sampling system penetration efficiencies. Utilizing the average penetration efficiencies with the greatest concentrations per mobility diameter, as shown in Fig. 4.16., a full average penetration efficiency dataset is graphed in Fig. 4.17. When comparing the full average penetration efficiency from measurements of the downstream portion of the AVL sampling system to the UTRC penetration efficiency model calculations, the full average penetration efficiency deviates from the model by an average of 5.39%, well within the measurement uncertainties of 14% that are quoted by TSI for a single measurement.

The difference in the standard deviations of the two penetration efficiency calculations is again due to the GE J-85 producing a more constant soot and gas composition over time compared to the Jing Mini-CAST.

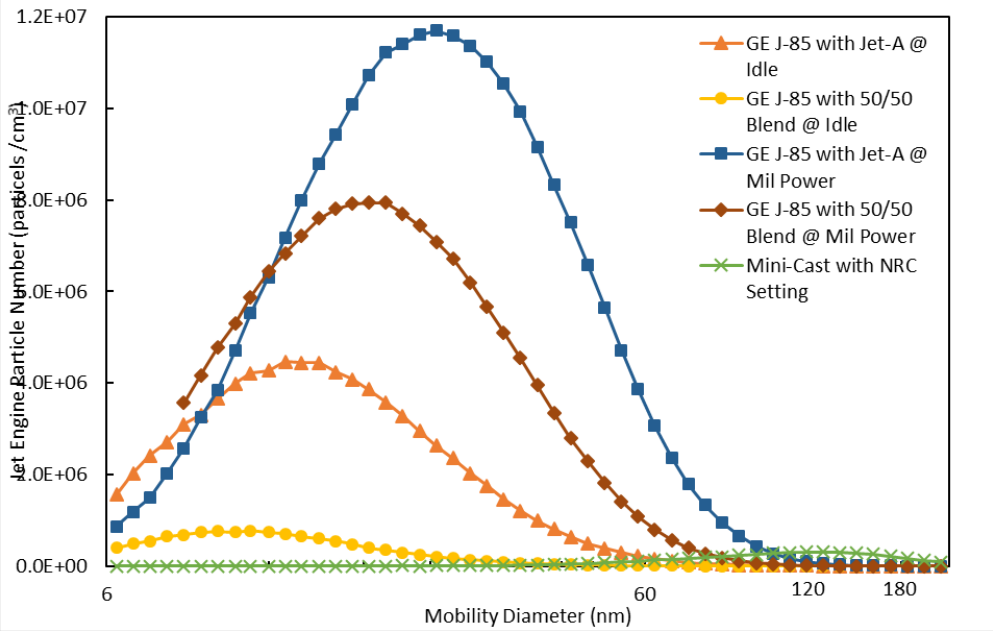

Figure 4.16. Measured Lognormal mobility diameter distributions produced by multiple sources, fuels, and settings recorded by the AFRL SMPS located at the dilutor one vent.

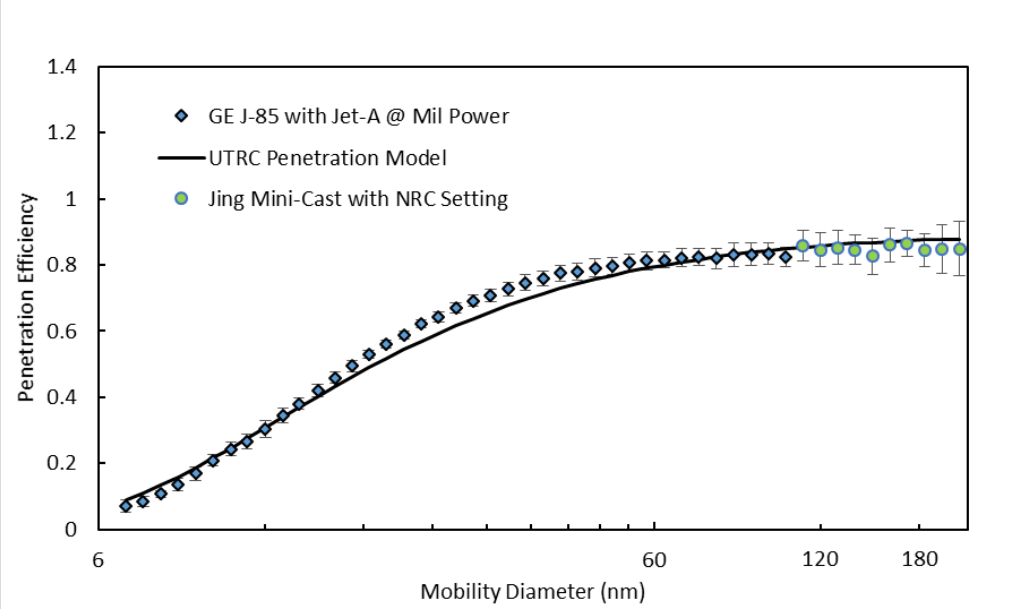

Figure 4.17. Complete mobility diameter average penetration efficiency for the downstream half of the AVL sampling system using measurements of mobility diameter distributions from two different particle sources compared to the UTRC model calculation.

Various Fuel, Source, and Setting Penetration Efficiencies

Using the procedure described previously for Fig. 4.4., average penetration efficiencies were determined for different fuel types, combustion sources, Mini-CAST settings, and power settings. These are shown in Figs. A.6.6. – A.6.10. in Appendix 6. The procedure described above for Fig. 4.17. was not performed due to the many combinations that could be created from the Figs. A.6.6. – A.6.10.

An example of the alternative fuel can be seen in Fig. 4.18. where the same GE J-85 with a power setting of Mil was utilized as in Fig. 4.12., but the fuel was a mixture of 50% Camelina and 50% Jet-A. This average penetration efficiency dataset shows close correlation, within about 4%, to the UTRC Modeled Penetration Efficiency from 9 nm (first dashed vertical line in Fig. 4.18.) up to about 100 nm (second dashed vertical line in Fig. 4.18.), where the concentration is well above zero as can be seen in Fig. 4.16. The concentration after 100 nm starts to approach zero and the standard deviation starts to increase. There was no data provided below 9 nm in this case, so a penetration efficiency below 9 nm was not determined.

An example of multiple settings is shown in Fig. 4.19., where the GE J-85 with Jet-A was utilized as in the above Fig. 4.17., but a power setting of idle was utilized. This average penetration efficiency dataset shows a close trend to the UTRC Modeled Penetration Efficiency from 6 nm up to about 62 nm, where the concentration is well above zero as can be seen in Fig. 4.16., but this is not the case after 62 nm where the concentration approaches zero. Figure 4.19. also shows one case where the measured penetration efficiency deviates from the model where the concentration is within acceptable levels from about 15 nm (first dashed vertical line in Fig. 4.19.) to 62 nm (second dashed vertical line in Fig. 4.19.). However, through the mobility diameter size range in question, the penetration efficiency deviates from the model by a maximum of 14% which is within the measurement uncertainty.

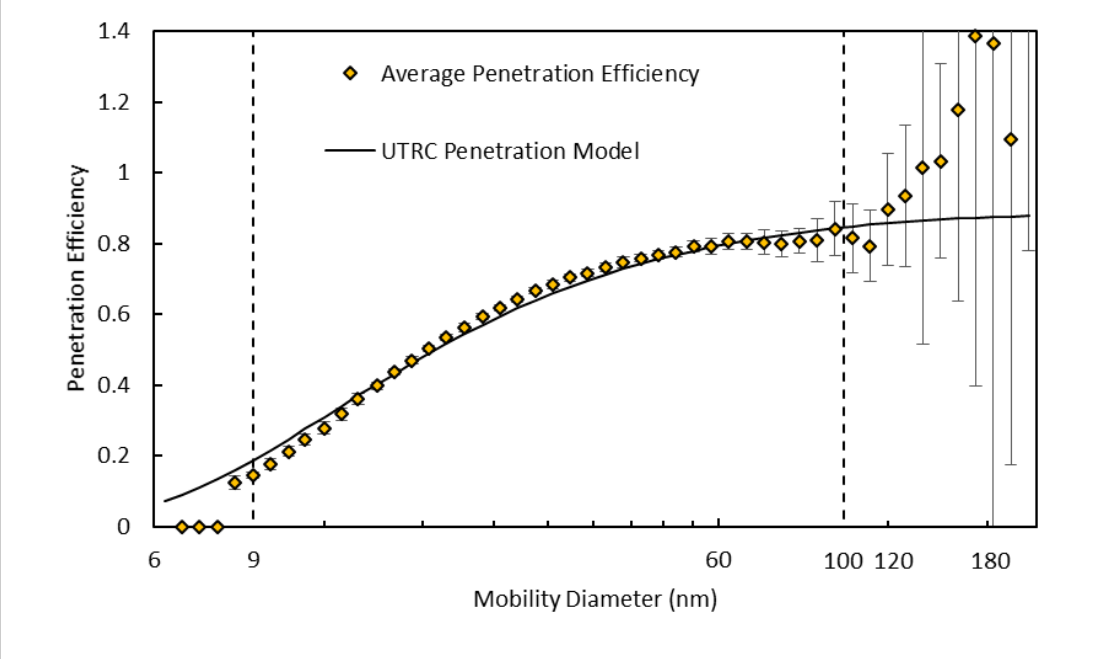

Figure 4.18. Downstream half of the AVL sampling system average penetration efficiency for the GE J-85 with 50/50 Camelina and Jet-A Blend Fuel at Mil power setting.

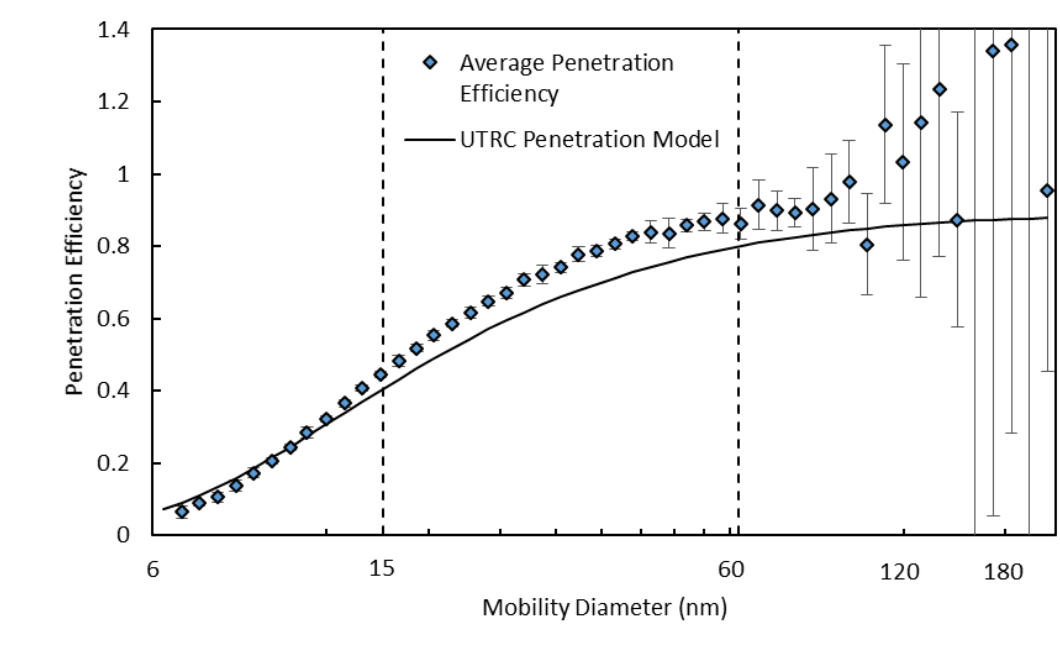

Figure 4.19. Downstream half of the AVL sampling system average penetration efficiency for the GE J-85 with Jet-A at idle power setting.

An example of another source and fuel can be seen in Fig. 4.20. where the Jing Mini-CAST with a VARIAnT1 setting was utilized. The Mini-CAST utilizes compressed propane and dry shop air to produce the soot source. The VARIAnT1 setting is a specific fuel to air ratio as well as other parameters that affect the particle morphology which was described previously. This average penetration efficiency dataset, Fig. 4.20., shows close correlation, within about 4%, to the UTRC Modeled Penetration Efficiency from about 62 nm to 212 nm where the concentration is well above zero, but this is not the case for mobility diameters smaller than about 62 nm (dashed vertical line in Fig. 4.20.) where the concentration approaches zero.

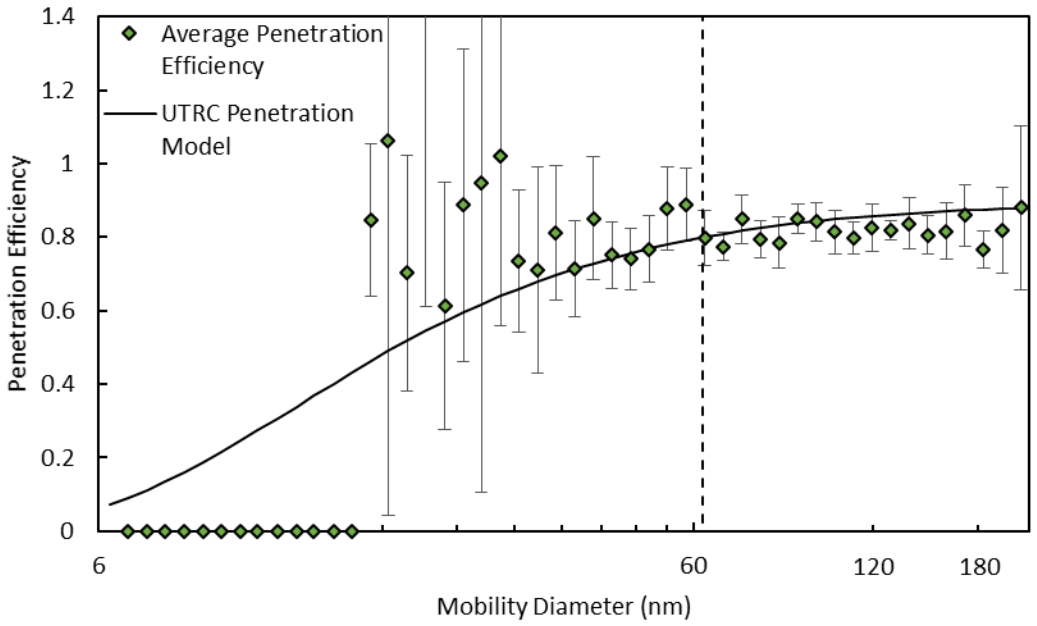

Figure 4.20. Downstream half of the AVL sampling system average penetration efficiency for the Jing Mini-CAST with the VARIAnT1 Setting.

All the average penetration functions have portions of them that show close correlation, within measurement uncertainties, to the model, at least where the standard deviation is consistently small. As the standard deviation increases the average penetration greatly deviates from the model, which again is due to the lack of particles at that mobility diameter. Using the standard deviation as the indicator, the Mini-CAST has a close agreement at the larger mobility diameter sizes, and the GE J-85 has a closer agreement at the smaller sizes.

MS&T Sampling System Penetration Efficiencies

The same procedures utilized to calculate the penetration efficiency for the full AVL sampling system were also utilized for full penetration efficiency for the full MS&T sampling system. As described in the setup section, the MS&T Sampling system refers to the section between the probe tip (TSI SMPS) and the inlet to the mass and number instruments (NRMRL SMPS). Since the NRMRL SMPS instrument was not operable through most of the campaign, the NVFEL SMPS measurements were utilized to create penetration efficiencies for the MS&T sample system. The MS&T APC penetration efficiency, described in the next section, was utilized to determine the concentration at the inlet of the mass or number instruments where the NRMRL SMPS is located. This measurement has a high uncertainty due to the high dilution from inlet to exit of the APC (up to 3390:1 by volume), and the high loss of particles especially at the small sizes through the APC VPR/dilution system. The high dilution ratio is needed to keep the CPC or particle counter in the APC within the measurement limits. This uncertainty is compounded by the fact that only two penetration efficiency measurements were acquired on the MS&T APC due to the NRMRL SMPS failure early in the campaign. The assumption that the penetration efficiency for the APC does not change over time adds more uncertainty to the determination of the penetration efficiencies. Only by utilizing a penetration modeled efficiency for the MS&T APC was a penetration efficiency of the MS&T sampling system able to be determined. Based on the UTRC APC penetration efficiency determined in a later section, this is a good assumption but adds uncertainties compared to directly measuring the particles in and out of the APC. Utilizing the best data with the highest concentrations and closest correlations between the measured penetration efficiencies and the UTRC calculated model penetration efficiencies, the Jing Mini-CAST with the NRC setting and the GE J-85 utilizing Jet-A as the fuel at a power setting of idle was utilized to determine a full average penetration efficiency measurement. This full average penetration efficiency measurement of the MS&T sampling system was compared to the UTRC calculation model within the mobility diameters of interest (6 nm to 212 nm) shown in Fig. 4.21.

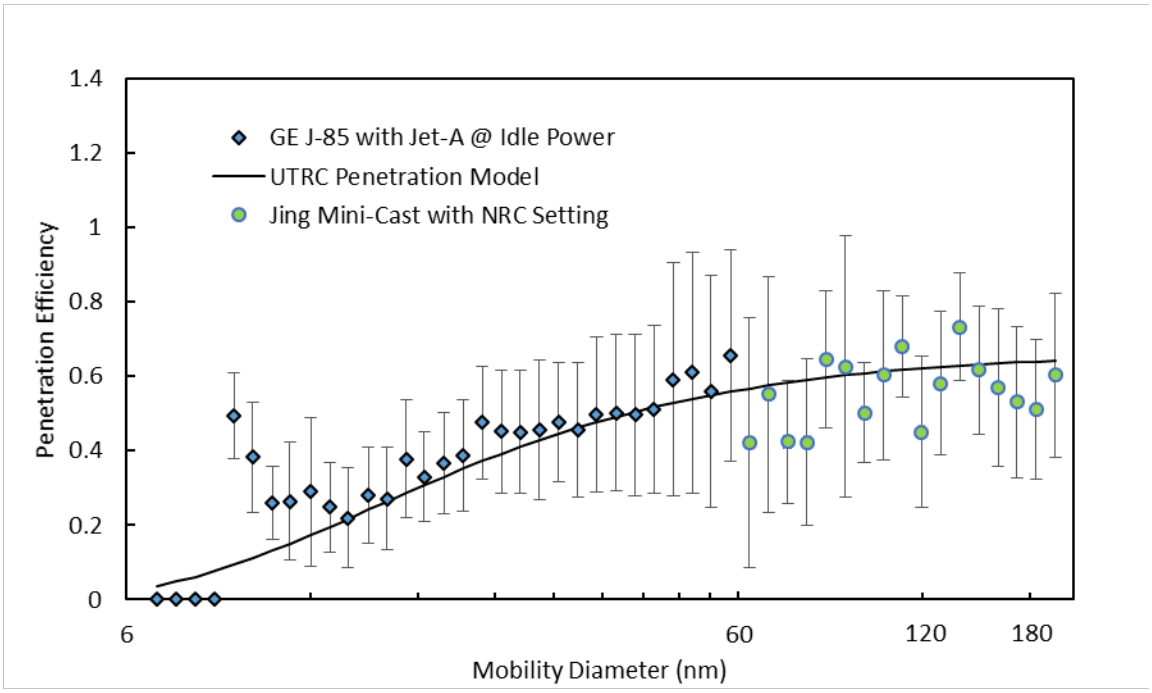

Figure 4.21. Complete mobility diameter average penetration efficiency for the MS&T sampling system using measurements of mobility diameter distributions from two different particle sources compared to the UTRC model calculation.

The same split point at about 59 nm was utilized to determine the transition from the GE J-85 penetration efficiencies to the Mini-CAST penetration efficiencies. When comparing the full average penetration efficiency from measurements to the UTRC penetration efficiency model calculations, the full average penetration efficiency deviates from the model by an average of 29.76%, outside of the measurement uncertainties of 14% that are quoted by TSI for a single measurement, which was expected due to the complicated assumptions. The average deviation from the model can be reduced to 11.84%, if the penetration efficiencies below 10.4 nm (dashed vertical line in Fig. 4.22.) are removed due to very minimal amount of particles below that mobility diameter which was observed at the NVFEL SMPS, as seen in Fig. 4.22.

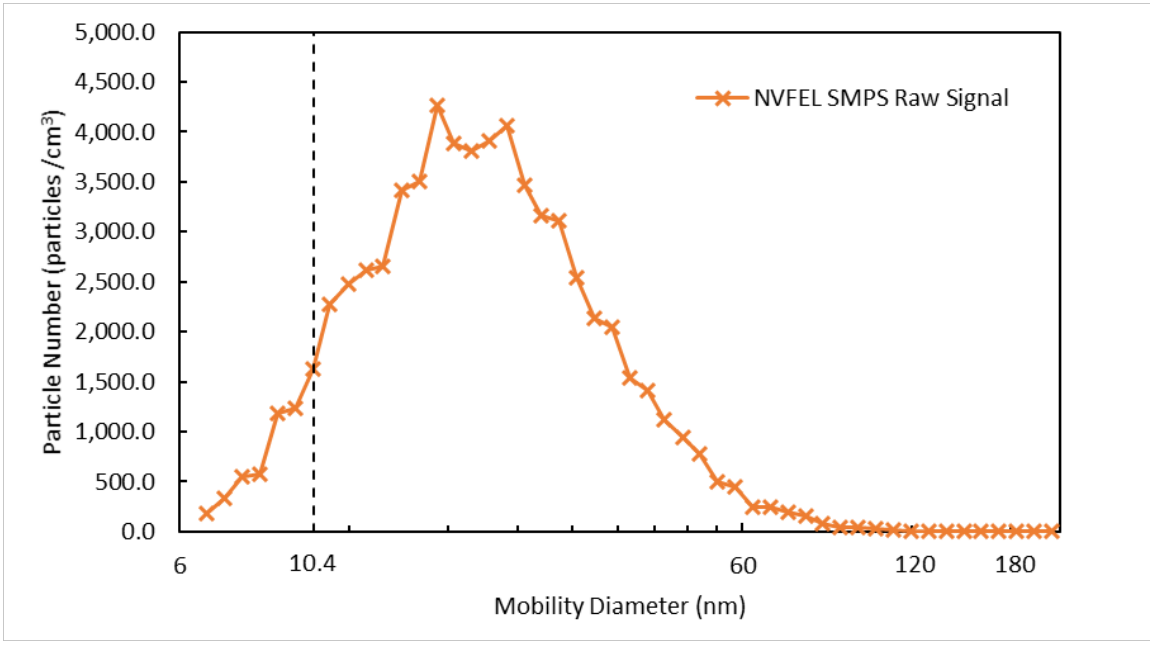

Figure 4.22. NVFEL SMPS scan on GE J-85 burning Jet-A at a power setting of idle.

Again, the difference in the standard deviations of the two penetration efficiency calculations observed in Fig. 4.21. is due to the GE J-85 producing a more constant soot and gas composition over time compared to the Jing Mini-CAST. The TSI and NVFEL SMPS instruments were set up to start the 3 minute measurement scan at the same point in time. This means they will be determining the concentration for a particular size bin at the same point in time. This measurement method would not create an issue if both SMPS instruments

would be analyzing the same sample simultaneously. Due to transit times of the particles from the front of the sampling system to the back where the NVFEL SMPS was located, characteristics of the sample may be different. If the source is variable, then the SMPS instruments will sample a different composition of particles.

Various Fuel, Source, and Setting Penetration Efficiencies

Using the procedure described above for Fig. 4.4., average penetration efficiencies were determined for different fuel types, combustion sources, Mini-CAST settings, and power settings. These are shown in Figs. A.6.11. – A.6.12. in Appendix 6. The procedure described above for Fig. 4.21. was not performed due to the many combinations that could be created from the Figs. A.6.11. – A.6.12.

An example of the alternative fuel in the GE J-85 was not determined for the MS&T sampling system, due to the lack of particles at all sizes and engine power settings.

An example of multiple settings is shown in Fig. 4.23., where the GE J-85 with Jet-A was utilized as in the above Fig. 4.21., but a power setting of Military (Mil) was utilized. This average penetration efficiency dataset shows a close correlation, within an average of 7.82%, to the UTRC Modeled Penetration Efficiency from about 16 nm (first dashed vertical line in Fig. 4.23.) up to about 90 nm (second dashed vertical line in Fig. 4.23.), where the concentration is well above zero. This is not the case below 16 nm or above 90 nm, where the concentration approaches zero at the NVFEL SMPS.

An example of another source and fuel can be seen in Fig. 4.24. where the Jing Mini-CAST with an NRC setting was utilized (also utilized in the Fig. 4.21.). The Mini-CAST utilizes compressed propane and dry shop air to produce the soot source. The NRC setting is a specific fuel to air ratio as well as other parameters that affect the particle morphology. This average penetration efficiency dataset shows a correlation, within an average of 13.7%, to the UTRC Modeled Penetration Efficiency from about 59 nm to 212 nm where the concentration is well above zero as can be seen in Fig. 4.5., but this is not the case for mobility diameters smaller than about 59 nm (dashed vertical line in Fig. 4.24.) where the concentration approaches zero. The large standard deviation error bars in the Fig. 4.24. are due to the very low concentration of particles, which is nearing the detection limits of the SMPS instruments.

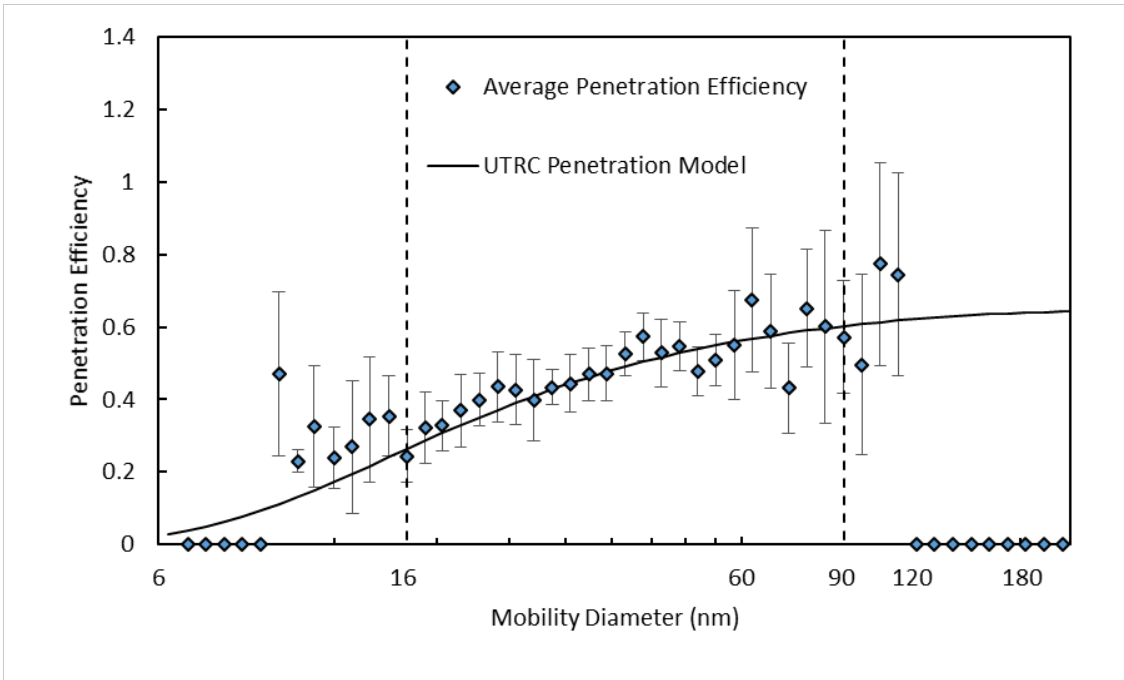

Figure 4.23. MS&T sampling system average penetration efficiency for the GE J-85 with Jet-A at Military (Mil) power setting.

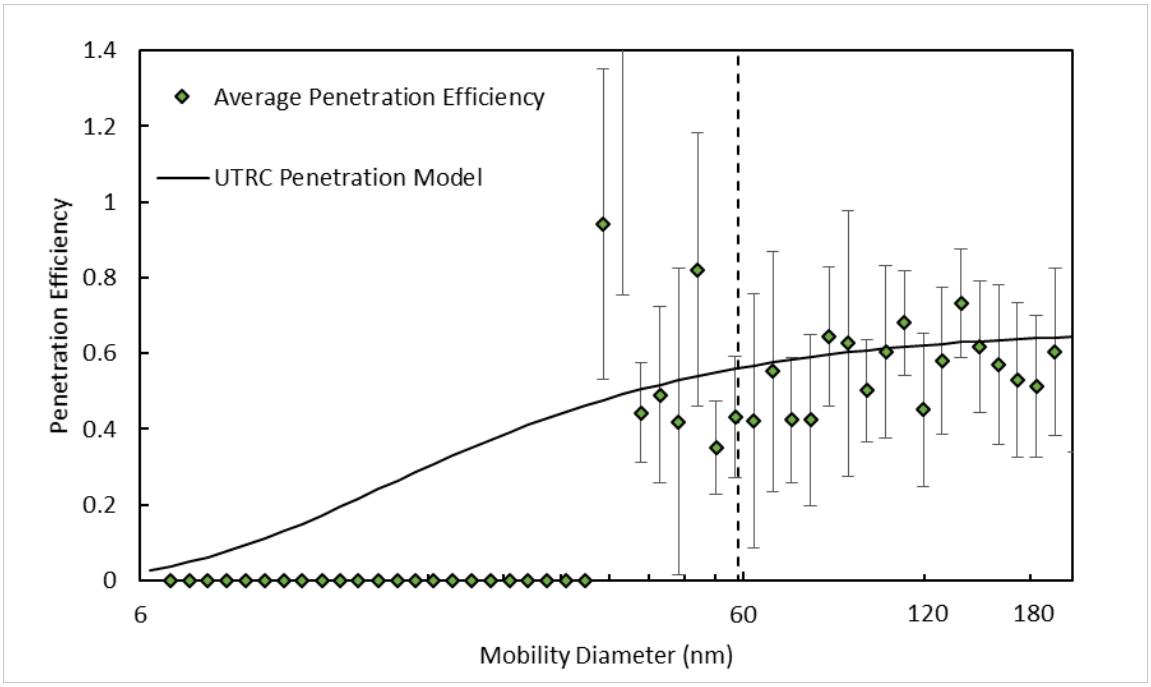

Figure 4.24. MS&T sampling system average penetration efficiency for the Jing Mini-CAST with the NRC Setting.

The average penetration functions that were applicable have portions that show close correlation, within measurement uncertainties, to the model. As the standard deviation increases, the average penetration greatly deviates from the model, which again is due to the lack of particles at the corresponding mobility diameter. Using the standard deviation as the indicator, the Mini-CAST has a close agreement at the larger mobility diameter sizes, and the GE J-85 has a closer agreement at the larger sizes. This is based on the assumptions that the penetration through the MS&T APC does not change over time, fuel, or source, which is proven to be a good assumption based on the UTRC APC penetration results in a later section. The issue that was observed with the low concentration of particles at the NVFEL SMPS inlet due to the high dilutions through the MS&T APC increases the uncertainty and presents question in this measurement. To better understand the penetration through the MS&T sampling system to compare with the UTRC calculated penetration model, this test would need to be conducted again with a functioning SMPS where the NRMRL SMPS was located.

APC Penetration Efficiencies

MS&T APC Penetration Efficiencies

The same procedures utilized to calculate the penetration efficiency for the full AVL sampling system were also utilized for the penetration efficiencies of the MS&T APC. As described in the setup section, the MS&T APC penetration measurements refer to measurements across the section between the inlet of the APC (NRMRL SMPS) and exhaust out of the APC (NVFEL SMPS). Only two MS&T APC penetration efficiencies were collected, Figs 4.25. and 4.26., due to the failure of the NRMRL SMPS.

These average penetration efficiencies show correlation to the model, but it is difficult to tell to what extent due to the limited number of particles illustrated in Fig. 4.27., showing the concentration vs. mobility diameter for the NVFEL SMPS. These are actual concentrations that the SMPS recorded and have not been corrected for dilution like all other measurements and penetrations.

Due to the issues observed with the NRMRL SMPS, little information is available for the penetration efficiency measurements through the MS&T APC. The issue that was observed with the low concentration of particles at the NVFEL SMPS inlet due to the high dilutions through the MS&T APC increases the uncertainty and presents question in the measurements that were collected. To better understand the penetration through the MS&T APC to compare with the UTRC calculated penetration model, this test would need to be conducted again with a functioning SMPS, where the NRMRL SMPS was located as well as at a lower dilution ration on the APC itself to increase the concentration on the outlet side.

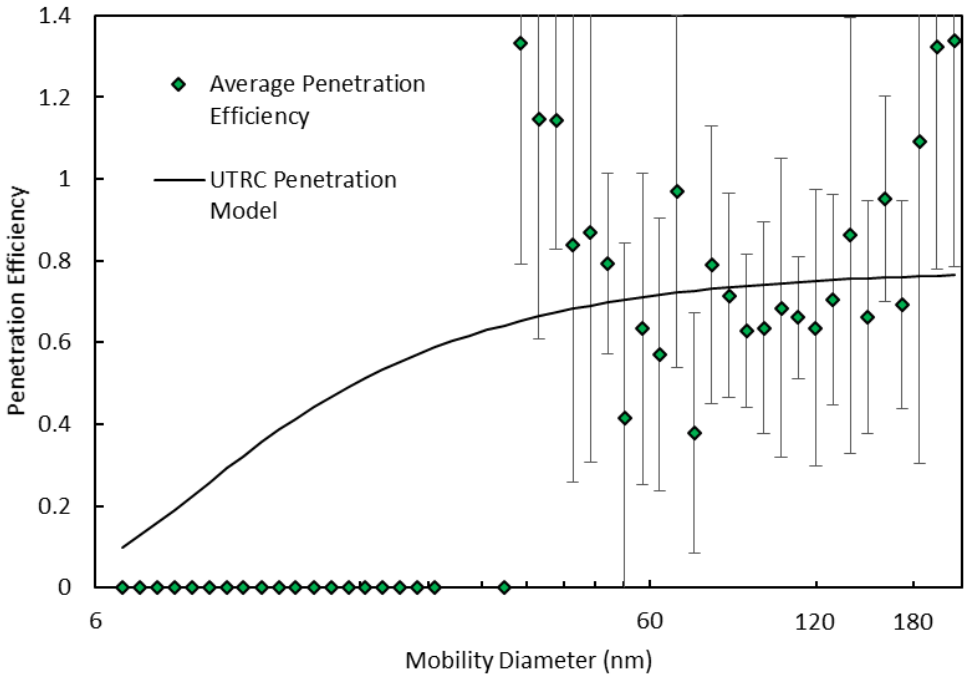

Figure 4.25. Average size dependent penetration data determined from measurements on the Jing Mini-CAST with an NRC setting compared to calculations from the UTRC model.

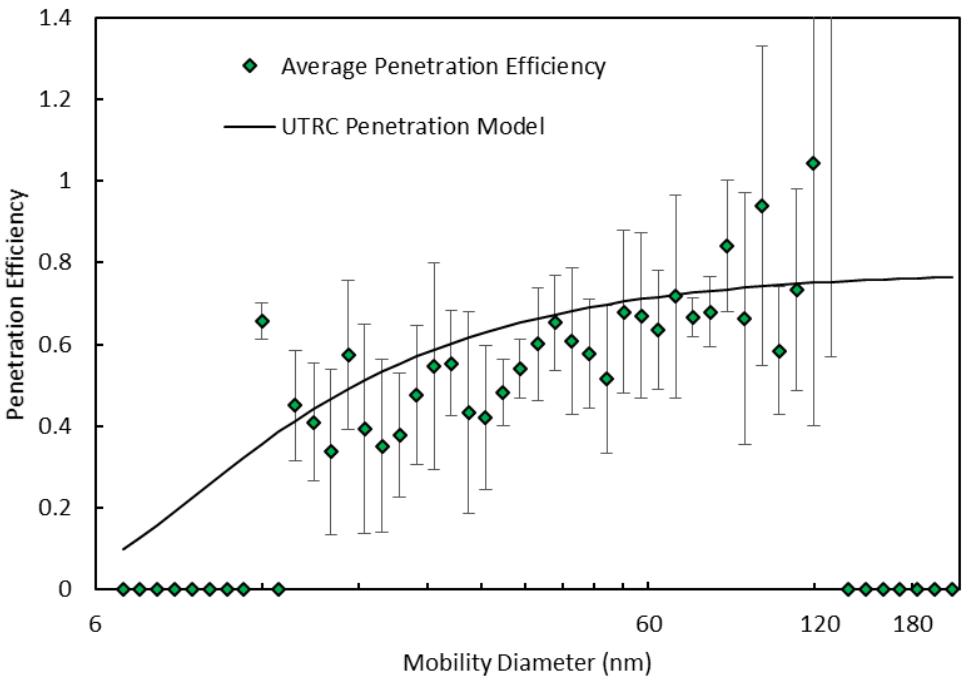

Figure 4.26. The average size dependent penetration curve determined from measurement on the Jing Mini-CAST with a VARIAnT1 setting compared to calculations from the UTRC model.

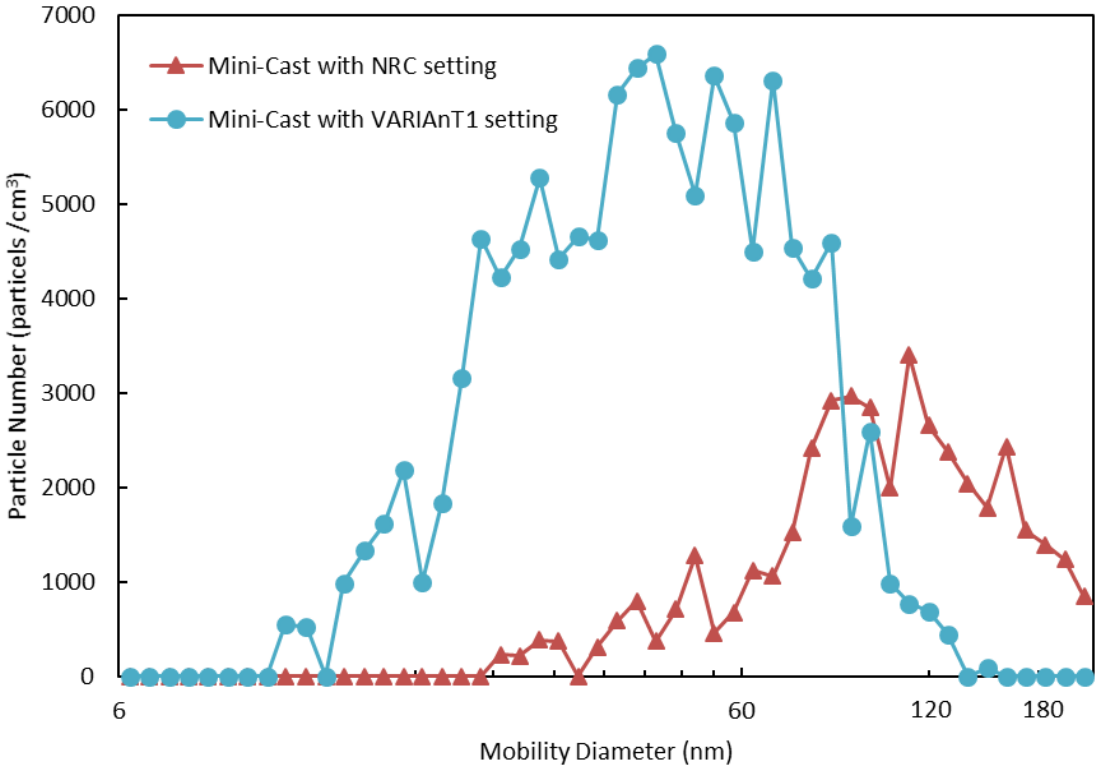

Figure 4.27. NVFEL SMPS mobility diameter distributions measured after the MS&T APC utilizing two settings on the Jing Mini-CAST.

UTRC APC Penetration Efficiencies

The same procedures utilized to calculate the penetration efficiency for the full AVL sampling system were also utilized for full penetration efficiencies for the UTRC APC, which was sampling from the ALV sampling system. As described in the setup section, the UTRC APC penetration measurements refer to the measurements between the inlet of the APC (AEDC SMPS) and exhaust out of the APC (UTRC SMPS). Once again, the measurements obtained from the UTRC SMPS have higher uncertainties compared to the other SMPS instruments, where the concentration is much higher. This is also due to the high dilution from inlet to exit of the APC (up to 3390:1), and the high loss of particles through the APC VPR/dilution system. Utilizing the best data with the highest concentrations, Fig 4.28., and closest correlations between the measured penetration efficiencies and the UTRC calculated model penetration efficiencies a full penetration efficiency measurement can be determined. In this case, the Jing Mini-CAST with the NRC setting and the GE J-85 operating on Jet-A as the fuel at a power setting of idle data sets were utilized to determine a full average penetration efficiency measurement. This full average penetration efficiency measurement of the UTRC APC was compared to the UTRC calculation model within the mobility diameters of interest (6 nm to 212 nm) shown in Fig. 4.29.

The split point at about 55 nm was utilized to determine the transition from the GE J-85 penetration efficiencies to the Mini-CAST penetration efficiencies. When comparing the full average penetration efficiency from measurements to the UTRC penetration efficiency model calculations, the full average penetration efficiency deviates from the model by an average of 5.5%, which is within measurement uncertainties of 14% that are quoted by TSI for a single measurement. The only locations where the 5.5% average difference from the model doesn't hold true is below 10.4 nm (dashed vertical line in Fig. 4.29.) where the concentration of particles is approaching the limit of detection of the SMPS instrument. The difference in the standard deviations of the two penetration efficiency measurements, observed in Fig. 4.29., is due to the GE J-85 producing a more constant soot and gas composition over time compared to the Jing Mini-CAST. The AEDC and UTRC SMPS instruments were set up to start the 3 minute measurement scan at the same point in time. This means they will be determining the concentration for a particular size bin at the same point in time. This measurement method would not create an issue if both SMPS instruments were analyzing the same sample simultaneously. Due to transit times of the particles from the inlet of the APC to the back where the UTRC SMPS was located, characteristics of the sample may be different. If the source is variable, then the SMPS instruments have the potential of sampling a different composition of particles.

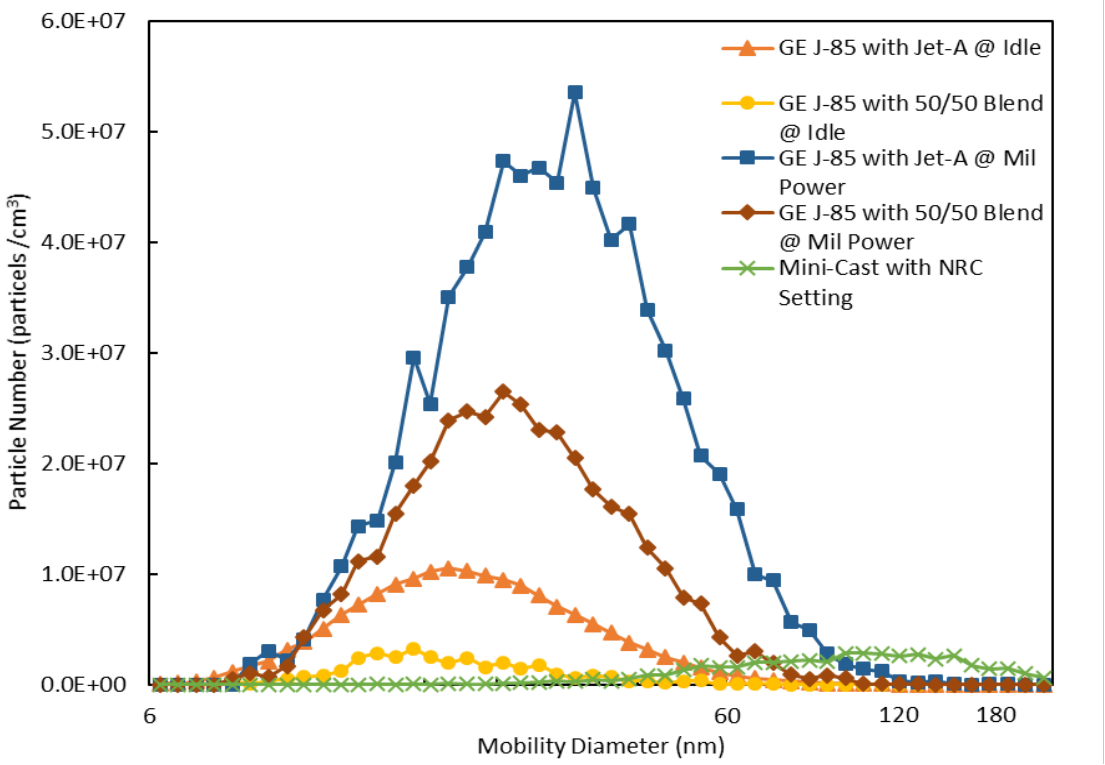

Figure 4.28. Measured Lognormal mobility diameter distributions produced by multiple sources, fuels, and settings recorded by the UTRC SMPS sampling from the outlet of the UTRC APC.

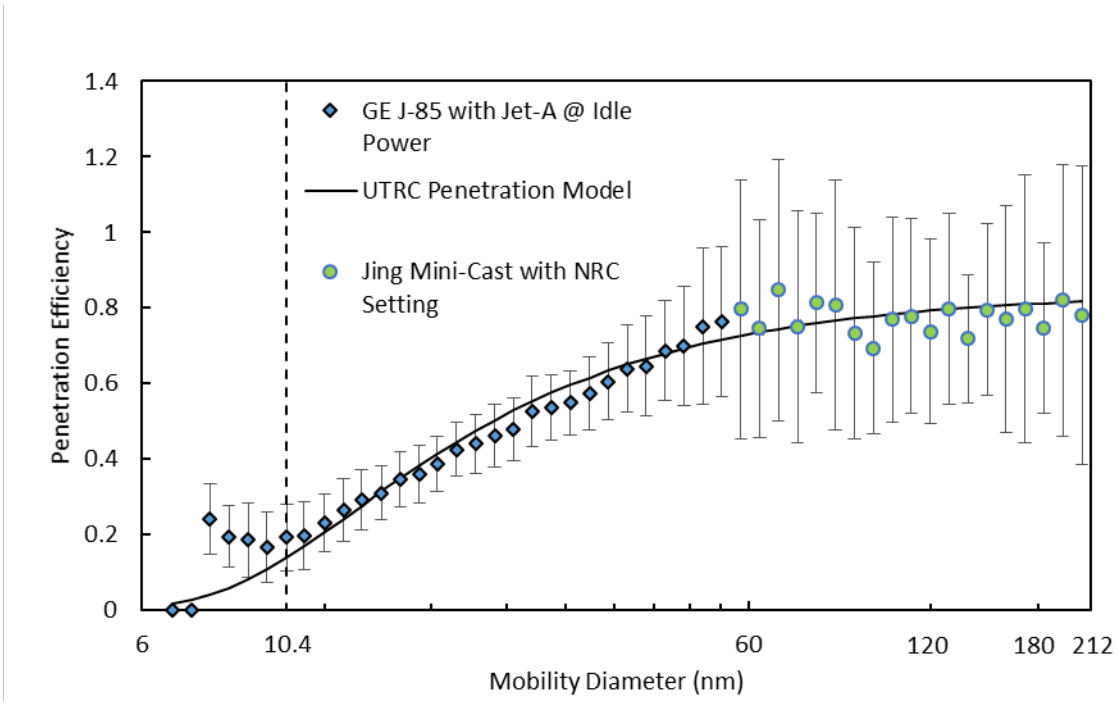

Figure 4.29. Complete mobility diameter average penetration efficiency for the UTRC APC using measurements of mobility diameter distributions from two different particle sources compared to the UTRC model calculation.

Various Fuel, Source, and Setting Penetration Efficiencies

Using the procedure described for Fig. 4.4., average penetration efficiencies were determined for different fuel types, combustion sources, Mini-CAST settings, and power settings. These are shown in Figs. A.6.13. – A.6.17. in Appendix 6. The procedure described above for Fig. 4.29. was not performed due to the many combinations that could be created from the Figs. A.6.13. – A.6.17.

An example of the alternative fuel can be seen in Fig. 4.30. where the same GE J-85 with a power setting of Idle was utilized as in Fig. 4.4., but the fuel was a mixture of 50% Camelina and 50% Jet-A. This average penetration efficiency dataset shows close correlation, within an average of 11.6%, to the UTRC Modeled Penetration Efficiency from 12 nm (first dashed vertical line in Fig. 4.30.) up to about 32 nm (second dashed vertical line in Fig. 4.30.), where the concentration is above zero as can be seen in Fig. 4.28., but this is not the case before 12 nm or after 32 nm, where the concentration approaches zero at the UTRC SMPS.

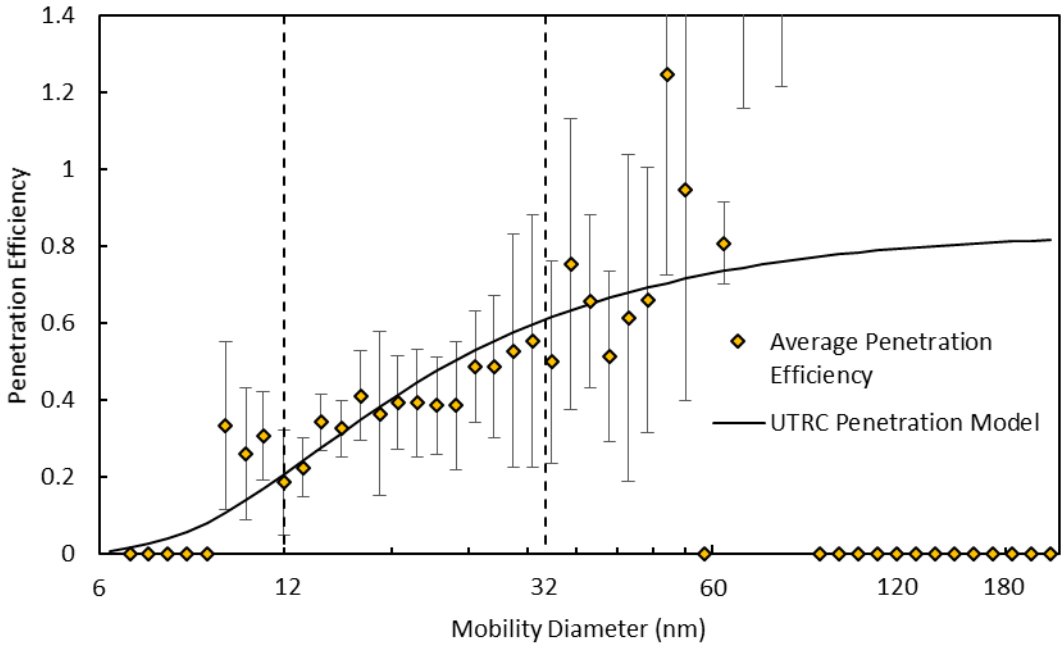

Figure 4.30. UTRC APC average penetration efficiency for the GE J-85 with 50/50 Camelina and Jet-A Blend Fuel at Idle power setting.

An example of multiple settings is shown in Fig. 4.31., where the GE J-85 with Jet-A was utilized as in the above Fig. 4.21. but a power setting of Military (Mil) was utilized. This average penetration efficiency dataset is not as close of a correlation as the other average penetration efficiencies shown thus far. The measured penetration efficiencies seem to match the model almost exactly where the mean diameter of the distribution takes place around 30 nm, Fig. 4.28. but starts to deviate as the mobility diameter starts to get larger or smaller and the concentration decreases. The standard deviation also starts to increase when moving up or down in size. The standard deviation also increases dramatically when outside the acceptable concentration ranges, which in this case is any mobility diameter less than about 10 nm (first dashed vertical line in Fig. 4.31.) and greater than about 110 nm (second dashed vertical line in Fig. 4.31.). The exponential increase in the penetration efficiency is notable at the lower sizes, as seen in previous graphs and is again due to the concentration approaching the limit of detection of the SMPS instrument. The measured penetration efficiencies, when compared to the UTRC calculated model penetration efficiencies, have an average of about 25%, within the range of 10 nm to 110 nm. This test would need to be performed again to determine if this is actually a deviation from the UTRC model or an issue due to the increased uncertainties associated with the difficult penetration measurements through the APC.

An example of another source and fuel can be seen in Fig. 4.32. where the Jing Mini-CAST with an NRC setting was utilized (also utilized in Fig. 4.29.). The Mini-CAST utilizes compressed propane and dry shop air to produce the soot source. The NRC setting is a specific fuel to air ratio as well as other parameters that affect the particle morphology. This average penetration efficiency dataset shows a correlation within an average of 15.4% to the UTRC Modeled Penetration Efficiency from about 58 nm (dashed vertical line in Fig. 4.32.) to 212 nm, where the concentration is well above zero as can be seen in Fig. 4.28. This is not the case for mobility diameters smaller than about 58 nm where the concentration approaches zero. The large standard deviation error bars in the Fig. 4.32. are due to the very low concentration of particles, which is nearing the detection limits of the SMPS instruments.

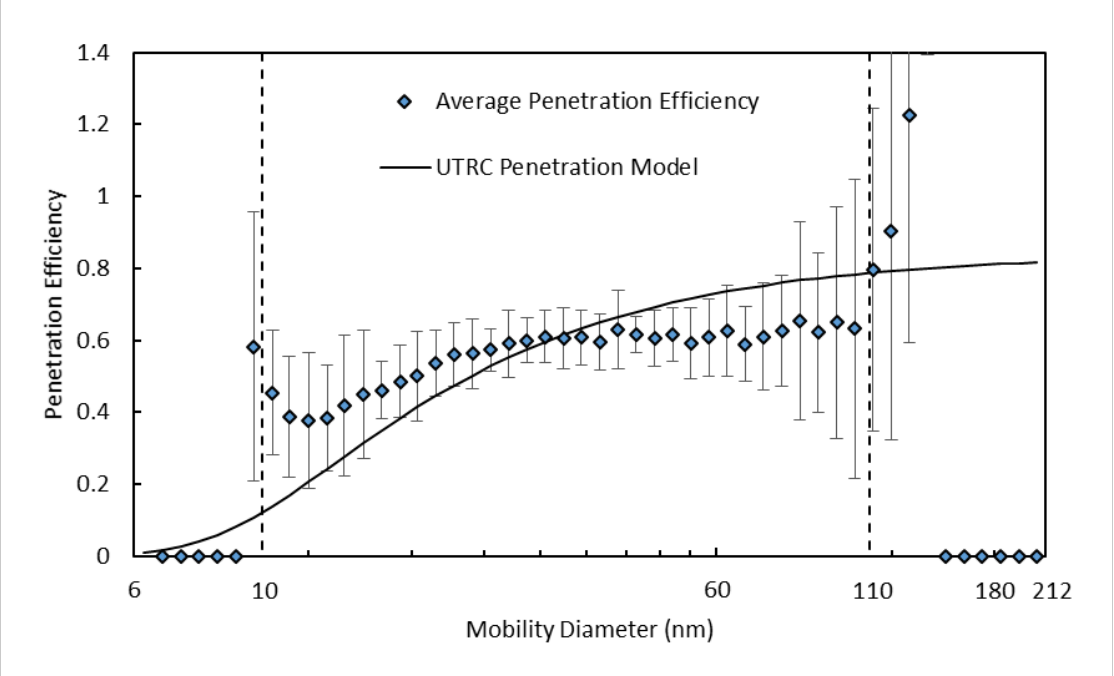

Figure 4.31. UTRC APC system average penetration efficiency for the GE J-85 with Jet-A at Military (Mil) power setting.

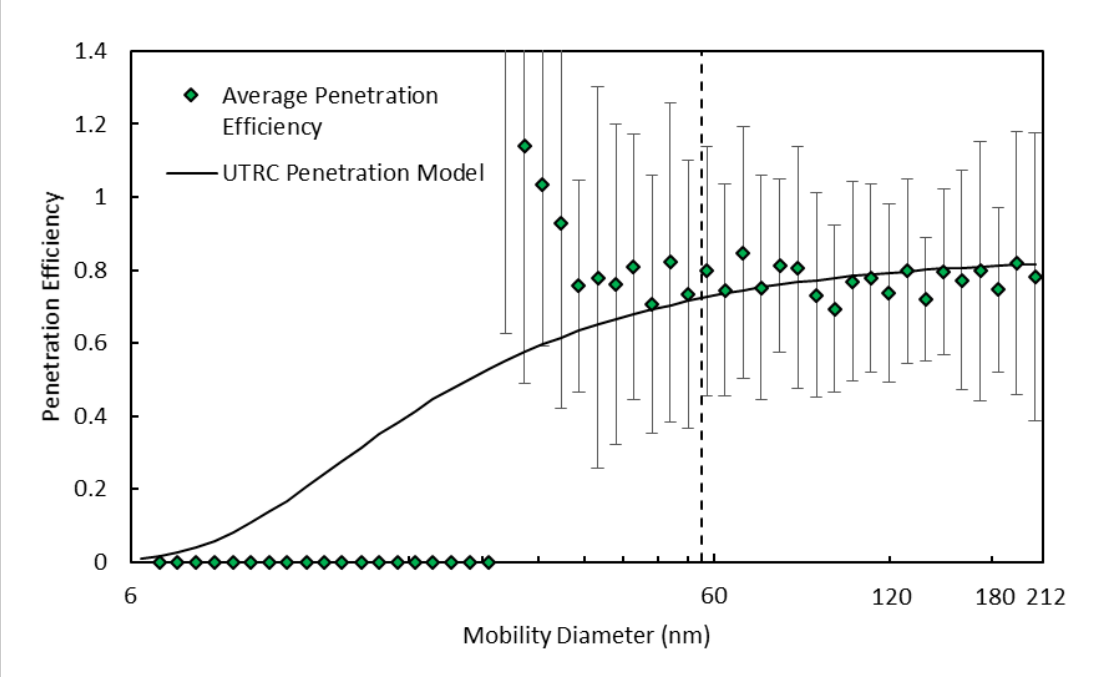

Figure 4.32. UTRC APC system average penetration efficiency for the Jing Mini-CAST with the NRC Setting.

The average penetration functions that were applicable have portions that show close correlation, within measurement uncertainties, to the model. As the standard deviation increases the average penetration greatly deviates from the model which is due to the lack of particles at that mobility diameter. Using the standard deviation as the indicator, the Mini-CAST has a close agreement at the larger mobility diameter sizes where the GE J-85 has a closer agreement at the smaller sizes. The issue that was observed with the low concentration of particles at the UTRC SMPS inlet due to the high dilutions through the UTRC APC increases the uncertainty and presents a question to the measurement validity. To better understand the penetration through the UTRC APC compared with the UTRC calculated penetration model, this test would need to be conducted again with a lower dilution ratio on the APC itself to increase the concentration on the outlet side for better UTRC SMPS measurements. Lowering the dilution ratio in the APC may increase the concentration to a point where the CPC in the APC is out of range, but for these penetration efficiency measurements this is not a concern. This was not performed during the campaign due to other test objectives that required the CPC measurement.

Penetration Efficiency Model Comparisons

From the results above, the measured penetration efficiencies match the UTRC calculated model in most cases, where the standard deviations are relatively low, within the measurement uncertainties of 14%. As a result, the UTRC calculated models will be utilized in this section for the comparisons of the two sampling systems and the penetration efficiency comparisons of the two APC instruments.

Sampling System Model Comparison

When comparing the models of the full sampling systems, Fig. 4.33., the AVL sampling system penetration is almost identical to the MS&T sampling system penetration. The greatest difference is at 212 nm mobility size, which has about a 6% deviation from each other. To get the difference between the two models here, the reference (here the MS&T Sampling System model) is subtracted from the calculated penetration efficiencies at each mobility diameter and then is divided by the reference. The average is taken of these values and is then multiplied by 100 to get a percent. The 6% difference is to be expected because each system was built to the ARP6320 specifications, which are very specific to enable the comparison of results for certification and regulation purposes.

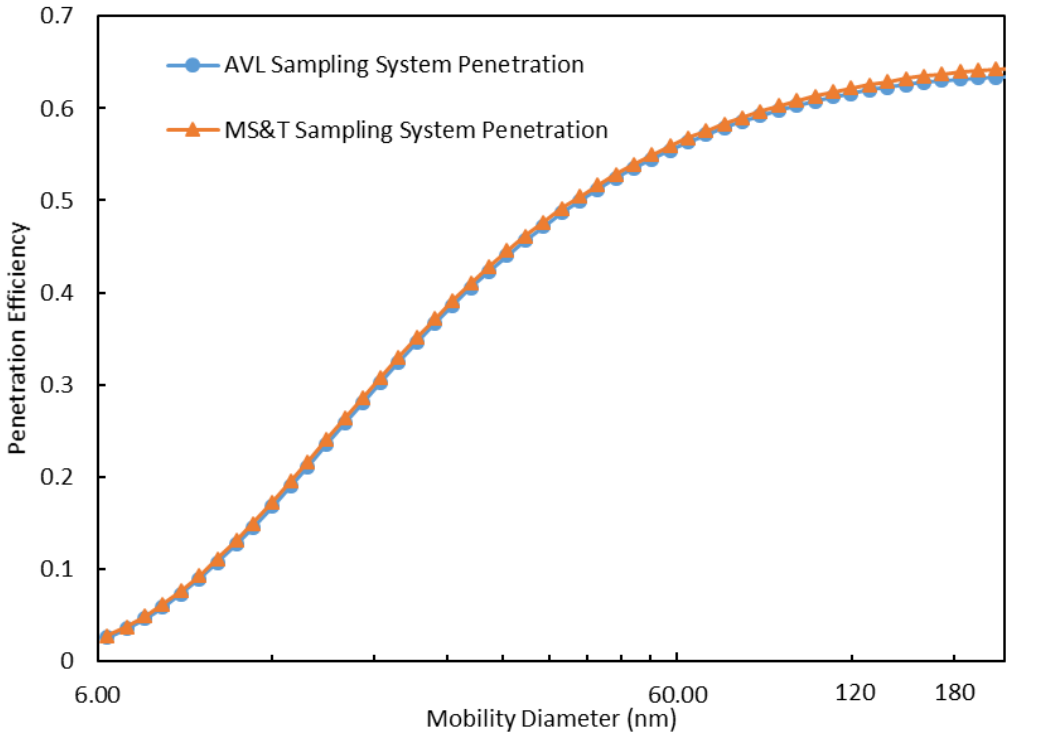

Figure 4.33. UTRC calculated model penetration efficiencies for both sampling systems.

VPR/Dilution System APC Model Intercomparison

When comparing the APC modeled penetration efficiencies of the UTRC APC with the MS&T APC, Fig. 4.34., they are very different and have a maximum of an 84% deviation from each other at the smallest mobility diameter of 6 nm. The calculation of this difference was performed as described in the sampling system model comparison section and the MS&T APC is the reference instrument in the calculation. The 84% deviation between the two models is due to the internal heating, thermophoretic losses, and diffusional losses for each particle counter and volatile particle remover that makes up the number counting instrument which in this case is the APC instruments. Due to these manufacturing differences, each APC must be calibrated and verified to account for the losses.

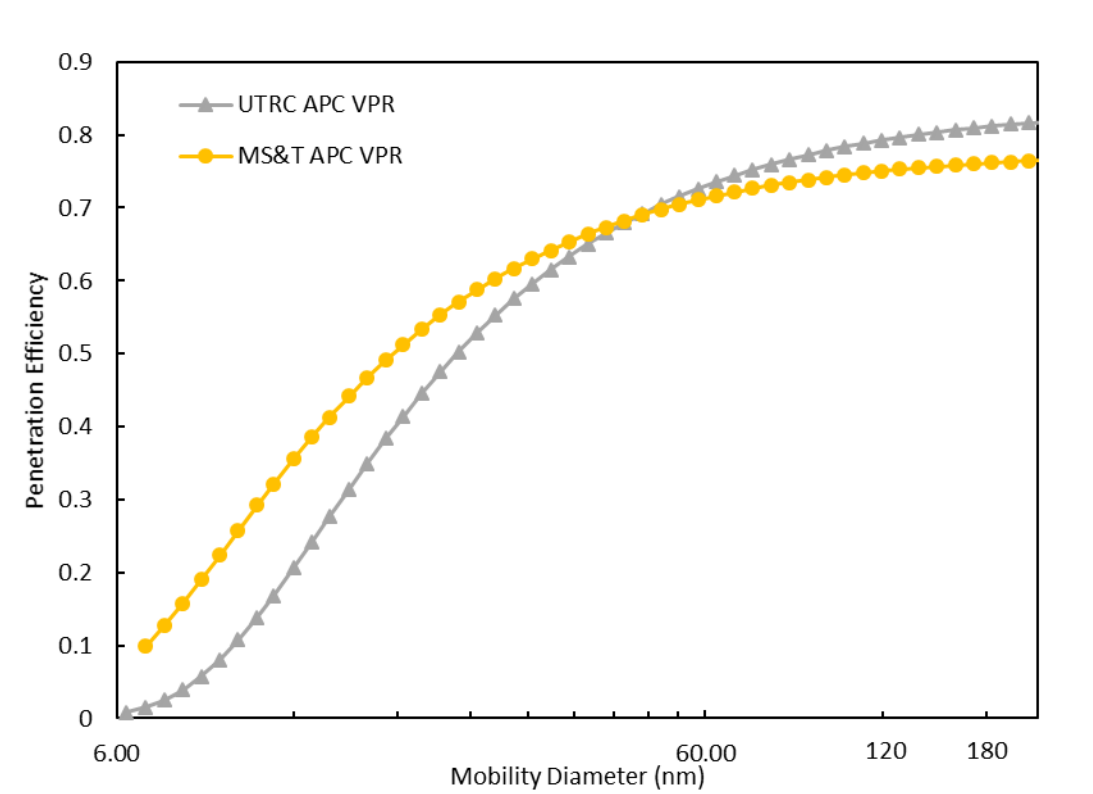

Figure 4.34. UTRC calculated model penetration efficiencies for both APC instruments.

Upstream and Downstream AVL Sampling System Model Comparison

Comparing the upstream half of the AVL Sampling system UTRC modeled penetration efficiency to the downstream half UTRC modeled penetration efficiency, most of the losses at the larger sizes were more predominate in the upstream half of the sampling system. In reference to the smaller sizes, the losses were more predominant in the downstream portion of the sampling

system, seen in Fig. 4.35., because of the long lengths of line. The long line lengths increase losses due to diffusional losses. This was expected from the model calculations shown in Fig. 2.1. The larger particles are primarily lost due to thermophoresis, which affects all size ranges because it is not size dependent. This is only the case because the larger particles are not affected by other loss mechanisms as much as small particles. At the Dekati Dilutor, the sample is mixed with nitrogen to dilute and cool the sample. The cooling is needed because the instruments cannot handle the extreme temperatures of the turbine exhaust. The nitrogen is also added to prevent condensation and to dilute the concentration of the sample to a reasonable level to keep the number instrument functioning properly in single particle counting mode.

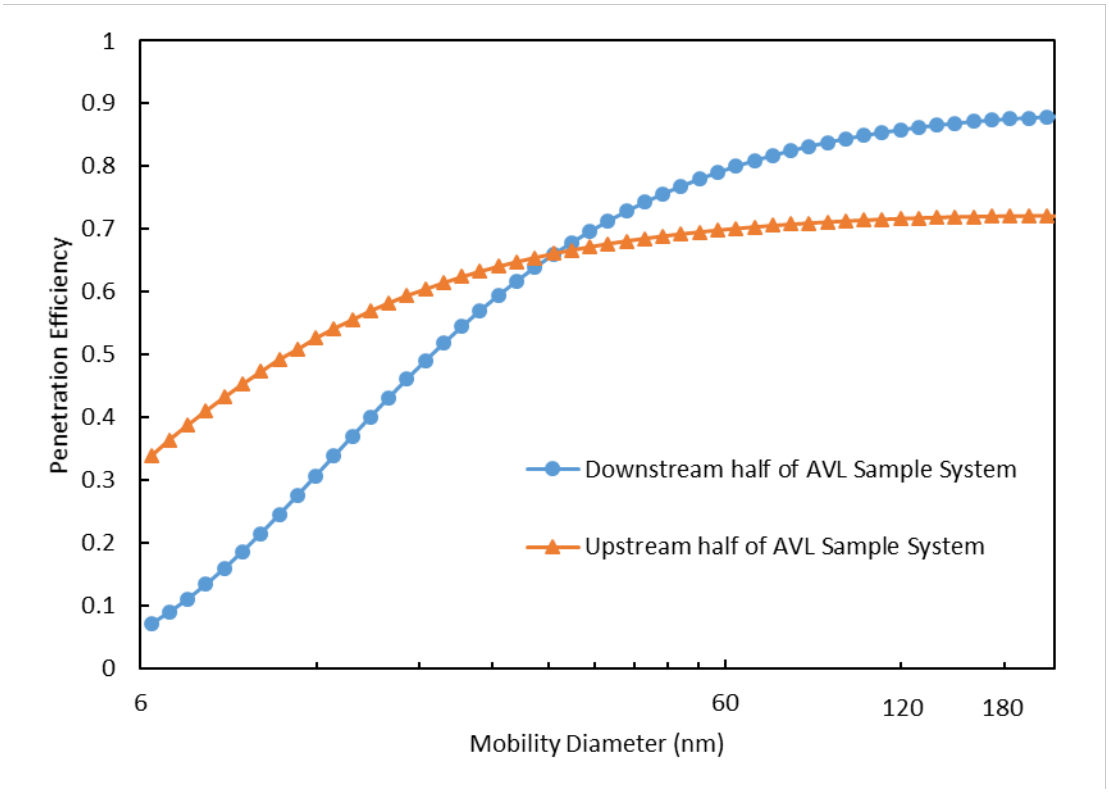

Figure 4.35. UTRC calculated model penetration efficiencies for upstream and downstream of the AVL sampling system.

Error and Uncertainty

Standard Deviation Calculation

A lot of assumptions and measurement error went into each calculation and measurement, respectively. Due to these assumptions, the SAE E-31 committee has quoted a ±25% uncertainty in the measurement, without accounting for the losses shown above. The committee is currently working to lower these

uncertainties and taking into account these models is one approach. One of the factors that could contribute to the model error would be the assumption of a constant density of the particles. A particle density of 1 g/cm^3 was assumed throughout. This is very unlikely due to the string like structure of these carbon particles. Utilizing Equation 4.1, the standard deviation was calculated for all measured penetration efficiencies which is illustrated in the results.

$$\sigma = \sqrt{\frac{1}{N-1}\sum_{i=1}^{N}(x_i - \mu_m)^2} \qquad \text{Equation 4.1}$$

where σ is the standard deviation of the penetration efficiencies data sets per mobility diameter, μ_m is the mean of all penetration efficiencies in the data set, x is the individual penetration efficiency values, and N is the number of penetration efficiencies in our data set.

CHAPTER FIVE

SUMMARY AND CONCLUSIONS

The objective of this thesis is to compare measured penetration efficiencies to the AIR6241 UTRC calculated penetration efficiency model to increase the viability and validity of using the model instead of performing penetration efficiency measurements on all ARP6320 compliant systems. The secondary objective is to compare the penetration efficiencies of the AVL sample system and the MS&T sample system to better validate the constraints in the ARP6320 to insure they are sufficiently constrained to minimize the effects of losses in the system and minimize the difference in these losses between systems.
To accomplish these objectives two ARP6320 non-volatile particle emission sampling systems, the MS&T and AVL sampling systems, along with six Scanning Mobility Particle Sizers (SMPS) instruments were utilized in the EPA VARIAnT2 test campaign. The SMPS instruments measured mobility diameter vs. concentrations at various locations on the sampling systems as described in Chapter 3. Taking the ratio of various SMPS results, penetration efficiencies were determined for both sampling systems and APC instruments. These results were compared to the results of the calculations performed (Chapter 2) using the UTRC calculated penetration efficiency models shown in the Results Section, Chapter 4.

Results and Discussion

The results were broken down into three main parts: AVL sampling system penetration efficiencies, MS&T sampling system penetration efficiencies, and APC penetration efficiencies.

For the AVL sampling system penetration efficiencies, the best correlation between the measured penetration efficiencies and the UTRC calculated model was determined and graphed in Fig. 4.7. The results showed a deviation of an average of 6.71%. The full AVL sampling system was broken into two parts: upstream and downstream halves. The best measured full average penetration efficiency for the upstream half of the AVL sampling system deviated from the model by an average of 5.52%, as seen in Fig. 4.12. The best measured full average penetration efficiency for the downstream half of the AVL sampling system deviated from the model by an average of 5.39%, as seen in Fig. 4.17. All of these penetration efficiencies correlated with the model well within the measurement uncertainties of 14% that are quoted by TSI for a single SMPS measurement.

The deviations between the calculated UTRC model penetration efficiencies and the determined penetration efficiencies from measured data were again calculated by taking the difference, the calculated UTRC model was subtracted from the penetration efficiencies at each mobility diameter, and then is divided by the calculated UTRC model. The average is taken of these values and is then multiplied by 100 to get a percentage. When comparing the measured MS&T sampling system penetration efficiencies to the UTRC calculated model penetration efficiencies, an average of 11.84% deviation was calculated using the method described above when ignoring the mobility diameters below 10.4 nm due to the lack of particles. This deviation again is well within the measurement uncertainties of 14% that are quoted by TSI for a single SMPS measurement. The 11.84% deviation could probably have been reduced if it wasn't for the failure of the NRMRL SMPS and the needed assumption that the penetration efficiency through the MS&T APC remained unchanged during the test campaign.

Two different APC instruments were utilized during the VARIAnT2 Test campaign, the UTRC APC and the MS&T APC, to measure the number of particles. The UTRC APC was located on the AVL sampling system and the MS&T APC was located on the MS&T sampling system. The best measured penetration efficiencies for the UTRC APC when compared to the UTRC calculated model penetration efficiencies deviated from each other by an average of 14.3%. This is close to the measurement uncertainties for a single SMPS measurement. The best measured penetration efficiencies for the MS&T APC, when compared to the UTRC calculated model penetration efficiencies, were not able to be determined due to a very limited amount of data. Only two penetration efficiency measurements were obtained on the Jing Mini-CAST source, due to the failure of the upstream instrument (NRMRL SMPS).

The biggest issues with making penetration efficiency measurements is the lack of particles at various sizes for the SMPS instruments to get an accurate reading. This was solved in most cases by combining the penetration efficiencies from two different sources (GE J-85 and Jing Mini-CAST). Even with combining the sources it was still not possible to get a full penetration efficiency measurement for the UTRC APC due to the lack of particles below 10.4 nm. This again was due to the high dilution ratio (~3390:1) of the APC needed to keep its number counting instrument (CPC) within range for all sources.

Other issues were observed that demonstrate how difficult these penetration measurements are, for instance the unknown cause in the deviation from the model in Figs. 4.9., 4.13., and 4.14. In all cases the measured penetration efficiencies deviated from the model. Also in all cases, when the measured penetration efficiency starts to deviate from the model, the standard deviation

starts to increase. This could be an indication of issues with SMPS instruments or changes in configurations between SMPS scans that were not documented.

Recommended Additional Research

Additional research is needed to determine the causes in the deviations in the models and to determine, in some instances, if the actual penetration efficiencies match the model with confidence. Also, to better understand the penetration efficiencies through the MS&T sampling system, the set of experiments would need to be completed again with a functioning SMPS where the NRMRL SMPS was located.

Other experiments could be conducted to lower the uncertainties and answer some of the issues observed when the measurements deviated from the model. These same experiments could help answer unexplained increases in standard deviations not due to low concentrations. In order to do this, the setup would need to be replicated and the experiments in question would need to be conducted again. This would be a costly undertaking in terms of time and resources which is not possible at this time.

Final Remarks

Based on the issues observed, the cost associated with these measurements, the delicate nature of making precise measurements with a lab instrument that is not meant for these conditions, and the uncertainties associated these measurements, the model presents a more consistent, with less uncertainty, prediction of the penetration efficiencies of these systems. These are some of the reasons SAE recommends the utilization of this UTRC penetration efficiency model over actual penetration efficiency measurements.

When comparing the calculated UTRC models and the penetration efficiencies from measurements, the ARP 6320 seems to have sufficiently constrained the recommended sample systems used for this type of measurement. This ensures similar measurements and the highest possible penetration efficiency.

LIST OF REFERENCES

1. Jing Ltd, CAST Principle, 2009, (http://sootgenerator.com/CAST_principle.htm)
2. Gunston, Bill (2006). World Encyclopedia of Aero Engines, 5th Edition. Phoenix Mill, Gloucestershire, England, UK: Sutton Publishing Limited. ISBN 0-7509-4479-X. (http://www.456fis.org/GENERAL_ELECTRIC_J85.htm)
3. P.Lobo, D.E.Hagen, P.D.Whitefield, D.J.Alofs, Physical Characterization of Aerosol Emissions from a Commercial Gas Turbine Engine, Journal of Propulsion and Power, Vol. 23, No. 5, September–October 2007.
4. R.P.Howard, K.M.Stephens, P.D.Whitefield, D.E.Hagen, S.L.Achterberg, E.A.Black, S.C.Herndon, M.T.Timko, R.C.Miake-Lye, J.S.Kinsey, and D.Gemmill, Interim Particulate Matter Test Method For The Determination Of Particulate Matter From Gas Turbine Engines, SERDP Project WP-1538, Final Report, 29-July 2011.
5. A.Crayford, M.Johnson, R.Marsh, Y.Sevcenco, D.Walters, P.Williams, S.Christie, W.Chung, A.Petzold, A.Ibrahim, D.Delhaye, P.Quincey ,P.Bowen, H.Coe, D.Raper, C.Wilson, SAMPLE III-SC01: Studying, sampling and measuring of aircraft particulate emissions, Final Report, 23rd October 2011 (http://easa.europa.eu/document-library/research-projects/easa2010fc10-sc01).
6. A.Crayford, M.Johnson, R.Marsh, Y.Sevcenco, D.Walters, P.Williams, A.Petzold, P.Bowen, J.Wang, D.Lister, SAMPLE III-SC02: Studying, sampling and measuring of aircraft particulate emissions, Final Report, 27th November 2012 (http://easa.europa.eu/document-library/research-projects/easa2010fc10-sc02).
7. A.Crayford, M.Johnson, A.Llamedo, P.Williams, P.Madden, R.Marsh, P.Bowen, SAMPLE III-SC03: Studying, sampling and measuring of aircraft particulate emissions, Final Report, 15th November 2013 (http://easa.europa.eu/document-library/research-projects/easa2010fc10-sc03).
8. A.Crayford, M.Johnson, Y.Sevcenco, P.Williams, SAMPLE III-SC05: Studying, sampling and measuring of aircraft particulate emissions, Final Report, 31st October 2014 (http://easa.europa.eu/document-library/research-projects/easa2010fc10-sc05).
9. L.Durdina, B.T.Brem, M.Abegglen, P.Lobo, T.Rindlisbacher, K.A.Thomson, G.J.Smallwood, D.E.Hagen, B.Sierau, J.Wang, Determination of PM mass emissions from an aircraft turbine engine using particle effective density, Atmospheric Environment, vol. 99, pp.500-507 (2014).

10. J.Kinsey, Characterization of Emissions from Commercial Aircraft Engines during the Aircraft Particle Emissions eXperiment (APEX) 1 to 3. U.S. EPA Report EPA-600/R-09/130, October 2009.
11. B.E.Anderson, A.J.Beyersdorf, C.H.Hudgins, J.V.Plant, K.L.Thornhill, E.L.Winstead, L.D.Ziemba, R.Howard, E.Corporan, R.C.Miake-Lye, S.C.Herndon, M.Timko, E.Woods, W. Dodds, B.Lee, G.Santoni, P.Whitefield, D.Hagen, P.Lobo, W.B.Knighton, D.Bulzan, K.Tacina, C. Wey, R.Vander Wal, A.Bhargava, J.Kinsey, D.S.Liscinsky, Alternative Aviation Fuel Experiment (AAFEX), NASA Report NASA/TM–2011-217059, February 2011.
12. P.Lobo, L.Durdina, G.Smallwood, T.Rindlisbacher, F.Siegerist, E.Black, Z.Yu, A.Mensah, D.Hagen, R.Miake-Lye, K.Thomson, B.Brem, J.Corbin, M.Abegglen, B.Sierau, P.Whitefield, J.Wang, “Measurement of Aircraft Engine Non-Volatile PM Emissions: Results of the Aviation-Particle Regulatory Instrumentation Demonstration Experiment (A-PRIDE) 4 Campaign”, Aerosol Sci. & Techn. 7, 472-484 (2015)
13. A.Bhargava, D.Liscinsky, R.McKinney, B.Anderson, A.Petzold, R.A.Miake-Lye, Characterizing Particulate Matter Emissions from Aircraft Engines, ASME Turbo Expo, paper no. GT2012-69598 (2012).
14. S.J.Yook and D.Y.H.Pui, Estimation of Penetration Efficiencies through NASA Sampling Lines, submitted to NASA Glenn Research Center (2005).
15. P.A.Baron and K.Willeke, Aerosol measurement: Principles, Techniques, and Applications, Wiley (2001).
16. SAE Aerospace, Aerospace Information Report 6504, Procedure for the Calculation of non-volatile Particulate Matter Sampling and Measurement System Penetration Functions and System Loss Correction Factors, September 2016.
17. SAE Aerospace, Aerospace Recommended Practice 6320, Procedure for the Continuous Sampling and Measurement of Non-Volatile Particulate Matter Emissions from Aircraft Turbine Engines, November 2016.
18. SAE Aerospace, Aerospace Information Report 6241, Procedure for the Continuous Sampling and Measurement of Non-Volatile Particle Emissions from Aircraft Turbine Engines.
19. D.B.Kittelson and J.H.Johnson, "Variability in Particle Emission Measurements in the Heavy-Duty Transient Test," SAE Paper No. 910738 (1991).
20. D.B.Kittelson, Expert Review of SAE E-31 Method to Estimate Emissions of Non-Volatile Particulate Matter (nvPM) from Aircraft Engines and Correct for Sample Train Losses, (unpublished report to U.S. EPA, contract EP-C-12-011, work assignment 2-22), August 8, 2013.

21. B.Giechaskiel, L.Ntziachristos, and Z.Samaras, Effect of ejector dilutors on measurements of automotive exhaust gas aerosol size distributions, Meas. Sci. Technol., vol 20, 045703, (2009).
22. L.C.Kenny, R.Gussman, and M.Meyer, Development of a Sharp-Cut Cyclone for Ambient Aerosol Monitoring Applications, Aerosol Science and Technology,32:4, 338-358 (2000).
23. AVL List GmbH, Graz – Austria, AVL APC 489 Particle Counter Manual /Product Guide, PN AT2858E, Rev. 07, November 2012.
24. H.Hollick, and D.Liscinsky, United Technologies Research Center Line Loss Tool, November 21, 2014.
25. D.B.Kittelson and J.H.Johnson, "Variability in Particle Emission Measurements in the Heavy-Duty Transient Test," SAE Paper No. 910738 (1991).
26. H.E.Hesketh, Fine Particles In Gaseous Media, Second Edition, Lewis Publishers, Inc. (1986).
27. AVL List GmbH, Graz – Austria, AVL Micro Soot Sensor AVL Conditioning Unit Operating Manual, PN AT2249E, Rev. 13, April 2013.
28. Artium Technologies, Inc., LII 300 User Manual, Rev. 8, 2014.
29. TSI Inc., 3938 SMPS_US_5001531_RevA_Web.pdf Manual

APPENDIX

Appendix 1. APC Calibrations .

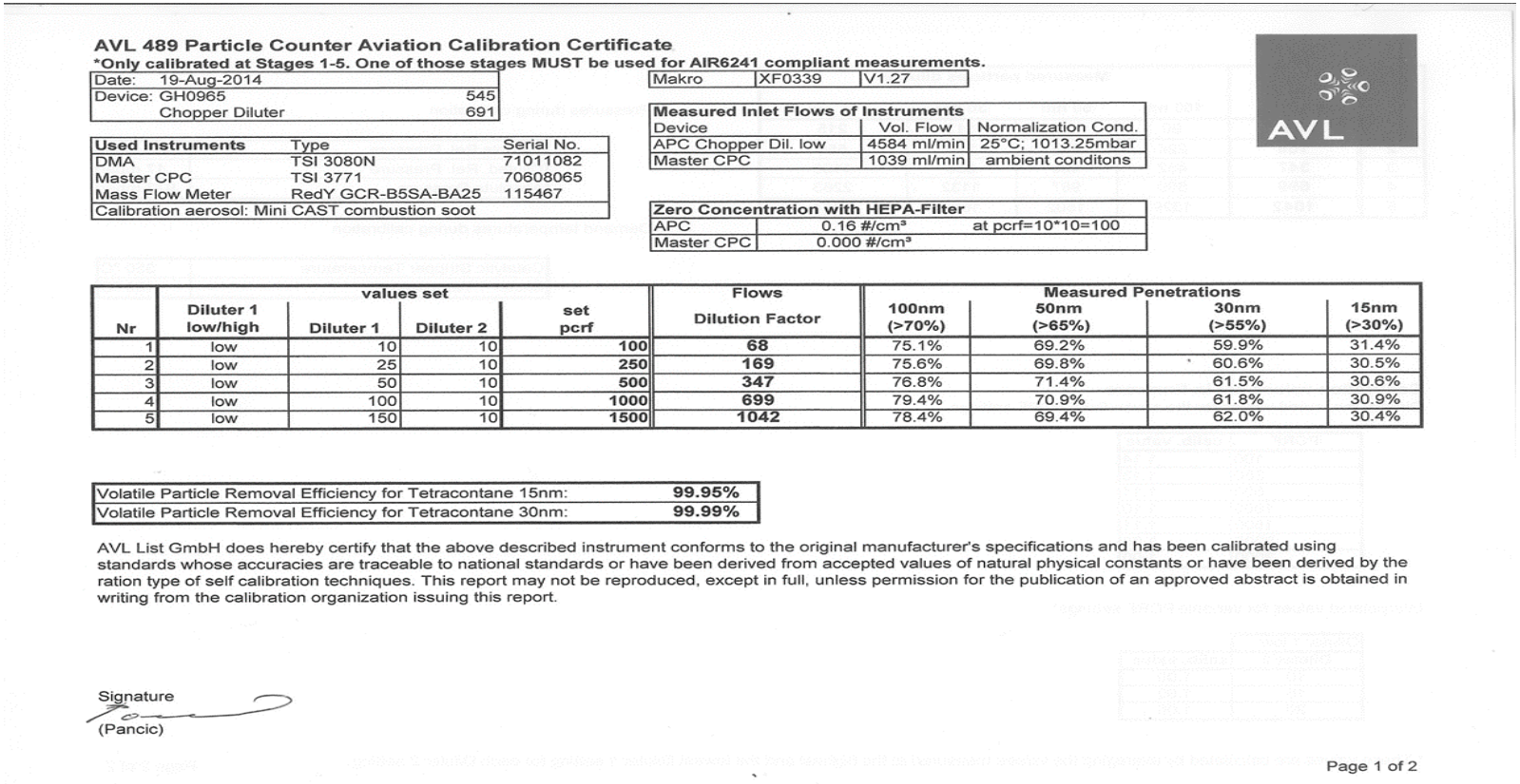

AVL 489 Particle Counter Aviation Calibration Certificate

***Only calibrated at Stages 1-5. One of those stages MUST be used for AIR6241 compliant measurements.**

Date:	19-Aug-2014	
Device:	GH0965	545
	Chopper Diluter	691

Makro	XF0339	V1.27

Used Instruments	Type	Serial No.
DMA	TSI 3080N	71011082
Master CPC	TSI 3771	70608065
Mass Flow Meter	RedY GCR-B5SA-BA25	115467
Calibration aerosol: Mini CAST combustion soot		

Measured Inlet Flows of Instruments		
Device	Vol. Flow	Normalization Cond.
APC Chopper Dil. low	4584 ml/min	25°C; 1013.25mbar
Master CPC	1039 ml/min	ambient conditons

Zero Concentration with HEPA-Filter		
APC	0.16 #/cm³	at pcrf=10*10=100
Master CPC	0.000 #/cm³	

Nr	values set: Diluter 1 low/high	Diluter 1	Diluter 2	set pcrf	Flows: Dilution Factor	Measured Penetrations: 100nm (>70%)	50nm (>65%)	30nm (>55%)	15nm (>30%)
1	low	10	10	**100**	**68**	75.1%	69.2%	59.9%	31.4%
2	low	25	10	**250**	**169**	75.6%	69.8%	60.6%	30.5%
3	low	50	10	**500**	**347**	76.8%	71.4%	61.5%	30.6%
4	low	100	10	**1000**	**699**	79.4%	70.9%	61.8%	30.9%
5	low	150	10	**1500**	**1042**	78.4%	69.4%	62.0%	30.4%

Volatile Particle Removal Efficiency for Tetracontane 15nm:	**99.95%**
Volatile Particle Removal Efficiency for Tetracontane 30nm:	**99.99%**

AVL List GmbH does hereby certify that the above described instrument conforms to the original manufacturer's specifications and has been calibrated using standards whose accuracies are traceable to national standards or have been derived from accepted values of natural physical constants or have been derived by the ration type of self calibration techniques. This report may not be reproduced, except in full, unless permission for the publication of an approved abstract is obtained in writing from the calibration organization issuing this report.

Signature

(Pancic)

Page 1 of 2

Figure A.1.1. UTRC APC calibration certification (Page 1 of 2).

Nr	Flows Dilution Factor	Measured particles dilution			
		100 nm	50 nm	30 nm	15 nm
1	**68**	90	98	113	215
2	**169**	224	243	280	556
3	**347**	452	486	565	1135
4	**699**	880	987	1132	2263
5	**1042**	1329	1502	1682	3434

Pressures during calibration

Sample Rel. Pressure	-45 mbar
Diluted. Rel. Pressure	17 mbar
Absolute Pressure	973 mbar

Demand temperatures during calibration

Catalytic Stripper Temperature	350 °C
Diluter 1 Temperature	150 °C

Calibration values set in firmware

Directly measured values for the seven fixed PCRF settings

PCRF	calib. value
100	1.14
250	1.13
500	1.11
1000	1.10
1500	1.11
2000	1.00
3000	1.00

Interpolated values for variable PCRF settings*

Diluter 1 low	
Diluter 2	**calib. value**
10	1.00
15	1.00
20	1.00

* These values are calculated by averaging the values measured at the highest and the lowest Diluter 1 setting for each Diluter 2 setting.

Page 2 of 2

Figure A.1.2. UTRC APC calibration certification (Page 2 of 2).

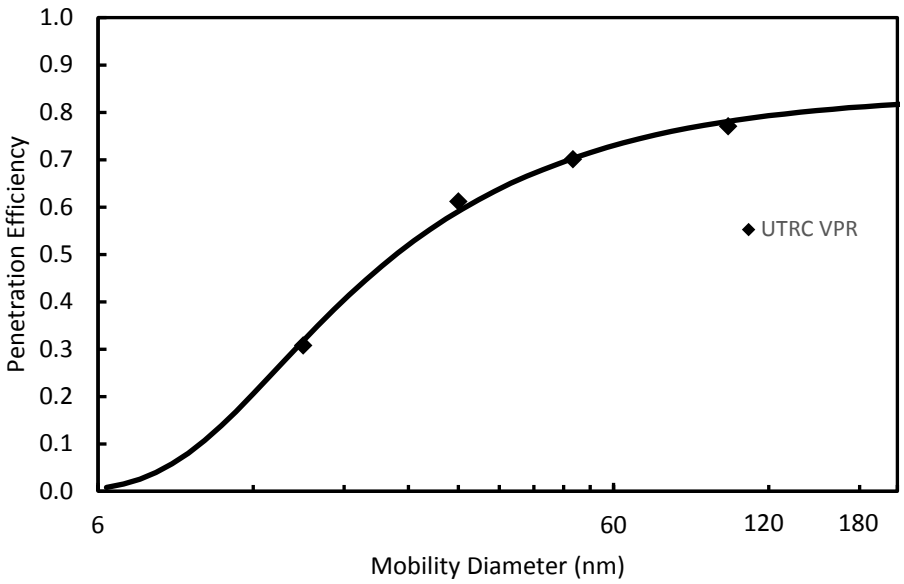

Figure A.1.3. UTRC APC calibration points fit to model.

AVL 489 Particle Counter Aviation Calibration Certificate

***Only calibrated at Stages 1-5. One of those stages MUST be used for AIR6241 compliant measurements.**

Date:	5-Mar-2015
Device: GH0965	410
Chopper Diluter	508

Makro	XF0339	V1.28b

Used Instruments	Type	Serial No.
DMA	TSI 3080N	71207121
Master CPC	TSI 3772	3772113102
Mass Flow Meter	RedY GCR-B5SA-BA25	137315
Calibration aerosol: APG combustion soot		

Measured Inlet Flows of Instruments		
Device	Vol. Flow	Normalization Cond.
APC Chopper Dil. low	4726 ml/min	25°C; 1013.25mbar
Master CPC	978 ml/min	ambient conditons

Zero Concentration with HEPA-Filter		
APC	0.11 #/cm³	at pcrf=10*10=100
Master CPC	0.001 #/cm³	

Nr	values set: Diluter 1 low/high	Diluter 1	Diluter 2	set pcrf	Flows: Dilution Factor	Measured Penetrations: 100nm (>70%)	50nm (>65%)	30nm (>55%)	15nm (>30%)
1	low	10	10	100	68	74.3%	69.5%	63.1%	44.1%
2	low	25	10	250	176	74.8%	73.4%	64.4%	43.0%
3	low	50	10	500	352	76.6%	72.4%	63.9%	42.2%
4	low	100	10	1000	718	78.5%	73.5%	65.0%	41.3%
5	low	150	10	1500	1048	73.9%	74.8%	62.5%	38.4%

Volatile Particle Removal Efficiency for Tetracontane 15nm:	**100.00%**
Volatile Particle Removal Efficiency for Tetracontane 30nm:	**100.00%**

AVL List GmbH does hereby certify that the above described instrument conforms to the original manufacturer's specifications and has been calibrated using standards whose accuracies are traceable to national standards or have been derived from accepted values of natural physical constants or have been derived by the ration type of self calibration techniques. This report may not be reproduced, except in full, unless permission for the publication of an approved abstract is obtained in writing from the calibration organization issuing this report.

Signature

(CELIK Caglayan)

Page 1 of 2

Figure A.1.4. MS&T APC calibration certification (Page 1 of 2).

Nr	Flows Dilution Factor	Measured particles dilution			
		100 nm	50 nm	30 nm	15 nm
1	**68**	93	99	109	156
2	**176**	236	241	274	411
3	**352**	458	486	549	832
4	**718**	917	978	1107	1740
5	**1048**	1417	1399	1676	2728

Calibration values set in firmware
Directly measured values for the seven fixed PCRF settings

PCRF	calib. value
100	1.12
250	1.09
500	1.09
1000	1.07
1500	1.10

Pressures during calibration

Sample Rel. Pressure	-49 mbar
Diluted. Rel. Pressure	16 mbar
Absolute Pressure	982 mbar

Demand temperatures during calibration

Catalytic Stripper Temp.	350 °C
Diluter 1 Temperature	150 °C

Specifications of the Catalytic Stripper

Oxidation efficiency: >99% for decane inlet concentration of 4%
Sulphur Storage Capacity: > 6mg

* These values are calculated by averaging the values measured at the highest and the lowest Diluter 1 setting for each Diluter 2 setting.

Figure A.1.5. MS&T APC calibration certification (Page 2 of 2).

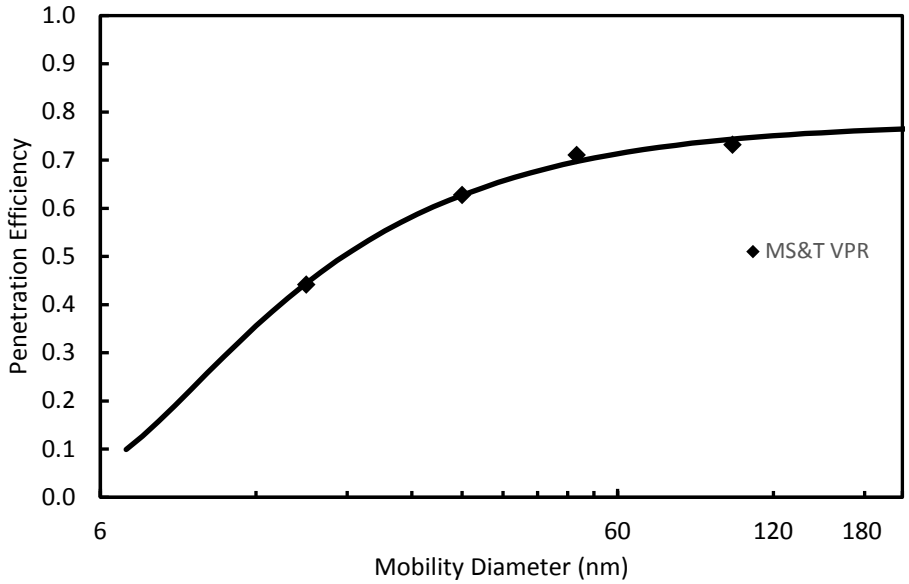

Figure A.1.6. MS&T APC calibration points fit to model.

Appendix 2. SMPS Calibrations

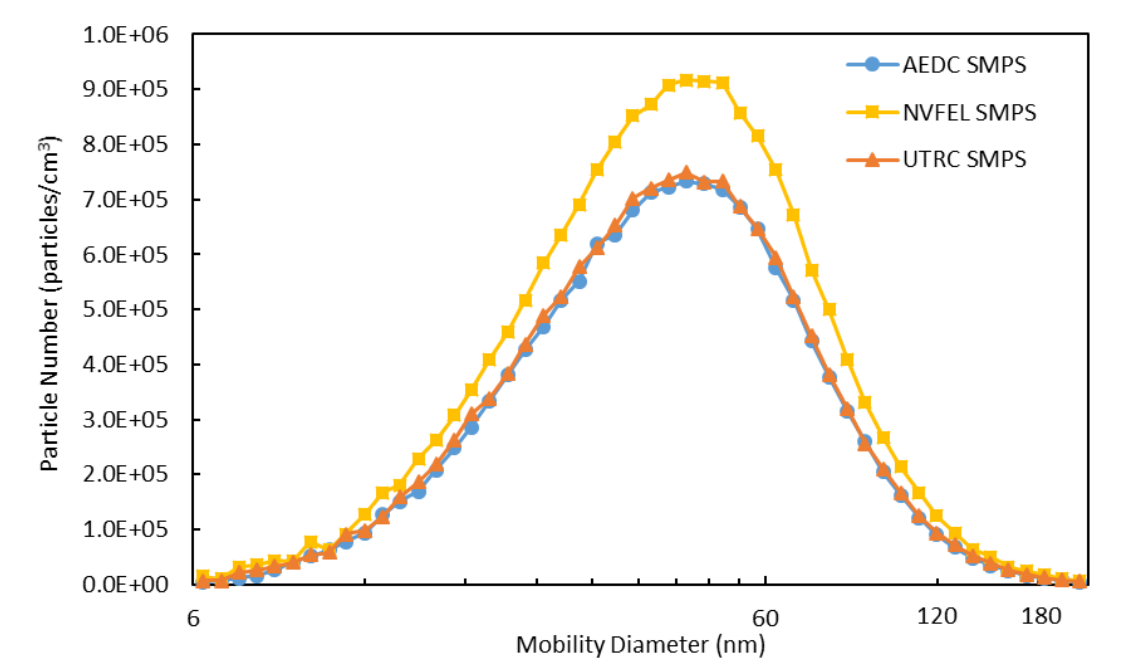

Figure A.2.1. Day 1 – AEDC, NVFEL, and UTRC SMPS morning calibration results – Group 1.

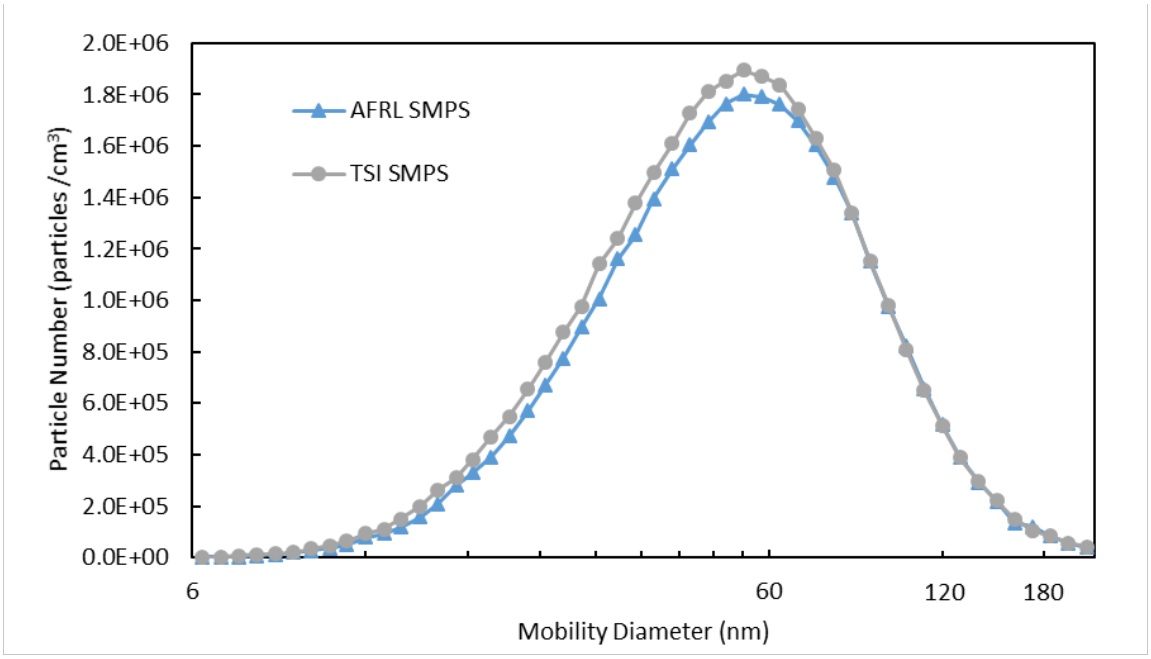

Figure A.2.2. Day 1 - AFRL and TSI SMPS morning calibration results – Group 2.

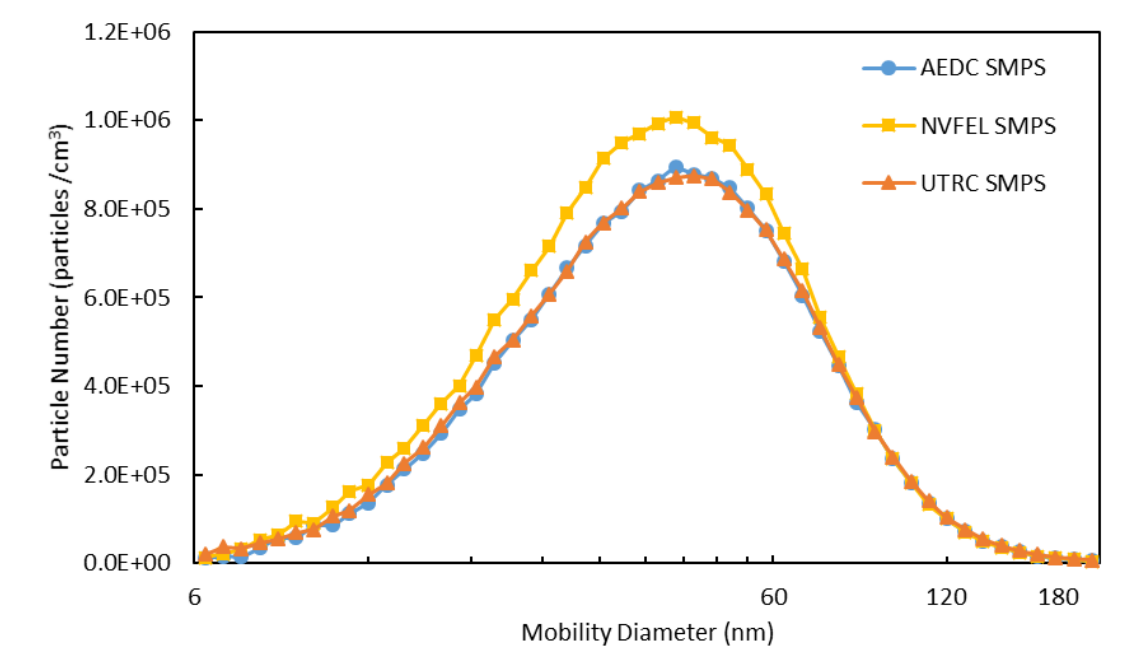

Figure A.2.3. Day 2 – AEDC, NVFEL, and UTRC SMPS morning calibration results – Group 1.

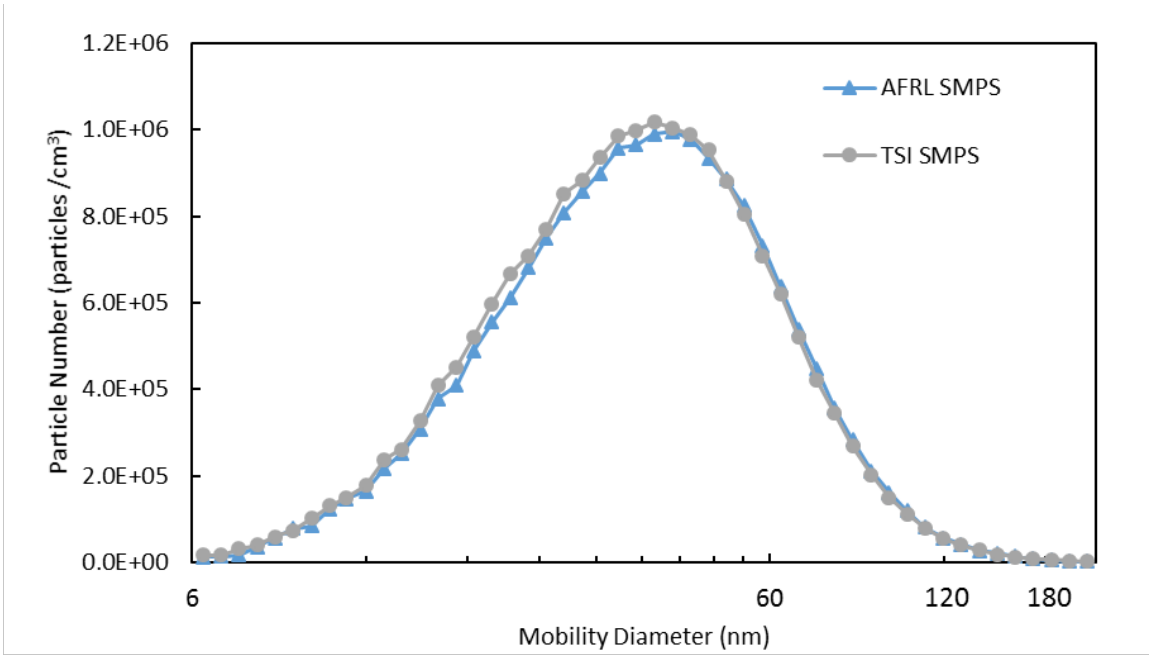

Figure A.2.4. Day 2 - AFRL and TSI SMPS morning calibration results – Group 2.

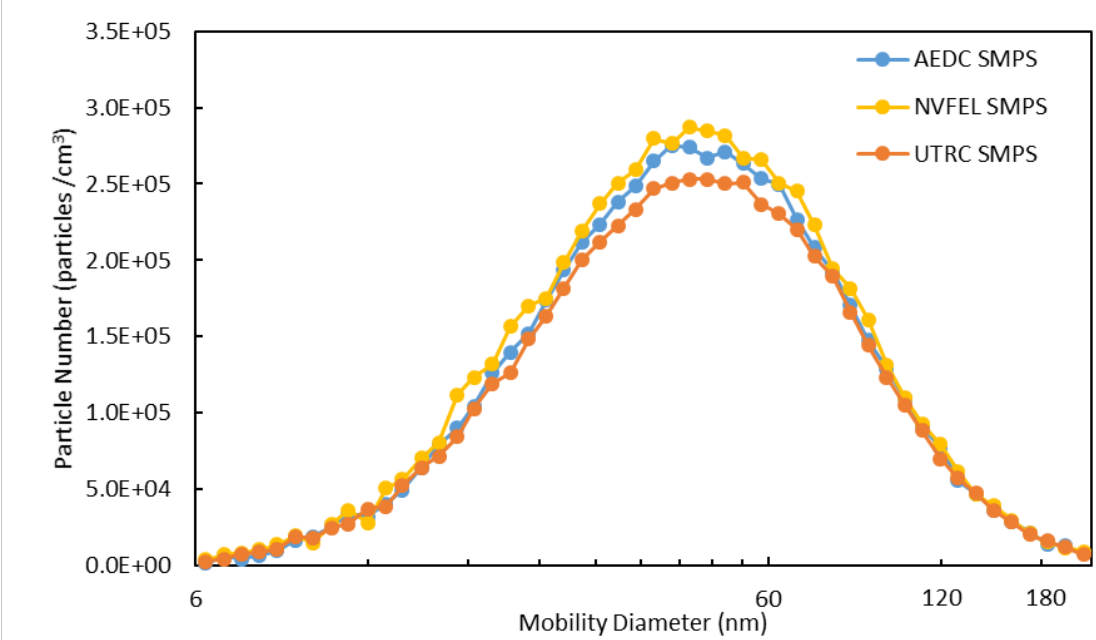

Figure A.2.5. Day 3 – AEDC, NVFEL, and UTRC SMPS morning calibration results – Group 1.

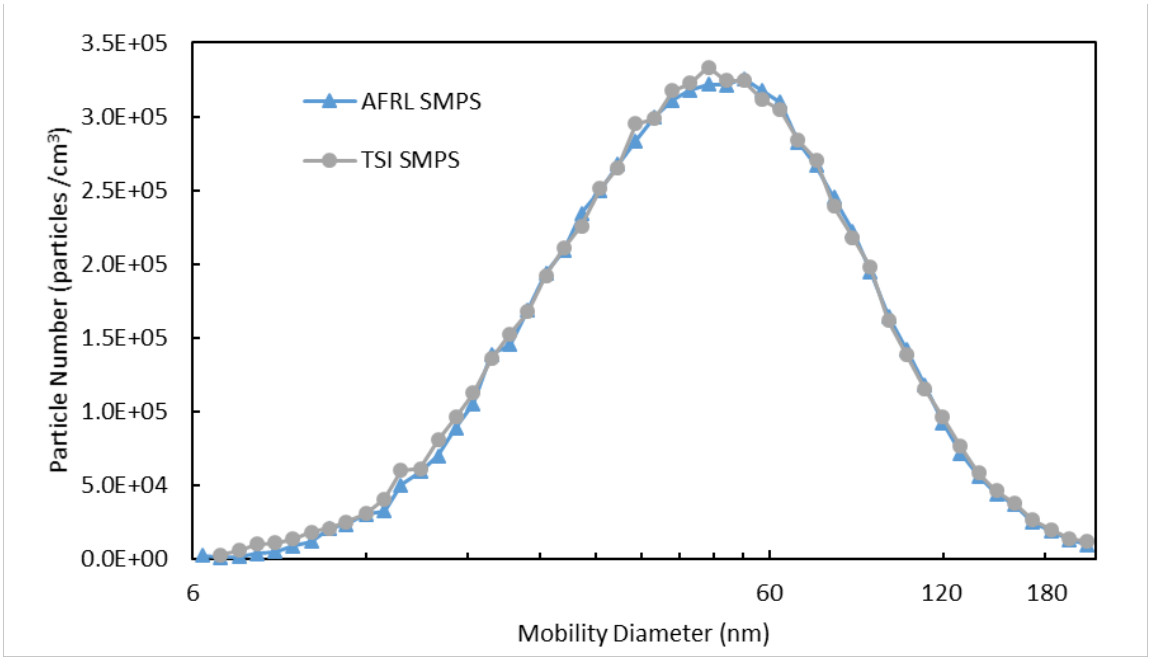

Figure A.2.6. Day 3 - AFRL and TSI SMPS morning calibration results – Group 2.

Appendix 3. MSS, LII and APC Description

AVL MSS

The Micro Soot Sensor (MSS) is a real-time non-volatile (nvPM) mass concentration measuring device. The MSS uses a photoacoustic method to quantify nvPM in units of particle mass per sample volume (mg/m^3), making it ideal for characterizing nvPM from aircraft engines (see Fig. A.3.1.). The MSS uses an embedded laser to expose sample gas to light of wavelength 808 ± 5 nm, causing cycles of rapid heating and cooling of the gas sample (Schindler et al., 2004). These cycles result in pressure fluctuations that are measured by a highly sensitive microphone detector. The measured pressure fluctuations provide the raw signal values that are then converted to mass concentrations. {Ref. 27}

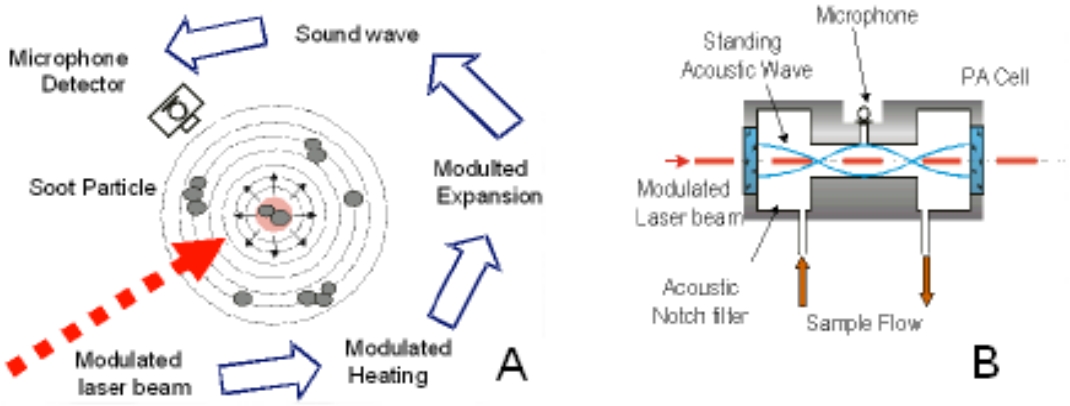

Figure A.3.1. The principle of photoacoustic measurement (A) and the photoacoustic cell design (B) {Ref. 27}.

AVL APC

The APC is a real-time non-volatile PM (nvPM) number counting device that reports particle number concentration values in units of particles per cubic centimeter (#/cm^3), making it ideal for characterizing nvPM from aircraft engines. To eliminate contributions of volatile particles the device employs a two stage dilution process coupled with a volatile particle remover (VPR). During first stage dilution, dilution air heated to 150°C is added to the exhaust sample at the chopper diluter. Following stage one dilution the sample is then transported to a catalytic stripper, or VPR, maintained at 350°C to drive off volatiles. After volatile removal in the catalytic stripper, stage two dilution cools the sample before entering the CPC, which uses light scattering detection to count particles. {Ref. 23}

The APC is described schematically in Fig. A.3.2.; a detailed instrument description and theory of operation is available in the APC User Manual {Ref. 23}.

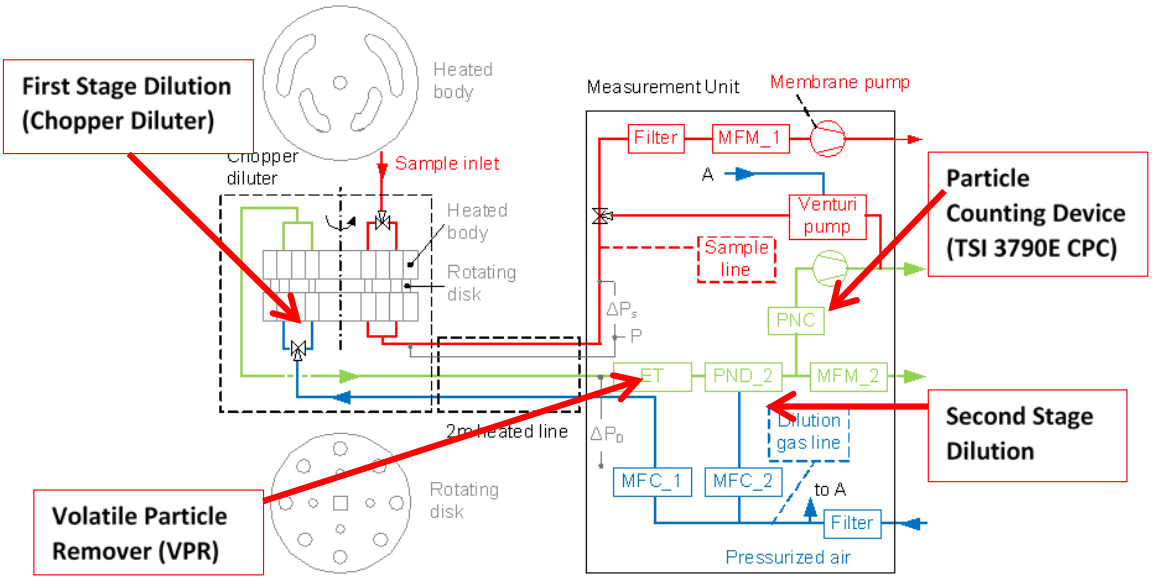

Figure A.3.2. Schematic of APC with key features specific to operation in aircraft engine emissions testing {Ref. 23}.

Artium LII300

The Artium LII300 is a real-time mass concentration measuring device. The LII quantifies nvPM in units of particle mass per sample volume (mg/m^3), making it ideal for characterizing nvPM from aircraft engines. The LII uses a laser induced incandescence technique in which solid particles absorb enough energy from a laser for their temperature to greatly increase. The particles reradiate part of this energy (they incandesce), which is then detected by two photomultipliers; the raw signal values are then converted to mass concentrations (see Snelling et. al, 2004). A general schematic of the LII measuring unit is provided in Fig. A.3.3. below. {Ref. 28}

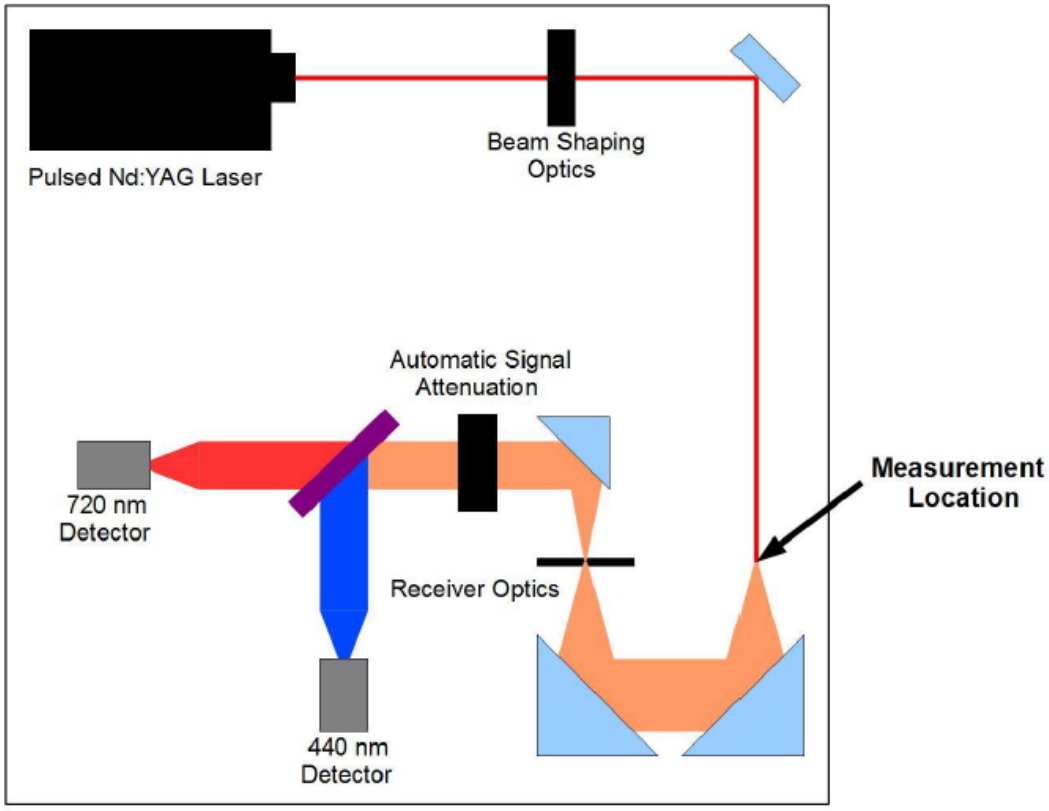

Figure A.3.3. Schematic showing the beam path used for measurement by the LII {Ref. 28}.

Appendix 4. Instrumentation List

Table A.4.1. Equipment & Description.

Equipment	Purpose
AEDC	
AEDC J85 Engine, Facility, Accommodations	Turbine Engine Particle Source
AEDC Probe-Rake System	Extractive Gas Sampling
Sampling Probes	Exhaust Sample to Instruments
Traversing Table	Horizontal Traverse of Sampling Probes
Pitot Probe(s)	Total Exhaust Flow Pressure
Total Temperature Probe(s)	Total Exhaust Flow Temperature
AEDC PM System	
AVL PM Sampling System	PM sampling flow control
AVL Micro Soot Sensor	nvPM Mass Concentration
Artium LII 300 (with lower detection option)	nvPM Mass Concentration
TSI Scanning Mobility Particle Sizer (SMPS)-Long DMA	Particle Size Distribution
CO2 Analyzer (1000 ppm) for PM Sampling Line	CO2 Concentration
AEDC Gas	
2-Multi-Gas Analyzer for Gases (Extractive FTIR based)	CO2, CO, NO, NOx, SO2, some HC speciation
2- FID (Total HC)	Total Unburned Hydrocarbons Concentration
2-Smoke Meter (TBD)	Smoke Number
2-NDIR CO2 analyzer	CO2 Concentration
Missouri University of Science and Technology (MST)	
MST PM Sampling System	PM sampling flow control
AVL APC	nvPM Particle Number Concentration
AVL MSS	nvPM Mass Concentration
Artium LII 300	nvPM Mass Concentration
CO2 analyzer	CO2 Concentration
EPA-Research Triangle Park	
TSI SMPS (3936); Long DMA (3081), classifier (3080); CPC (3025A)	Particle Size Distribution

Table A.4.1. Continued Equipment & Description

Equipment	Purpose
EPA-Research Triangle Park	
LII 300 (borrowed from Environmental-Canada)	EC/OC mass concentrations
483 MSS (borrowed from AVL)	nvPM Mass Concentration
Mini-CAST 5201 (prototype)	Particle Source
Licor CO2	Dog House CO2 Concentration
EPA-Ann Arbor	
5201 C model Mini-CAST burner with internal flow controller	Particle Source (backup to John's)
TSI SMPS (3936); Long DMA and classifier	Particle Size Distribution
2 - TSI CPCs (3776); n-butanol	To be connected to SMPSs
2 - TSI CPCs (3025A); n-butanol	
6201 Mini-CAST burner	
ATM220 Atomizer Instrument (yellow)	Generating DOS particles for SMPS characterization
EDU570 Diffusion Dryer	
UTRC	
TSI SMPS (3936); Long DMA and classifier	Particle Size Distribution
AVL Aerosol Particle Counter (APC)	nvPM Particle Number Concentration
AFRL	
TSI SMPS (3936); Long DMA, classifier and CPC	Particle Size Distribution
TSI	
TSI SMPS (3936); Long DMA and classifier	Particle Size Distribution

Appendix 5. Measurement Parameters

List of Parameters Collected

AEDC_AVL_Time
AEDC_AVL_EpochTime
AEDC_AVL_MeasurementStatus
AEDC_AVL_HEATER_T1_CMD
AEDC_AVL_HEATER_T2_CMD
AEDC_AVL_HEATER_T4_CMD
AEDC_AVL_HEATER_T5_CMD
AEDC_AVL_HEATER_T1_1_CMD
AEDC_AVL_HEATER_HL1_CMD
AEDC_AVL_V0_CMD
AEDC_AVL_MS_FlowRate
AEDC_AVL_MS_GasTemp
AEDC_AVL_MS_MeasCellTemp
AEDC_AVL_MS_RelPressure
AEDC_AVL_MS_TECHumidity
AEDC_AVL_MS_ConcentrationSensor
AEDC_AVL_MS_AbsPressure
AEDC_AVL_MS_LeakValue
AEDC_AVL_MS_MaxsumAtFrequency
AEDC_AVL_MS_Contamination_Real
AEDC_AVL_MS_Contamination_Imaginary
AEDC_AVL_MS_Contamination_Sum
AEDC_AVL_MS_Contamination_Phase
AEDC_AVL_MS_Meas_Real
AEDC_AVL_MS_Meas_Imaginary
AEDC_AVL_MS_Meas_Sum
AEDC_AVL_MS_Meas_Phase
AEDC_AVL_MS_Zeroing_Real
AEDC_AVL_MS_Zeroing_Imaginary
AEDC_AVL_MS_Zeroing_Sum
AEDC_AVL_MS_Zeroing_Phase
AEDC_AVL_MS_Zeroing_Amplification
AEDC_AVL_MS_DiffPressure
AEDC_AVL_MS_LaserDiodeTemp
AEDC_AVL_MS_LaserDiode_Curr
AEDC_AVL_MS_Second
AEDC_AVL_MS_ParamLeakCheckDeadVol
AEDC_AVL_MS_ParamLeackCheckTestPressure

AEDC_AVL_MS_ParamLeakCheckLeakLimit
AEDC_AVL_MS_LinCheckLaserFactor
AEDC_AVL_MS_LinCheckSpeakerFactor
AEDC_AVL_MS_DevID
AEDC_AVL_MS_Version
AEDC_AVL_MS_State4
AEDC_AVL_MS_ParamChanged
AEDC_AVL_MS_ResultChanged
AEDC_AVL_MS_ErrorStatus
AEDC_AVL_MS_RequestStatus
AEDC_AVL_Measure_Time
AEDC_AVL_Heaters_Enable
AEDC_AVL_Heater_T1_SP
AEDC_AVL_Heater_T2_SP
AEDC_AVL_Heater_T4_SP
AEDC_AVL_Heater_T5_SP
AEDC_AVL_Heater_Line_HL1_SP
AEDC_AVL_V0_SP
AEDC_AVL_V1
AEDC_AVL_V2
AEDC_AVL_V3
AEDC_AVL_V4
AEDC_AVL_MFC_Sample_Pump
AEDC_AVL_CO2_Sample_Pump
AEDC_AVL_AVL_483_MeasTime
AEDC_AVL_P1_Probe
AEDC_AVL_P2_Diluent_Gas
AEDC_AVL_P3_Vent
AEDC_AVL_P4_Pre_Heated_Line
AEDC_AVL_P5_Post_Heated_Line
AEDC_AVL_P6_Splitter_2
AEDC_AVL_P7_MFC
AEDC_AVL_P8_Atmosphere
AEDC_AVL_MFC_Flow_Rate
AEDC_AVL_CO2_Concentration_Diluted
AEDC_AVL_CO2_Concentration
AEDC_AVL_PO_2_Air_High_Switch
AEDC_AVL_PO_1_Air_Low_Switch
AEDC_AVL_T1_Splitter_1
AEDC_AVL_T1_1_Line
AEDC_AVL_T2

AEDC_AVL_T3
AEDC_AVL_T4
AEDC_AVL_T4_1
AEDC_AVL_T5
AEDC_AVL_T6
AEDC_AVL_T7
AEDC_AVL_T8
AEDC_AVL_T_HL1
AEDC_AVL_T_HL2
AEDC_AVL_T3_1
AEDC_AVL_T4_2
AEDC_AVL_MFC_Filter_Delta_Pressure
AEDC_AVL_System_State_Change_Time
AEDC_AVL_Probe_Delta_Pressure
AEDC_AVL_MFC_Filter_Plugged
AEDC_AVL_Heated_Line_Delta_Pressure
AEDC_AVL_Heated_Line_APC_MSS
AEDC_AVL_E31_Hibernate
AEDC_AVL_E31_HibernateEnabled
AEDC_AVL_E31_Warmup
AEDC_AVL_E31_WarmupEnabled
AEDC_AVL_E31_Pause
AEDC_AVL_E31_PauseEnabled
AEDC_AVL_E31_Standby
AEDC_AVL_E31_StandbyEnabled
AEDC_AVL_E31_LeakCheckGL
AEDC_AVL_E31_LeakCheckGLEnabled
AEDC_AVL_E31_LeakCheckPM
AEDC_AVL_E31_LeakCheckPMEnabled
AEDC_AVL_E31_BackpurgeGL
AEDC_AVL_E31_BackpurgeGLEnabled
AEDC_AVL_E31_BackpurgeDiluter
AEDC_AVL_E31_BackpurgeDiluterEnabled
AEDC_AVL_E31_AmbientMeasurement
AEDC_AVL_E31_AmbientMeasurementEnabled
AEDC_AVL_E31_Diluter1Check
AEDC_AVL_E31_Diluter1CheckEnabled
AEDC_AVL_E31_Diluter2Check
AEDC_AVL_E31_Diluter2CheckEnabled
AEDC_AVL_E31_Measure
AEDC_AVL_E31_MeasureEnabled

AEDC_AVL_E31_Manual
AEDC_AVL_E31_ManualEnabled
AEDC_AVL_E31_ManualEnabled_ORV
AEDC_AVL_V5
AEDC_AVL_V0_SP_Test
AEDC_AVL_MFC_Filter_Plugged_Pressue
AEDC_AVL_Heater_T1_1_SP
AEDC_AVL_Heater_PWM_Freq
AEDC_AVL_APC_EmissionIndex
AEDC_AVL_MS_EmissionIndex
AEDC_AVL_MS_RelPresError
AEDC_AVL_Device1_Flow_SP
AEDC_AVL_Device2_Flow_SP
AEDC_AVL_Device3_Flow_SP
AEDC_AVL_MFC_SP
AEDC_AVL_Dilution_Ratio
AEDC_AVL_APC_ParticlesPCcmm
AEDC_AVL_P2_DilutentGas_bar
AEDC_AVL_APC_DilutedParticlesPCcmm
AEDC_AVL_DeviceSuiteFlowSum
AEDC_AVL_MeasureStartFlag
AEDC_AVL_Leak_Mass_Number_Store
AEDC_AVL_Leak_Particle_Number_Store
AEDC_AVL_PC_ErrChannel
AEDC_AVL_PC_ParticlesPCcm
AEDC_AVL_PC_PND1
AEDC_AVL_PC_PND2
AEDC_AVL_PC_PCRFcurrent
AEDC_AVL_PC_ParameterChanged
AEDC_AVL_PC_ResultChanged
AEDC_AVL_PC_DeviceStatus
AEDC_AVL_PC_TimeReady
AEDC_AVL_PC_TemperaturVPR
AEDC_AVL_PC_TemperaturePND1
AEDC_AVL_PC_PressureAbsolute
AEDC_AVL_PC_FlowCPCBypass
AEDC_AVL_PC_SampleLineTemp
AEDC_AVL_PC_SampleRelPressure
AEDC_AVL_PC_MassFlowRDexcess
AEDC_AVL_PC_CPCButanolLevel
AEDC_AVL_PC_CPCNozzlePressure

AEDC_AVL_PC_CPCOrificePressure
AEDC_AVL_PC_DFSelection
AEDC_AVL_PC_DF
AEDC_AVL_PC_Concentration_DFcorrected
AEDC_AVL_PC_ResponseCheckResult
AEDC_AVL_PC_ResponseCheckFlag
AEDC_AVL_PC_ButanolBottleLevel
AEDC_AVL_APC_DFIdentifier
AEDC_AVL_FEB_Heat_Cool
AEDC_AVL_Start_PC_set_DF
AEDC_AVL_MS_Online
AEDC_AVL_Dilution_Factor
Facility_Time
Facility_T5
Facility_N1
Facility_PLA01
Facility_TraversePos
Facility_TGASPROBE3
Facility_TGASPROBE2
Facility_TGASPROBE1
Facility_TTPROBE3
Facility_TTPROBE1
Facility_PVACUUM
Facility_PMSTPROBE1
Facility_PTPITOTPROBE3
Facility_PTPITOTPROBE1
Facility_PAMB01
Facility_TAMB1
Facility_PAEDCPROBE2
Facility_PSHEDPROBE3
Facility_PSMOKEPROBE4
AEDC_GL_Time
AEDC_GL_MGA1_Samp_T
AEDC_GL_Cold_Ref1
AEDC_GL_MGA1_Flow
AEDC_GL_HFID1_Flow
AEDC_GL_HFID1
AEDC_GL_MGA1_Samp_P
AEDC_GL_MGA2_Samp_In_Line_T
AEDC_GL_HFID2_Line_T
AEDC_GL_MGA2_Line_T

AEDC_GL_MGA2_Samp_T
AEDC_GL_Cold_Ref2
AEDC_GL_MGA2_Samp_P
AEDC_GL_HFID2
AEDC_GL_MGA2_Flow
AEDC_GL_HFID2_Flow
AEDC_GL_DH_Dilute_CO2
AEDC_GL_MGA1_Time
AEDC_GL_MGA1_CO2 % span
AEDC_GL_MGA1_CO Low-Mid span
AEDC_GL_MGA1_H2O%
AEDC_GL_MGA1_Temp
AEDC_GL_MGA1_Pressure
AEDC_GL_MGA2_Time
AEDC_GL_MGA2_CO2 % span
AEDC_GL_MGA2_CO Low-Mid span
AEDC_GL_MGA2_H2O%
AEDC_GL_MGA2_Temp
AEDC_GL_MGA2_Pressure
AEDC_GL_Spectrum ID 1
AEDC_GL_Spectrum ID 2
MST_APC_Time
MST_APC_Conc. PNC
MST_APC_Conc. PCRF Corr.
MST_APC_DF
MST_APC_Sample Mass Flow (25°C)
MST_APC_Excess Diluted Mass Flow (25°C)
MST_APC_Temp. ET
MST_APC_Temp. PND1
MST_APC_Temp. Sample Line
MST_APC_Sample Relative Pressure
MST_APC_Diluted Relative Pressure
MST_APC_Temp. Condenser
MST_APC_Temp. Saturator
MST_APC_Pressure Flow Orifice
MST_APC_Pressure Nozzle
MST_APC_Raw Concentration PNC
MST_APC_APC Inlet Pressure
MST_APC_Error
MST_APC_Mean Conc. PCRF Corr.
MST_APC_Conc. DF Corr.

MST_APC_Mean Conc. DF Corr.
MST_CO2_Time
MST_CO2_CO2
MST_CO2_H2O
MST_CO2_H2O
MST_CO2_Cell_Temperature
MST_CO2_Cell_Pressure
MST_CO2_CO2_Absorption
MST_CO2_H2O_Absorption
MST_MKS_Time
MST_MKS_SAM
MST_MKS_CO2 #1
MST_MKS_CO2 #2
MST_MKS_LII
MST_MKS_Annex 16
MST_Pressures_HHMMSS
MST_Pressures_SAM
MST_Pressures_dP2
MST_Pressures_P2a
MST_Pressures_P1
MST_Pressures_P3
MST_Pressures_Cell Amb
MST_Pressures_Rack Amb
MST_Pressures_CO2 CAL
MST_Pressures_Driver Press
MST_Pressures_Total Flow
MST_TC_HHMMSS
MST_TC_SAM
MST_TC_Rack Amb
MST_TC_SPB1 60
MST_TC_T1 (SPB1 160)
MST_TC_T2 (DEK Dump)
MST_TC_Cell Amb
MST_TC_N/A
MST_TC_SPB2 60
MST_TC_T3 (Exit SPB2)
MST_TC_HL-A
MST_TC_HL-B
MST_TC_HL-D
MST_TC_HL-E
MST_TC_N/A

MST_TC_N/A
MST_TC_N/A
MST_TC_N/A
Doghouse_CO2_Time
Doghouse_CO2_CO2
Doghouse_CO2_CellTemp
Doghouse_CO2_CellPres
SMPS_Software_Version
SMPS_Impactor(cm)
DMA_Model
SMPS_CPC_Model
SMPS_Detector_Sample_Flow(L/min)
SMPS_Reference_Gas_Viscosity(Pa*s)
SMPS_Reference_Mean_Free_Path(m)
SMPS_Reference_Gas_Temperature(K)
SMPS_Reference_Gas_Pressure(kPa)
SMPS_Sutherland_Constant(K)
SMPS_Tube_Length(cm)
SMPS_Tube_Diameter(cm)
SMPS_Channels/Decade
SMPS_Multiple_Charge_Correction
SMPS_Nanoparticle_Agglomerate_Mobility_Analysis
SMPS_Diffusion_Correction

Appendix 6. Additional Penetration Efficiency Measurements

Note: Penetration Efficiencies were not available for all settings, sources, and fuels due to issues with the setup or instrumentation.

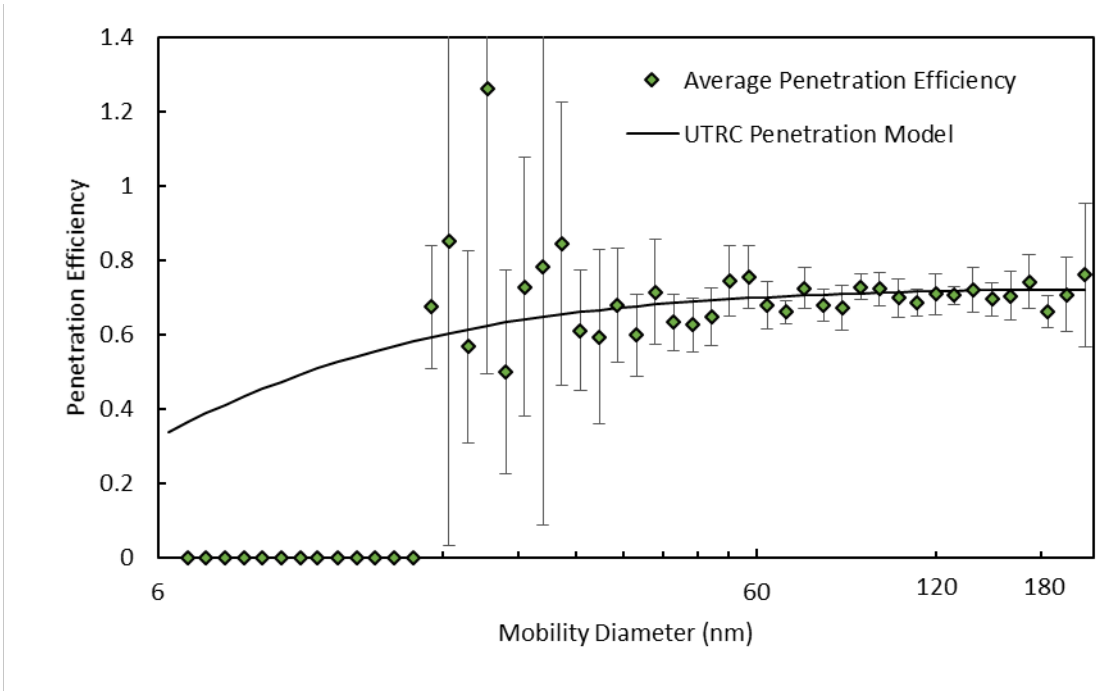

Figure A.6.1. Upstream half of AVL Sampling System average penetration efficiency for the Jing Mini-CAST with VARIAnT1 Setting.

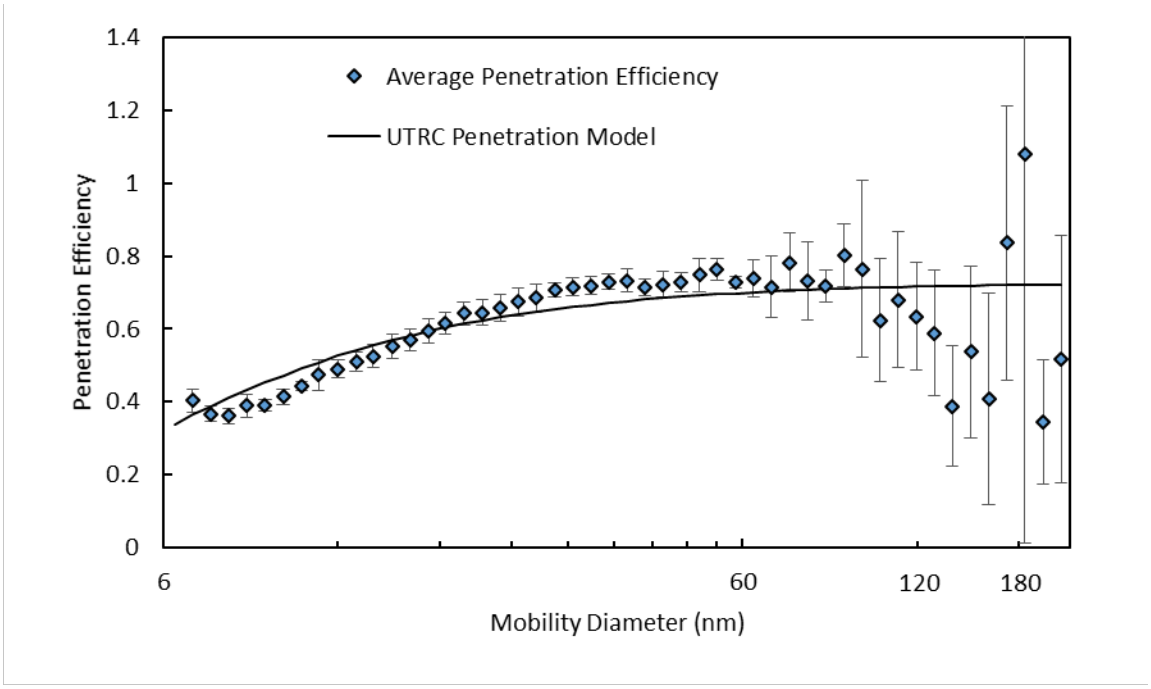

Figure A.6.2. Upstream half of AVL Sampling System average penetration efficiency for the GE J-85 with Jet-A Fuel at idle power setting.

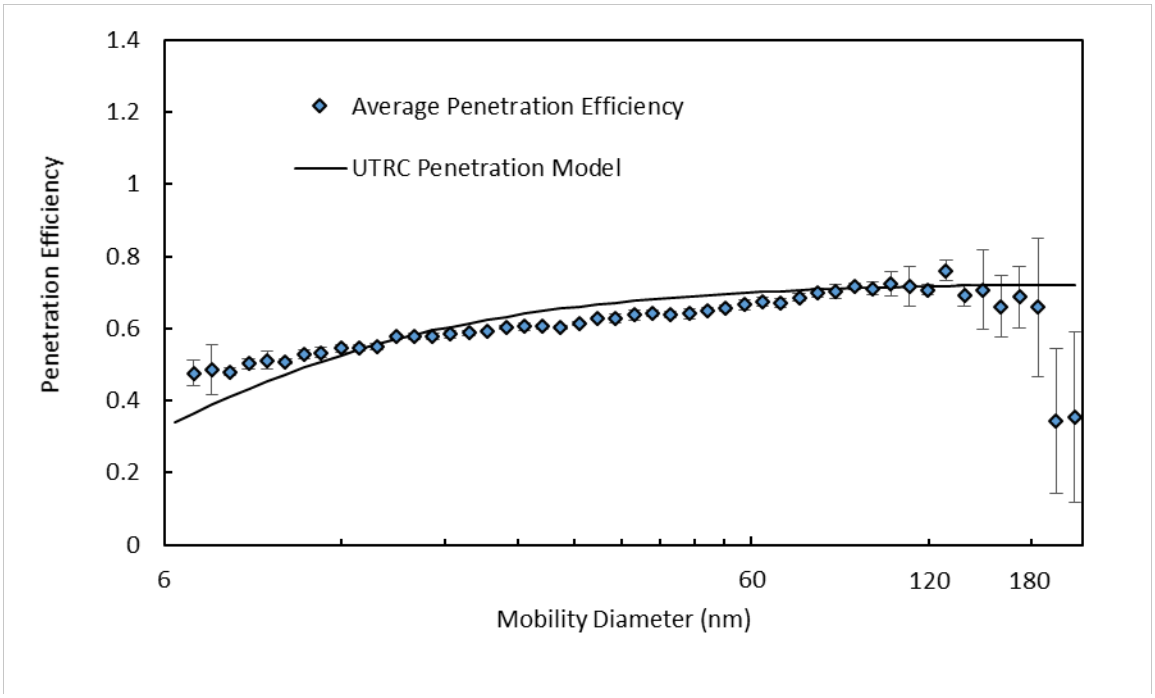

Figure A.6.3. Upstream half of AVL Sampling System average penetration efficiency for the GE J-85 with Jet-A Fuel at middle power setting.

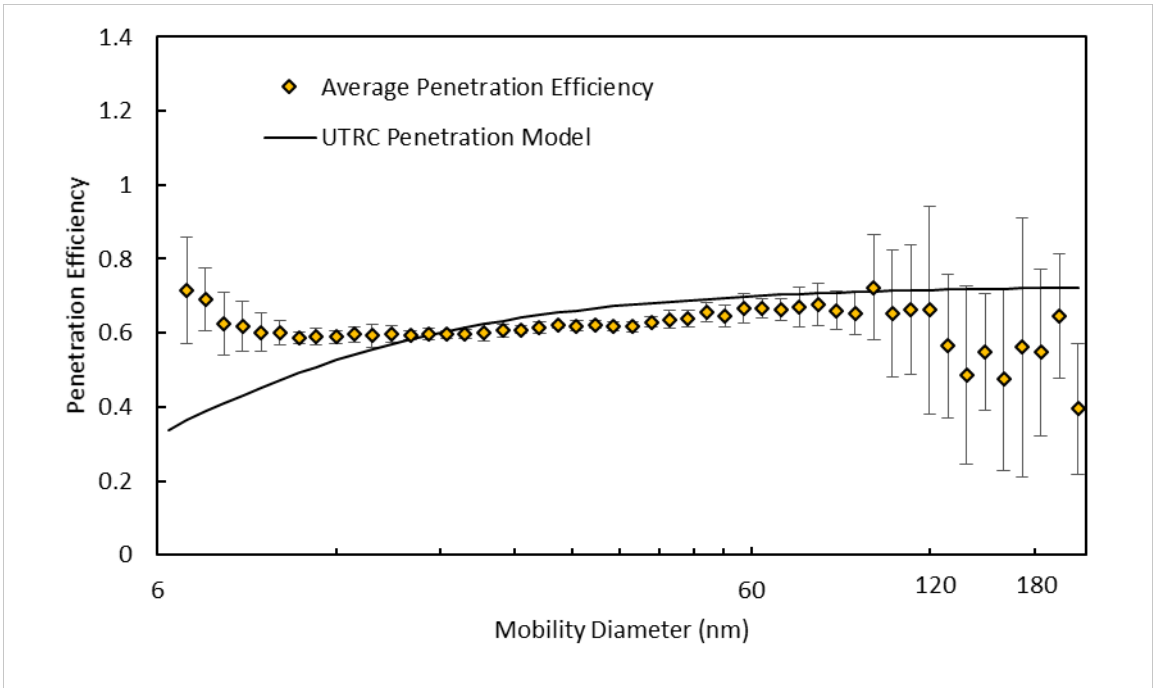

Figure A.6.4. Upstream half of AVL Sampling System average penetration efficiency for the GE J-85 with 50/50 Camelina and Jet-A Blend Fuel at middle power setting.

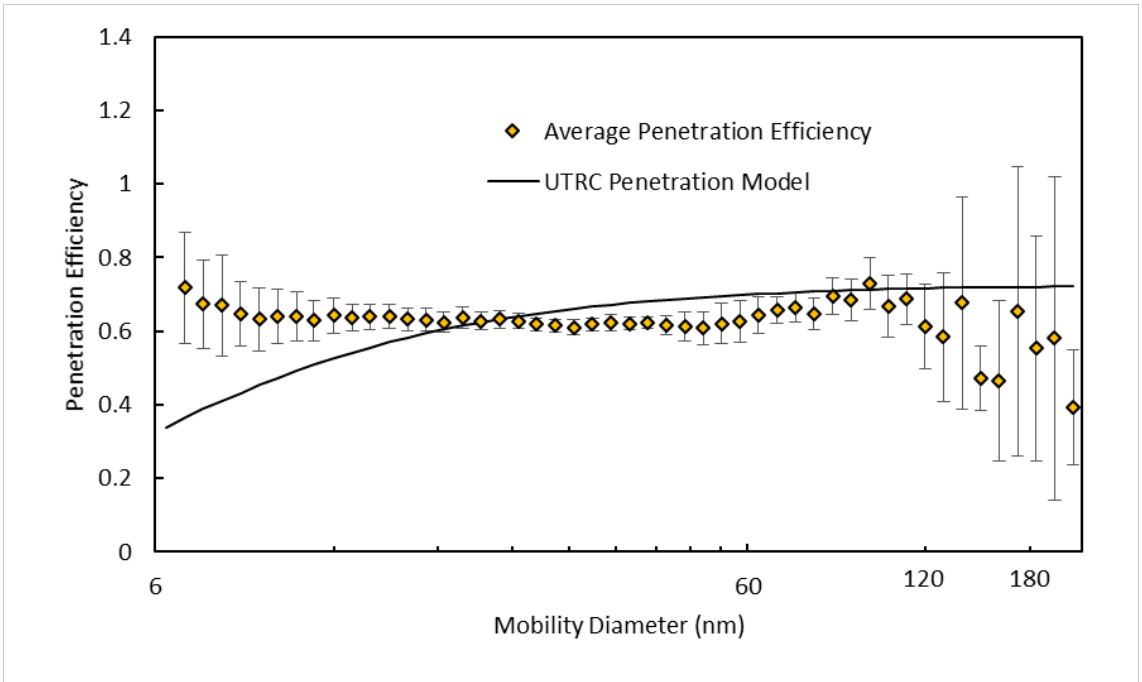

Figure A.6.5. Upstream half of AVL Sampling System average penetration efficiency for the GE J-85 with Jet-A Fuel at Military power setting.

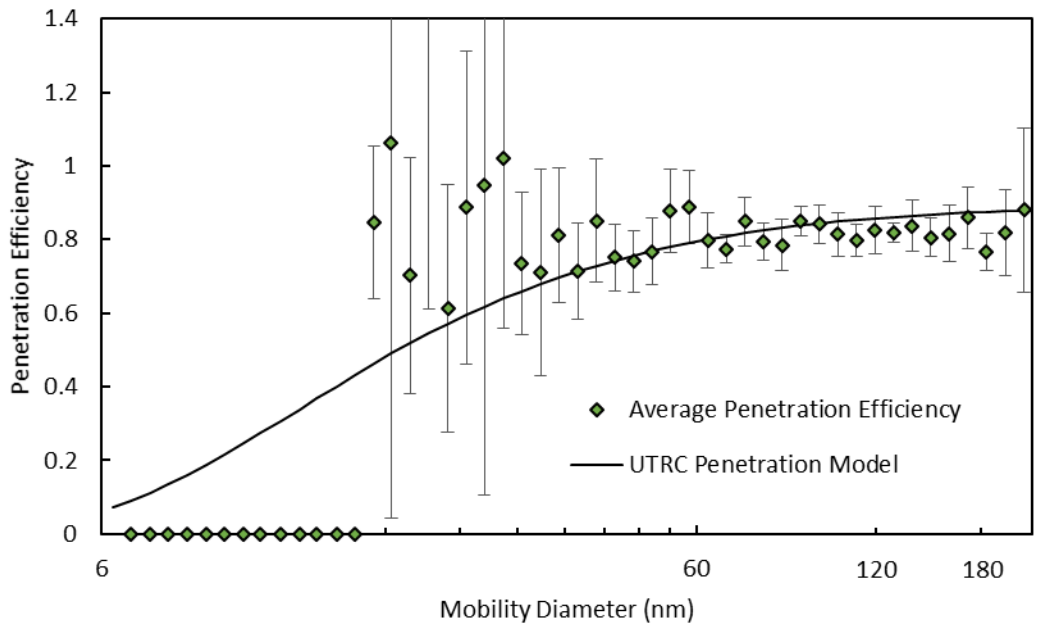

Figure A.6.6. Downstream half of AVL Sampling System average penetration efficiency for the Jing Mini-CAST with NRC Setting.

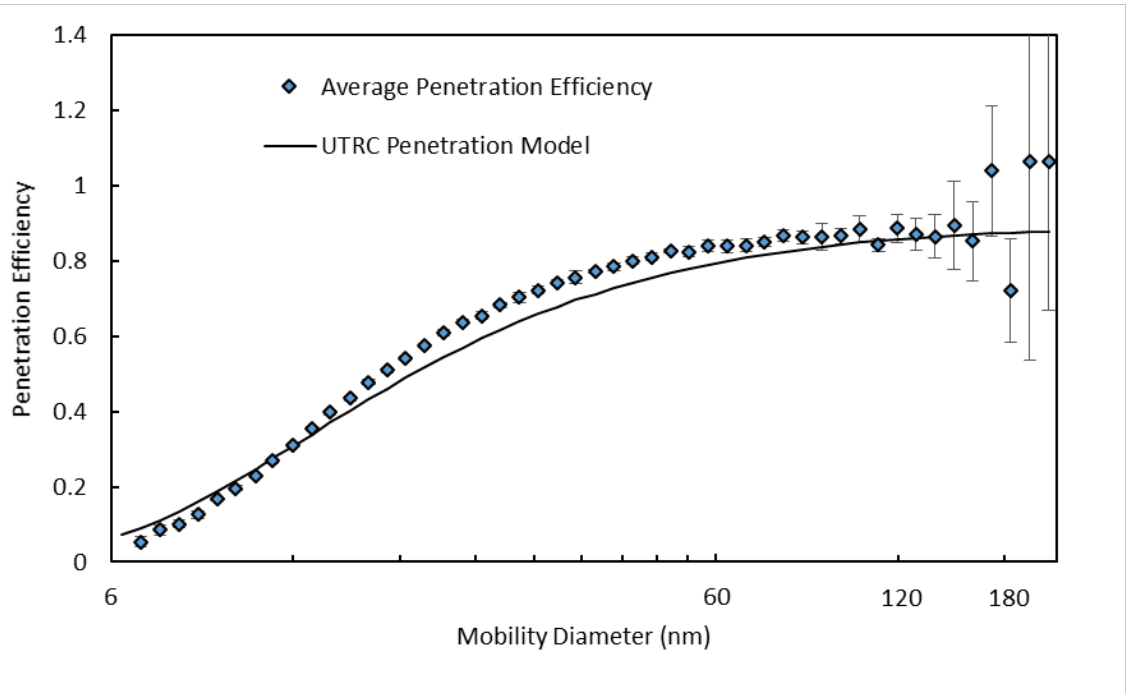

Figure A.6.7. Upstream half of AVL Sampling System average penetration efficiency for the GE J-85 with Jet-A Fuel at middle power setting.

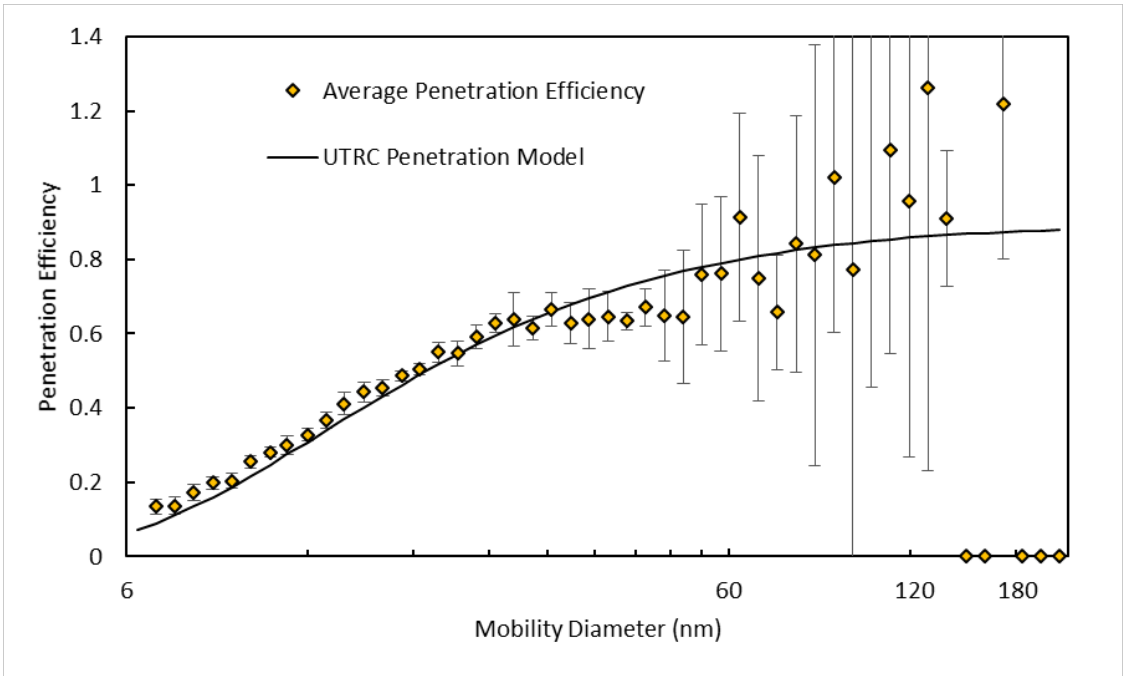

Figure A.6.8. Upstream half of AVL Sampling System average penetration efficiency for the GE J-85 with 50/50 Camelina and Jet-A Blend Fuel at idle power setting.

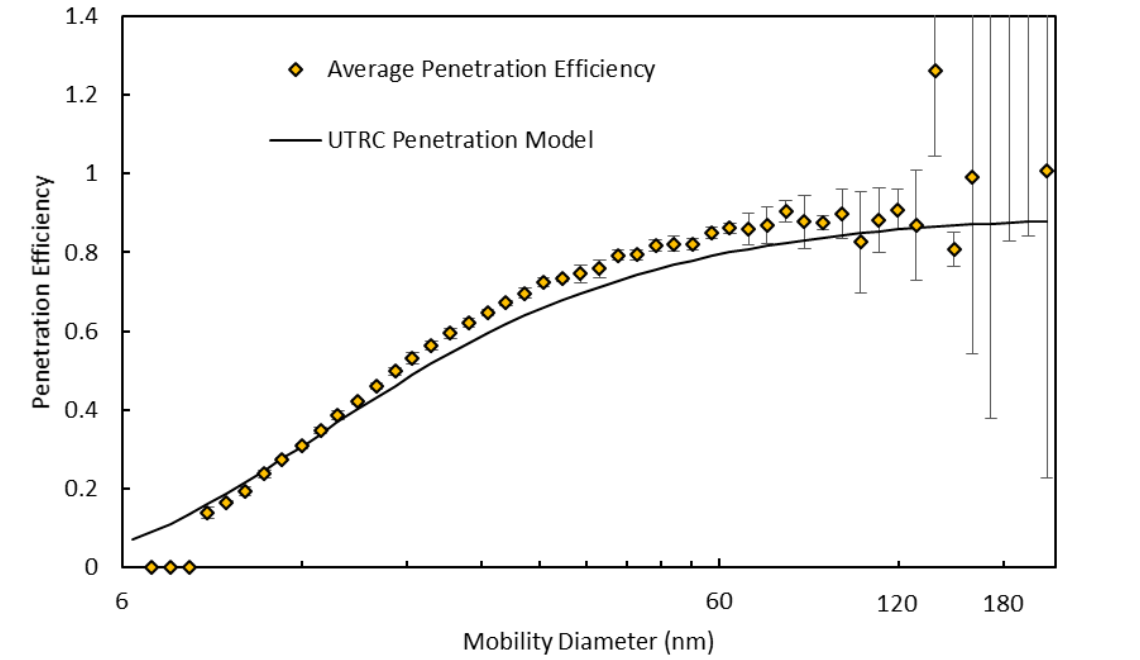

Figure A.6.9. Upstream half of AVL Sampling System average penetration efficiency for the GE J-85 with 50/50 Camelina and Jet-A Blend Fuel at middle power setting.

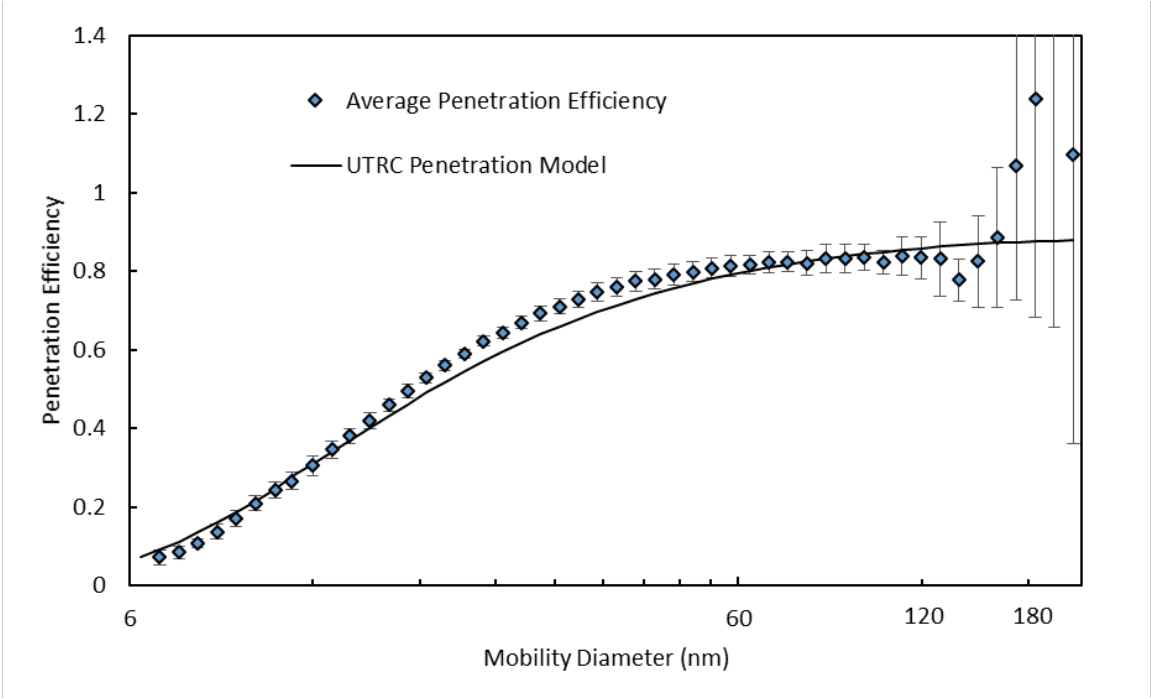

Figure A.6.10. Upstream half of AVL Sampling System average penetration efficiency for the GE J-85 with Jet-A Fuel at Military power setting.

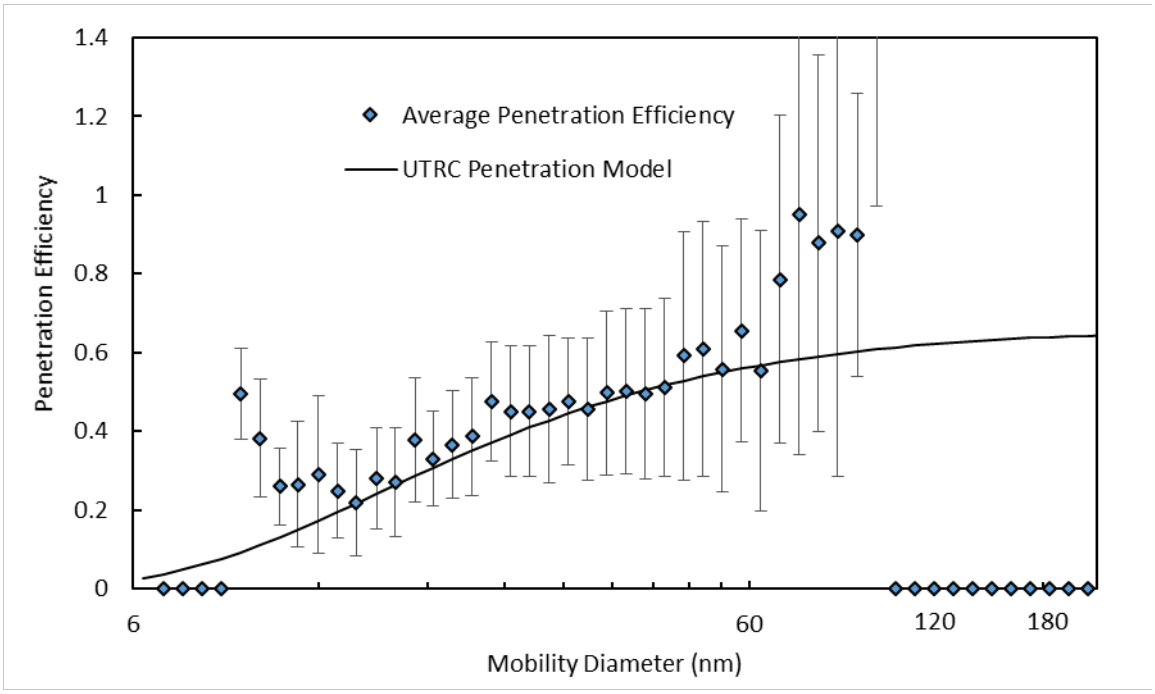

Figure A.6.11. MS&T Sampling System average penetration efficiency for the GE J-85 with Jet-A Fuel at idle power setting.

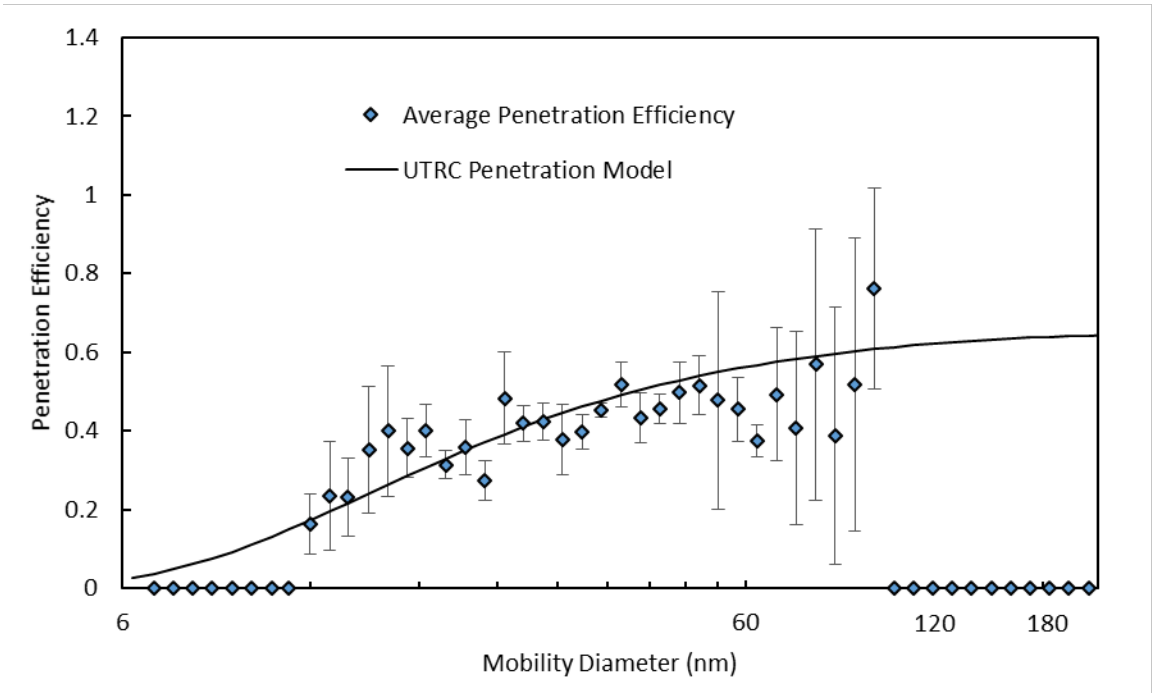

Figure A.6.12. MS&T Sampling System average penetration efficiency for the GE J-85 with Jet-A Fuel at middle power setting.

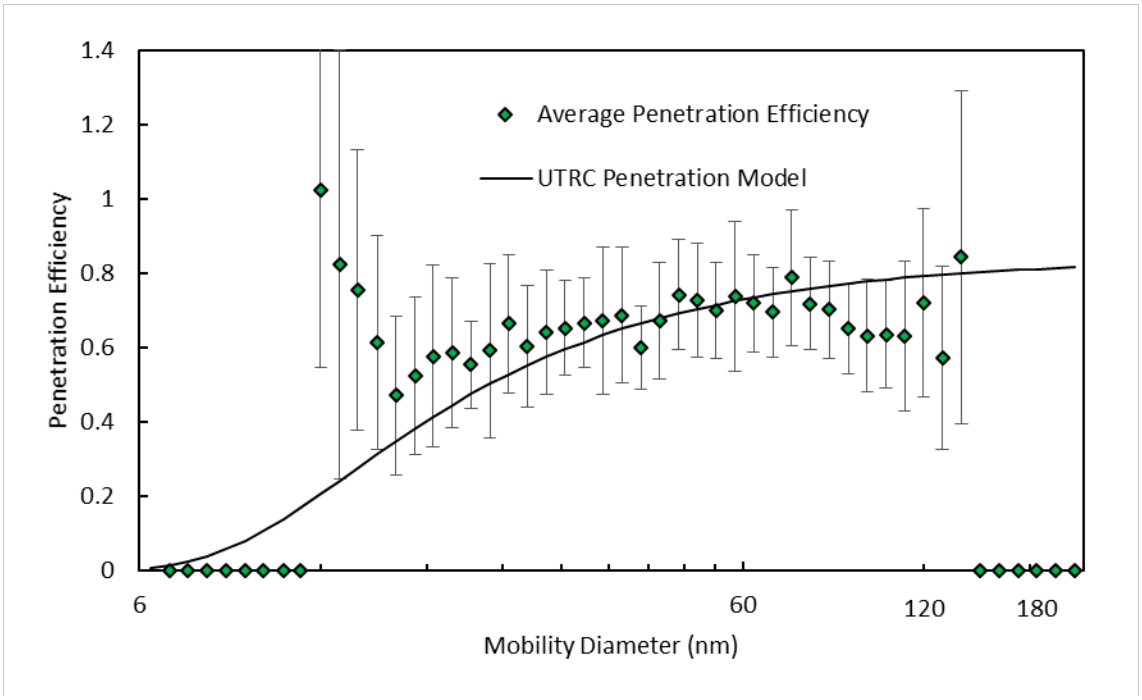

Figure A.6.13. UTRC APC average penetration efficiency for the Jing Mini-CAST with VARIAnT1 Setting.

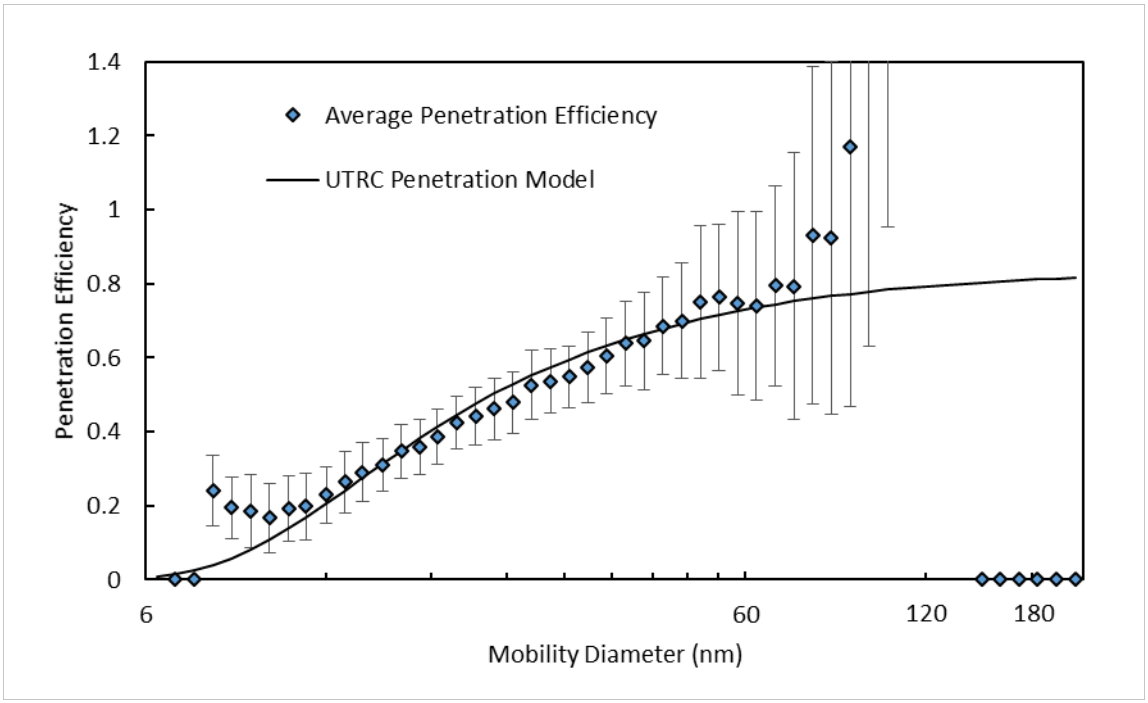

Figure A.6.14. UTRC APC average penetration efficiency for the GE J-85 with Jet-A Fuel at idle power setting.

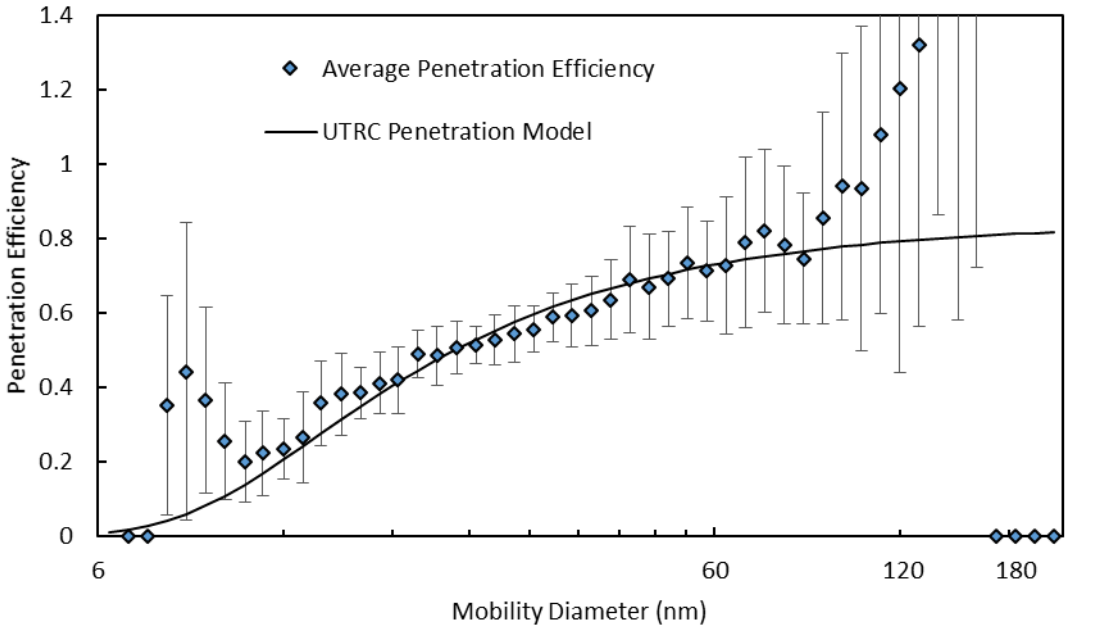

Figure A.6.15. UTRC APC average penetration efficiency for the GE J-85 with Jet-A Fuel at middle power setting.

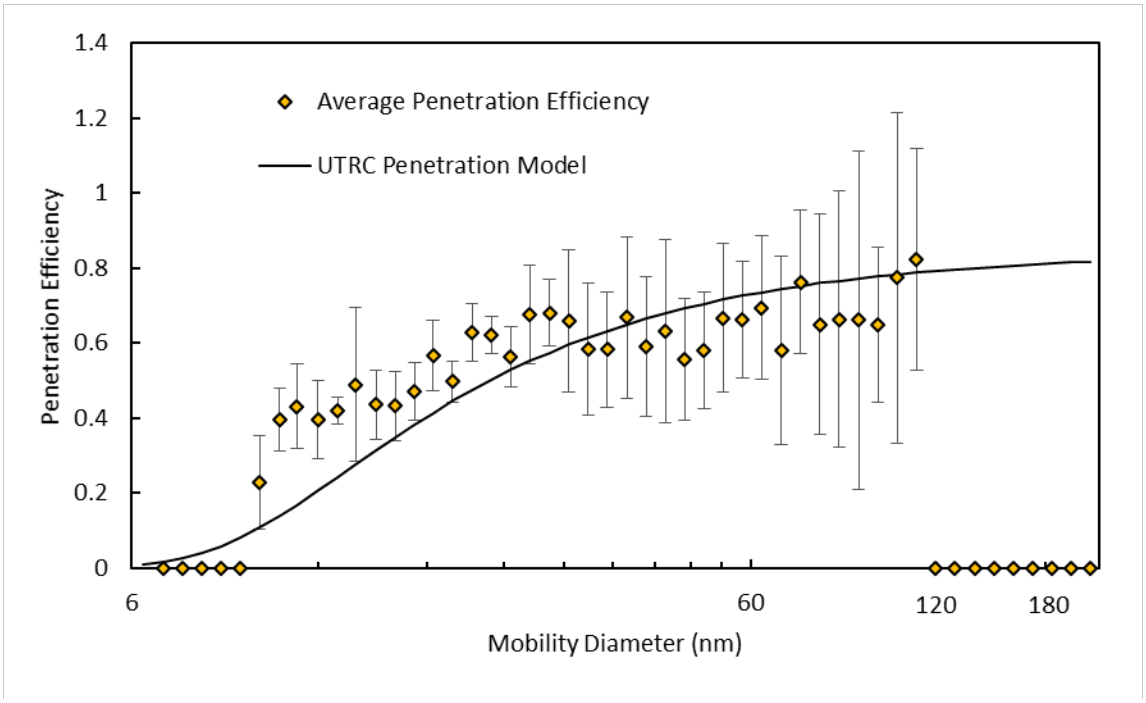

Figure A.6.16. UTRC APC average penetration efficiency for the GE J-85 with 50/50 Camelina and Jet-A Blend Fuel at middle power setting.

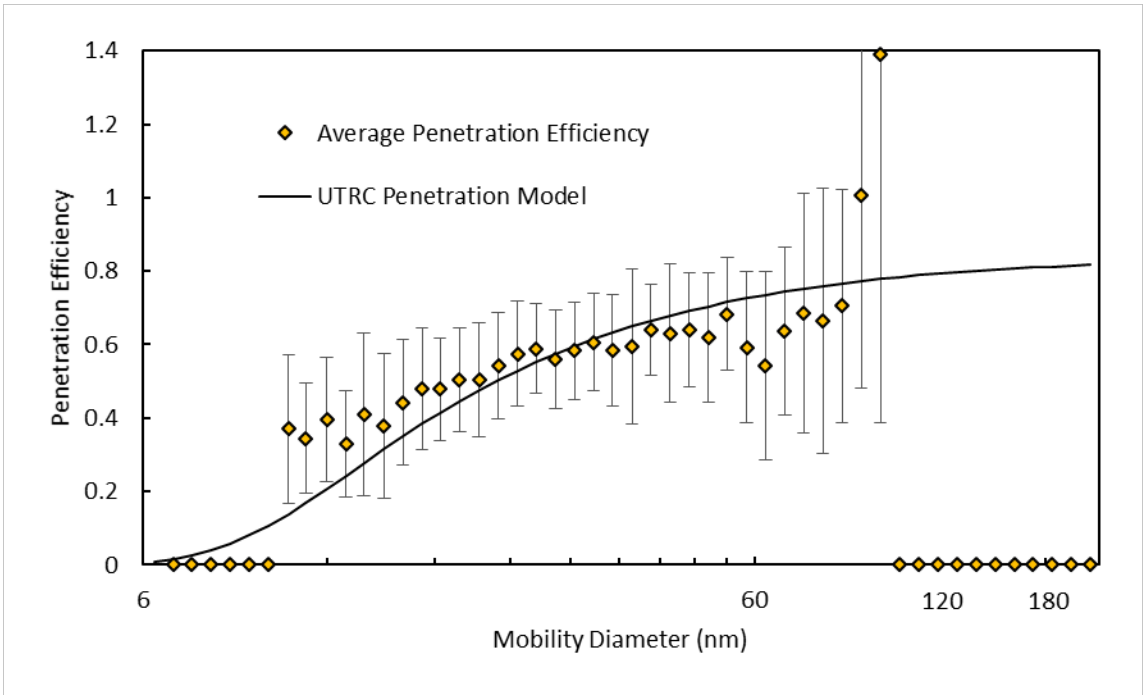

Figure A.6.17. UTRC APC average penetration efficiency for the GE J-85 with 50/50 Camelina and Jet-A Blend Fuel at Military power setting.

Note: Penetration Efficiencies were not available for all settings.

Appendix 7. Acronyms and Symbols

Table A.7.1. Acronyms definitions.

Acronyms	Definition
US EPA NVFEL	United States Environmental Protection Agency
NVFEL	National Vehicle and Fuel Emissions Laboratory (US EPA Branch)
AEDC	Arnold Engineering Development Complex
UTSI	University of Tennessee Space Institute
UoM	University of Minnesota
SMPS	Scanning Mobility Particle Sizer
UTRC	United Technologies Research Center
VARIAnT2	Variable Response In Aircraft Non-Volatile Particle Matter Testing
ARP	Aerospace Recommended Practice
MS&T	Missouri University of Science and Technology
AVL	Anstalt für Verbrennungskraftmaschinen List
nvPM	Non-volatile Particle Matter
MSS	Micro Soot Sensor
LII	Laser Induced Incandescence
APC	AVL Particle Counter
PTFE	Polytetrafluoroethylene
GL	Gas Line
PTS	Particle Transport System
VPR	Volatile Particle Remover
CPC	Condensation Particle Counter
DMA	Differential Mobility Analyzer
Jing Mini-CAST	Jing Mini-Combustion Aerosol Standard
GE	General Electric
PRF	Propulsion Research Facility
Mil	Military
A.I.M.	Aerosol Instrument Manager
TSI SMPS	SMPS owned by TSI (On Loan for Test)
AEDC SMPS	SMPS owned by AEDC
AFRL	Air Force Research Laboratory
AFRL SMPS	SMPS owned by AFRL (On Loan for Test)
UTRC SMPS	SMPS owned by UTRC (On Loan for Test)

Table A.7.1. Continued Acronyms definitions.

Acronyms	Definition
NRMRL	National Risk Management Research Laboratory (US EPA Branch)
NRMRL SMPS	SMPS owned by NRMRL
NVFEL SMPS	SMPS owned by NVFEL
DOS	Dioctyl sebacate
NaCl	Sodium chloride
K	Measure of temperature in degrees kelvin

Table A.7.2. Symbols Defined.

Parameter symbols	Descriptions	Units	Values
T_{gasi}	Temperature of the carrier gas of ith segment of the sampling line. (This is typically the line segment wall control temperature, T_{linei}, except when two adjoining segments differ in temperature.	Kelvin	Measured
T_{linei}	Line segment wall control temperature of the ith segment of the sampling line.	Kelvin	Measured
T_{EGT}	Performance-predicted engine exit exhaust gas temperature	Kelvin	Measured
P_i	Pressure of the carrier gas in the ith segment of the sampling line, assumed constant throughout the ith segment and equal to 101.325 kPa	Kilopascals	Measured
Q_i	Flow rate of the carrier gas through the ith segment of the sampling line (Collection Part segment flow rates are estimated)	Standard liters per minute (slpm)	Measured

Table A.7.2. Continued Symbols Defined.

Parameter symbols	Descriptions	Units	Values
ID_i	Inside diameter of the ith segment of the sampling line	Centimeters	Measured
L_i	Length of the ith segment of the sampling line	Centimeters	Measured
θ_{bi}	Total angle of bends in the ith segment of the sampling line	Degrees	Measured
$\eta_{VPR}(15)$, $\eta_{VPR}(30)$, $\eta_{VPR}(50)$, $\eta_{VPR}(100)$	VPR penetration fractions at particle diameters of 15 nm, 30 nm, 50 nm, and 100 nm; used to determine VPR penetration function	Dimensionless	Provided by manufacturers
cyclone separator D_{50}	Cyclone separator particle diameter at which 50% of particles diameters of 50 nm,D_{50}, pass through; used to determine cyclone separator penetration function	Nanometers (nm)	Provided by manufacturers
cyclone separator sharpness, $(D_{16}/D_{84})^{0.5}$	Ratio of cyclone separator particle diameters at which 16% and 84% of particles with diameters of 16 nm ,D_{16}, and 84 nm ,D_{84}, pass through; used to determine cyclone separator penetration function	Dimensionless	Provided by manufacturers
μ_0	Reference carrier gas viscosity, Evaluated at 296 K and 101 kPa	Grams per centimeter seconds (g/cm•s)	1.83×10^{-4}
λ_0	Mean free path, Evaluated at 296 K and 101 kPa, assumed constant	Nanometers (nm)	67.3
ρ	Assumed effective density of the Non-Volatile particles	Grams per centimeter cubed (g/cm^3)	1

Table A.7.2. Continued Symbols Defined.

Parameter symbols	Descriptions	Units	Values
D_m	Mobility diameter of the non-Volatile Particle	Nanometers (nm)	Measured
η	Penetration Efficiency	Dimensionless	Calculated
i	Sample System Segment, max of 10 segments	Dimensionless	1, 2, .., 10
$\eta_{difi}(D_m)$	Penetration Efficiencies due to only diffusional losses in the ith segment of the sampling line per mobility diameter	Dimensionless	Calculated
$V_{d,diff}$	Deposition speed	Seconds	Calculated
Q_i	Gas flow in the ith sampling line segment	Cubic centimeters per second (cm^3/s)	Measured
Re	Reynolds Number	Dimensionless	Calculated
Sc	Schmidt Number	Squared grams per square centimeters squared seconds ($g^2/cm^2 \cdot s^2$)	Calculated
D	Diffusion Coefficient	Squared centimeters per second (cm^2/s)	Calculated
k_B	Boltzmann constant	Grams squared centimeters per squared seconds degrees kelvin $(g \cdot cm^2)/(s^2 \cdot K)$	$1.38x10^{-16}$
ρ_{gas}	Density of the carrier gas	Grams per centimeter cubed (g/cm^3)	Calculated

Table A.7.2. Continued Symbols Defined.

Parameter symbols	Descriptions	Units	Values
μ	Viscosity of the carrier gas in question	Grams per centimeter seconds (g/cm•s)	Measured
T_0	Reference Temperature	Kelvin	296.15
C_c	Cunningham slip correction factor	Dimensionless	Calculated
$\eta_{bi}(D_m)$	Penetration Efficiencies due to only inertial particle losses in the ith segment of the sampling line per mobility diameter	Dimensionless	Calculated
θ_{bi}	Total angle of bends in the ith segment of the sampling line	Degrees	Measured
Stk	Dimensional Stokes number	Dimensionless	Calculated
$\eta_{thermoi}$	Penetration Efficiencies due only to thermophoresis in the ith segment of the sampling line	Dimensionless	Calculated
$\eta_{eleci}(D_m)$	Penetration Efficiencies due to only electrostatic losses per ith segment of sampling line per mobility diameter	Dimensionless	Calculated
C	Coulombic charge for a proton	Coulomb	1.6E-19
ε	Electrical permittivity of the particles through the line	Squared Coulomb second squared per gram per cubic centimeter ($C^2s^2/g/cm^3$)	8.85E-21

Table A.7.2. Continued Symbols Defined.

Parameter symbols	Descriptions	Units	Values
h_{gas}	Carrier gas convective heat transfer coefficient	Watts per squared centimeters degrees kelvin ($W/(cm^2 \cdot K)$)	$5.68x10^{-4}$
C_p	Constant pressure carrier gas specific heat, assuming Air as carrier gas	Joules per grams degree kelvin ($J/(g \cdot K)$)	1.01
Pr	Prandtl number	dimensionless	Calculated
K_{th}	Thermophoretic coefficient	dimensionless	Calculated
C_s	Slip coefficient	dimensionless	1.17
C_m	Soot momentum coefficient	dimensionless	Calculated
C_t	Thermal coefficient	dimensionless	Calculated
k_{gas}	Thermal conductivity of the carrier gas	Watts per squared centimeters degrees kelvin ($W/(cm^2 \cdot K)$)	Calculated
K_n	Knudsen number	Inverse nanometers squared (nm^{-2})	Calculated
k_p	Particle thermal conductivity	Watts per squared centimeters degrees kelvin ($W/(cm^2 \cdot K)$)	Calculated
T_{in}	Temperature of the gas entering the sampling line	Kelvin	Measured
T_{exit}	Equilibrated sample particulate and gas temperature which is approximately the temperature of the sampling line wall	Kelvin	~433.15

Table A.7.2. Continued Symbols Defined.

Parameter symbols	Descriptions	Units	Values
$\eta_{dil}(D_m)$	Diluter1 penetration efficiencies per mobility size, value is considered constant	Dimensionless	1
$\eta_{spl}(D_m)$	Splitter penetration efficiencies per mobility size, value is considered constant	Dimensionless	1
$\eta_{cyc}(D_m)$	Cyclone penetration efficiencies per mobility diameter	Dimensionless	Calculated
$\eta_{APC}(D_m)$	AVL Particle Counter Penetration Efficiencies per mobility diameter	Dimensionless	Calculated
$\eta_{VPR}(D_m)$	Volatile Particle Remover (VPR) penetration efficiencies per mobility diameter	Dimensionless	Calculated
$\eta_{VPRdiff}(D_m)$	VPR penetration efficiency due to diffusional losses	Dimensionless	Calculated
η_{VPRth}	VPR penetration efficiency due to thermophoretic losses	Dimensionless	Calculated
ψ	Deposition parameter, D x L_{VPR}/Q_{VPR}	Dimensionless	Calculated
Q_{VPR}	Carrier gas flow in the VPR	Cubic centimeters per second (cm^3/s)	Measured
$\eta_{total}(D_m)$	Total penetration efficiencies for sampling system and APC per mobility diameter	Dimensionless	Calculated
$\eta_{totalspl}(D_m)$	Total penetration efficiencies for sampling system only per mobility diameter	Dimensionless	Calculated

Table A.7.2. Continued Symbols Defined.

Parameter symbols	Descriptions	Units	Values
σ	Standard deviation of the penetration efficiencies data sets per mobility diameter	Dimensionless	Calculated
μ_m	Mean of all penetration efficiencies in the data set	Dimensionless	Calculated
x	Individual penetration efficiency values	Dimensionless	Calculated
N	Number of penetration efficiencies in our data set	Dimensionless	Calculated

Appendix 8. UTRC Model Inputs and Assumptions

Table A.8.1. Sampling and measurement System Input Parameters {Ref. 16}.

Parameter symbols	Descriptions	Units
T_{gasi}	Temperature of the carrier gas of ith segment of the sampling line. (This is typically the line segment wall control temperature, T_{linei}, except when two adjoining segments differ in temperature.	K
T_{linei}	Line segment wall control temperature of the ith segment of the sampling line.	K
T_{EGT}	Performance-predicted engine exit exhaust gas temperature	K
P_i	Pressure of the carrier gas in the ith segment of the sampling line, assumed constant throughout the ith segment and equal to 101.325 kPa	kPa
Q_i	Flow rate of the carrier gas through the ith segment of the sampling line (Segment one flow rates are estimated)	slpm
ID_i	Inside diameter of the ith segment of the sampling line	cm
L_i	Length of the ith segment of the sampling line	cm
θ_{bi}	Total angle of bends in the ith segment of the sampling line	degrees
ηVPR(15), ηVPR(30), ηVPR(50), ηVPR(100)	VPR penetration fractions at particle diameters of 15 nm, 30 nm, 50 nm, and 100 nm; used to determine VPR penetration function	dimensionless
cyclone separator D50	cyclone separator particle diameter at which 50% of particles diameters of 50 nm,D50, pass through; used to determine cyclone separator penetration function	nm
cyclone separator sharpness, (D16/D84)0.5	Ratio of cyclone separator particle diameters at which 16% and 84% of particles with diameters of 16 nm ,D16, and 84 nm ,D84, pass through; used to determine cyclone separator penetration function	dimensionless

Table A.8.2. Assumed Carrier Gas and Particle Properties used in the Particle Transport Calculations {Ref. 16}.

Carrier gas properties	**Value**	**Units**	**Notes**
composition	air	-	
viscosity, μ_0	1.83×10^{-4}	g/cm•s	Evaluated at 296 K and 101 kPa, not at STP temperature conditions
mean free path, λ_0	67.3	nm	Evaluated at 296 K and 101 kPa, not at STP temperature conditions
Particle properties	**Value**	**Units**	**Notes**
ρ, density	1	g/cm^3	Assumed effective density of the Non-Volatile particles
thermal conductivity	0.2	W/cm•K	Assumed thermal conductivity
size range	6 to 212	nm	particle diameter

VITA

Brandon Hoffman was born in New Bremen, OH, to parents of Melinda and Craig Hoffman. He is the older of two children and Lana Hoffman is his sister. He graduated from New Bremen High School. Throughout childhood he showed interest in engineering especially electronics. After graduation these interests lead him to pursue a degree in Electronic Engineering Technology. In 2008 he graduated from James A. Rhodes State Community College with his Associates Degree. While at Rhodes State he meet Paige Hoffman and they had one child, Mr. Oliver Hoffman. He continued to pursue his interest in engineering at Miami University in Oxford, Ohio, where he received a Baccalaureate degree in Electro-Mechanical Engineering Technology in 2011. After graduation from college he pursued a career in Engineering at Yuma Proving Ground, an Army testing facility and one of the largest military instillations in the world. He soon moved closer to Ohio and pursued a career in aerospace engineering at Arnold Engineering Development Complex (AEDC), one of the world's premier aerospace testing facilities. While at AEDC Brandon enrolled in graduate course work at the University of Tennessee Space Institute. The work completed in this document satisfies his requirement for a Master of Science degree in Aerospace Engineering.0